# LASER ASSISTED MICRO MILLING WITH MINIMUM QUANTITY LUBRICATION AND VORTEX COOLING

A Thesis

Presented to

The Academic Faculty

By:

Pushparghya Deb Kuila

In Partial Fulfillment

Of the Requirements for the Degree

Master of Science in Mechanical Engineering

Georgia Institute of Technology

August 2016

# LASER ASSISTED MICRO MILLING WITH MINIMUM QUANTITY LUBRICATION AND VORTEX COOLING

Approved by:

Dr. Shreyes Melkote, Advisor
School of Mechanical Engineering
Georgia Institute of Technology

Dr. Steven Y. Liang
School of Mechanical Engineering
Georgia Institute of Technology

Dr. Chris Saldana
School of Mechanical Engineering
Georgia Institute of Technology

Date approved: July 18, 2016

# ACKNOWLEDGEMENTS

First and most importantly I would like to thank God. I would like to thank My family and many friends for all the moral support during such difficult times. This project would not have been possible to have been completed without the help of my brother Alberto Bucciarelli. I owe very much of what I learned for this project due to Alberto. I would like to greatly thank Ken Voronin for being such a great industry mentor and giving me the motivation to continue my education after my undergrad. I would like to greatly thank the students, faculty, and staff of the PMRC for help with the many practical and administrative needs of this project. I would like to thanks the students of the PMRC for putting up with whinny sounds of the micro mill when we were running experiments. I would like to thank greatly Steven Sheffield, Louis Boulanger, Brandon Royal, and Nathan Mauldin for their expertise machining help for fabricating the many parts needed for this project. Thanks for the many many tools borrowed by the Invention Studio over the course of two years. Many thanks to the Kyle, Anh, and JJ Martino for helping fix the electronic and computer systems of the LAMM. Many of the high-quality microscopic images would not have been possible without the help and training given by Institute of Electronics and Nanotechnology. I would like to thank our sponsor for providing the funding for this project. I would like to thank Dr. Melkote for his guidance as an advisor and giving me a chance at this project. I would also like to thank Dr. Liang and Dr. Saldana for their time to be on my committee.

# TABLE OF CONTENTS

# LIST OF TABLES

# LIST OF FIGURES

# NOMENCLATURE

| | |
|---|---|
| LAM | Laser Assisted Machining |
| LAMM | Laser Assisted Micro Milling |
| HAZ | Heat Affected Zone |
| MQL | Minimum Quantity Lubrication |
| BUE | Built-up Edge |
| $V_{b\_max}$ | Maximum flank wear |
| SEM | Scanning Electron Microscope |
| $HR_c$ | Rockwell Hardness C Scale |
| EDS | Electron Dispersive Spectroscopy |
| $S_a$ | Areal arithmetic average surface roughness |
| $t$ | Instantaneous uncut chip thickness |
| $R$ | Tool cutting edge radius |
| $F_{ty}$ | Tensile yield strength |
| $F_{tu}$ | Ultimate tensile strength |
| $T(x,y,z)$ | Temperature distribution |
| $P$ | Laser power |
| $d_s$ | Laser spot diameter |
| $d$ | Center-to-center laser-tool distance |
| $\alpha$ | Absorptivity to laser irradiation |
| $q$ | Heat intensity |
| $K$ | Thermal conductivity |
| $\kappa$ | Thermal diffusivity |
| $C$ | Specific heat |
| $\rho$ | density |
| $U$ | Heat source velocity |
| $q_0$ | Average heat intensity of the laser spot |
| $R_l$ | Fraction of heat conducted into the chip |
| $\theta$ | Angular position |
| $\theta_0$ | Room temperature |
| $\theta_s$ | Temperature Rise |
| $J$ | Mechanical equivalent of heat |
| $\Upsilon$ | Shear strain |
| $u_s$ | Specific cutting energy |
| $k_0$ | Shear yield stress |
| $\phi_0$ | Shear angle |
| $\alpha_r$ | Radial rake angle |
| $V_c$ | Cutting speed |

|  |  |
|---|---|
| $f_t$ | Feed per tooth |
| $a_p$ | depth of cut |
| $F_x$, $F_y$, $F_z$ | Force components in the X, Y, Z directions |

# SUMMARY

As applications in medical, electronics, and aerospace industries continue to demand miniaturization of parts, manufacturing processes capable of creating microscale features are necessary. For part features of moderate complexity and low aspect ratios, micro milling is usually the most practical option because of its high material removal rates and relatively low capital cost. Micro milling refers to milling with end milling tools less than 1 mm in diameter. Micro end mills are prone to breaking easily due to their small size. Additional limitations in micro milling arise from the well-known size effect, which leads to increased ploughing and reduced tool life. Workpiece and tool life limitations also arise when micromachining difficult-to-cut metals such as a high nickel content alloyed steel A-286 (~ 42 $HR_c$), which is the work material of interest in this thesis.

Considerable research has been conducted to overcome these limitations and to generally enhance micromachinability. Prior investigations consider the use of wet assist, minimum quantity lubrication (MQL), vortex cooling, and laser assisted micro milling (LAMM) to overcome some of the limitations. In particular, prior investigations of LAMM have shown that by using a laser *in situ* to thermally soften the workpiece in front of the cutting tool, stresses in the tool are greatly reduced thereby reducing tool wear and improving the dimensional accuracy. However, a systematic comparison of the micromachinability of wet assist and LAMM is lacking. In addition, there is no prior work comparing the performance of MQL and vortex cooling on the tool condition and micromachinability in LAMM. Therefore, the first objective of this thesis is to analyze and compare micro milling under dry cutting, wet cutting, and LAMM. The second objective is to evaluate the performance of LAMM in the presence of MQL and vortex cooling.

A limited duration full factorial micro milling experiment was carried out using a range of cutting parameters to understand the micromachinability of a difficult-to-cut high nickel content alloyed steel A-286 (~ 42 $HR_c$) in dry cutting, wet cutting, and LAMM. Results showed that LAMM maintained a more precise depth of cut, yielded lower resultant cutting forces than dry cutting, and reduced the tool diameter wear by 29% compared to dry cutting and by 22% compared to wet cutting. However, LAMM resulted in built-up edge on the tool faces.

An extended duration LAMM tool life test was conducted using the best cutting conditions identified in the factorial experiment. As the tool wore, the grooves developed a tapered and rounded cross section, and non-uniform burrs formed at the groove edges. The tool wore rapidly in the first 50 $mm^3$ of material removal but reached a steady state thereafter. Built-up edge formation was prevalent and tended to increase over the test duration.

Finally, the use of MQL and vortex cooling methods were experimentally investigated to ameliorate the built-up edge caused by LAMM. The addition of MQL further enhanced the groove dimensional accuracy of LAMM, lowering the change in groove width by 41%. The addition of MQL to LAMM prevented built-up edge formation. Vortex cooling allowed for better chip removal and cooling of the tool and decreased the average resultant cutting force by 15%. Overall, the LAMM+MQL II case (corresponding to an air flow rate of 50 l/min) was found to be the best test condition with the least tool wear, least built-up edge, and the least change in groove dimensions. Physically-based explanations for these results are given. The thesis concludes by describing potential topics for future research.

# CHAPTER 1: INTRODUCTION

## 1.1 Motivation and problem statement

As applications in medical, electronics, and aerospace industries continue to demand miniaturization of parts, manufacturing processes capable of creating microscale features are necessary. Among subtractive manufacturing processes, the following processes are commonly used to create microscale features: electrochemical machining (ECM), electrical discharge machining (EDM), laser machining, micro grinding, and micro milling. For part features of moderate complexity and relatively low aspect ratios, micro milling is usually the most practical option because of its high material removal rates and relatively low capital cost. Micro milling uses end milling tools that are less than 1 mm in diameter. In the last decade, the role of micro milling as a subtractive micromachining process has increased, and it has been used for commercial applications. Figure 1.1-1.3 show examples of a commercially available micro milling machine, an example of a micro milled impeller, and the relative scale of micro end milling tool, respectively.

Figure 1.1: Example of commercial micro milling machine (Microgantry® by Kugler GmbH).

Figure 1.2: Fluid impeller part, machined in a 5-axis micro mill (Microlution Inc.).

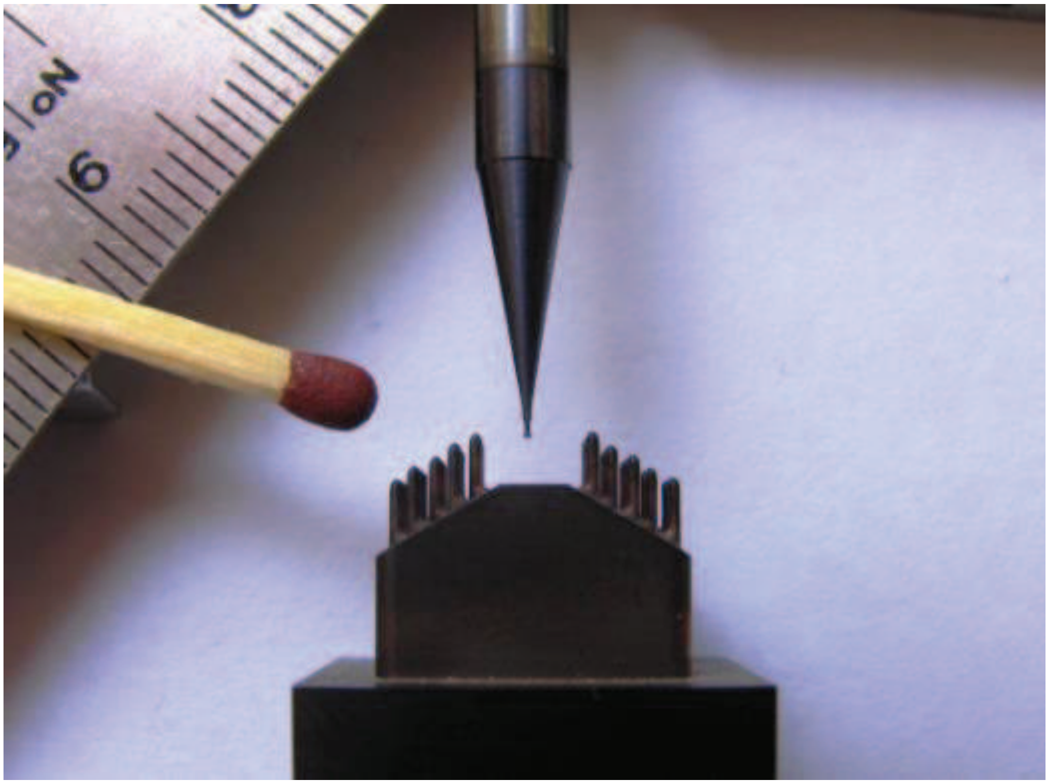

Figure 1.3: Micro mold machined using micro milling (Mold Making Technology).

### 1.1.1 Limitations of micro milling

Micro end mills are fragile and have a tendency to break easily due to their small size. Additional difficulties in micro milling arise from the well-known size effect [1], which is encountered when the uncut chip thickness and grain size of the material being cut are comparable to the tool cutting edge radius, as depicted in Figure 1.4. Size effect is characterized by a significant amount of ploughing and rubbing as opposed to material removal through shearing, which is common in conventional or macroscale machining operations. This effect significantly increases the specific cutting forces and tool wear in comparison to macroscale milling.

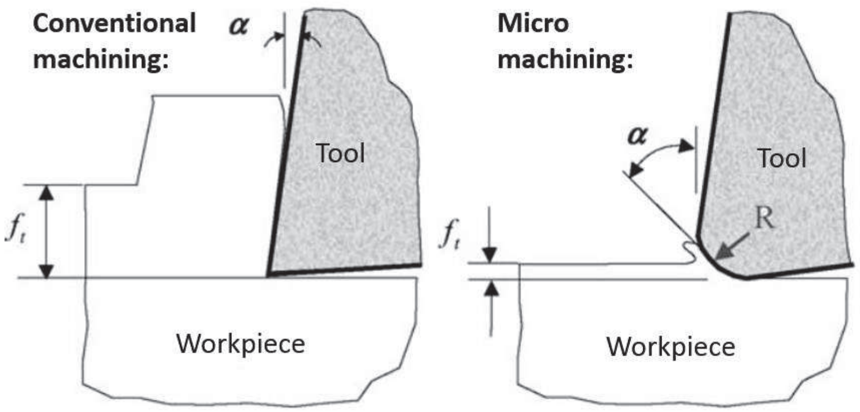

Figure 1.4: Size effect: conventional machining (left), micromachining (right); figure adapted from [2].

Additional limitations arise from micromachining difficult-to-cut materials such as superalloys including titanium and nickel base alloys, and high nickel content stainless steels such as A-286, which is the work material of interest in this thesis. Difficult-to-cut materials such as stainless steels, titanium alloys, and nickel base alloys are challenging from a standpoint of micro milling, because they lead to rapid tool wear and poor overall machinability.

### 1.1.2 Hybrid methods

To overcome the difficulties encountered in micro milling of difficult-to-cut materials, particularly tool wear, several solution approaches have been developed and implemented. The first and most common approach is to use a coolant, also referred to as wet assist in this thesis, which is often used in machining to lubricate and cool the tool-workpiece interfaces and convect the heat generated by plastic deformation and frictional interaction of the tool and workpiece. The second approach consists of Minimum Quantity Lubrication (MQL). This lubrication method mixes air with atomized oil droplets to better access and lubricate the tool-workpiece interfaces [3]. As a result, the tool temperature is lowered, which in turn reduces tool wear and therefore enhances tool life. MQL is also becoming more common due to its limited oil usage, ~ 10 ml/hr in contrast to ~ 1,000 ml/hr in conventional flood cooling. The third approach is to use Ranque-Hilsch vortex tubes and similar forms of air cooling methods [4]. Vortex tubes take in compressed air, cooling it down before delivering an output of cold air directed at the tool-workpiece interfaces [5, 6], thereby reducing tool wear and improving micromachinability.

The fourth approach involves laser assisted micro milling (LAMM). In this process, shown schematically in Figure 1.5, a laser is focused a short distance in front of the tool's path of travel to thermally soften the high strength workpiece, thereby lowering the cutting forces and the stresses imposed on the cutting tool. The reduced stress leads to lower tool wear and therefore improved machinability.

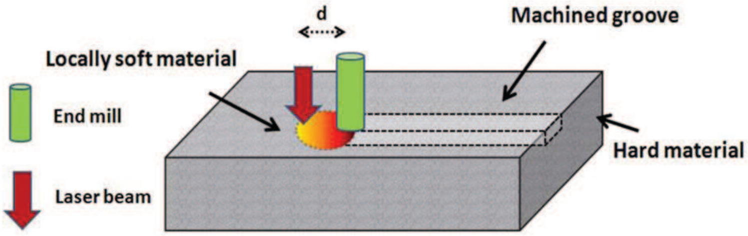

Figure 1.5: LAMM schematic [7].

Though LAMM has the potential to enhance machinability, a systematic investigation comparing micro milling using wet assist, MQL, vortex cooling, and LAMM is lacking. Furthermore, there are no prior studies on cooling and lubrication methods that can be used with LAMM to enhance micromachinability of difficult-to-cut materials. These limitations provide the motivation for the research described in this thesis.

## 1.2 Research objectives

This thesis investigates the use of laser assisted micro milling process to address the limitations in micromachining a difficult-to-cut material. Specifically, a high nickel content alloyed steel – A-286 – is targeted as an example of a difficult-to-cut material with industrial applications. The micromachinability of A-286 during micro milling using various assist methods such as wet, MQL, and vortex cooling are systematically compared with LAMM. To further enhance the micromachinability of and tool life in the LAMM process, the thesis also investigates the benefits and limitations of combining MQL and vortex cooling with LAMM. The primary research objectives of this thesis are:

- To analyze and compare micro milling under dry cutting and wet assist conditions with LAMM.

- To evaluate the performance of LAMM in the presence of MQL and vortex cooling.

### 1.2.1 Proposed approaches

The stated research objectives are accomplished through several analytical and experimental investigations summarized in Figure 1.6.

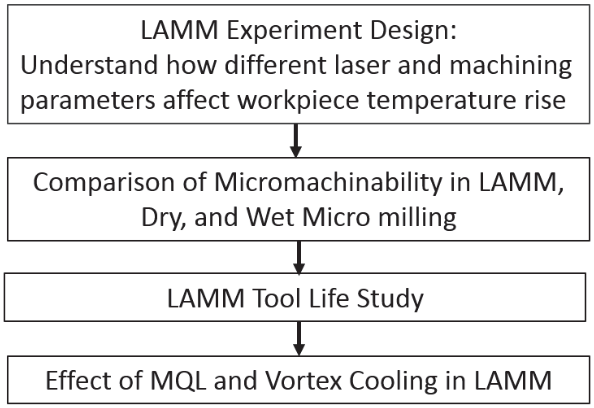

Figure 1.6: Overall research plan.

Proper LAMM experiment design required an understanding of the temperature rise in the workpiece material due to laser irradiation. A previously developed analytical model was used to understand the influence of different laser and machining parameters on the temperature rise in the workpiece. From this analysis, the initial laser parameters used in the LAMM experiments were identified.

A full factorial limited duration micro groove (or slot) milling experiment was performed with the following factors: assist condition (dry, wet, LAMM), and cutting conditions such as cutting speed, feed, and axial depth of cut. The primary objective of the experiment was to identify the best cutting conditions (cutting speed, feed, and depth of cut) for each assist condition. Micromachinability was characterized through measurement and analysis of the cut surface morphology, groove dimensions, tool condition, burr formation, and cutting forces.

An extended duration LAMM test was conducted using the best cutting conditions identified above to evaluate the tool life in LAMM. Micromachinability was again characterized by monitoring the groove condition, tool wear, burr formation, and cutting forces.

Finally, the use of MQL and vortex cooling methods was experimentally investigated to ameliorate the built-up edge caused by LAMM. Cut groove dimensions, surface roughness, burr dimensions, tool wear, and cutting forces were compared and analyzed.

## 1.3 Thesis outline

This chapter provided a basic introduction to micro milling, micro milling limitations, assist methods, LAMM, and the research objectives designed to investigate the efficacy of LAMM in micro milling a difficult-to-cut steel alloy. Chapter 2 provides an overview of prior research on micro milling, flood cooling, MQL, vortex cooling, LAMM, and combined hybrid processes. Chapter 3 discusses the thermal model used for initial selection of the laser parameters. LAMM equipment configuration, workpiece material, and end mill tools used in the experiments are also described in this chapter. Chapter 4 presents the results of an experimental evaluation of LAMM and its comparison with dry cutting and wet assist methods. Chapter 5 presents the results of the LAMM tool life study. Chapter 6 investigates the benefits and limitations of using MQL and vortex cooling to enhance tool life and micromachinability in LAMM. Chapter 7 summarizes the main conclusions and original contributions of this thesis. In addition, suggestions for future work are presented.

# CHAPTER 2: LITERATURE REVIEW

## 2.1 Introduction

This chapter reviews prior research related to micro milling and several heating, cooling, and lubrication methods – termed assist methods in this thesis – used to improve micromachinability with an emphasis on micro milling of difficult-to-cut metals. This chapter begins by providing an overview of micro milling considering specific aspects such as the size effect, cutting forces, tool coatings, and cutting parameters. In addition, the chapter provides an overview of influential research on the following assist methods: wet assist, Minimum Quantity Lubrication (MQL), vortex cooling, LAMM, and combined processes. This chapter concludes by highlighting the limitations of prior research, identifying where knowledge is lacking, and how this thesis addresses these limitations.

## 2.2 Literature review

### 2.2.1 Micro milling

As discussed in Chapter 1, one of the main difficulties in micro milling arises from the small size of the tool which limits the force it can withstand without breaking, especially when cutting difficult-to-cut materials. Even when the tool does not break, tool life is limited when cutting difficult-to-cut metals. Another characteristic of micro milling is the well-known size effect [1]. Size effect is characterized by a significant amount of ploughing and rubbing rather than shearing seen in conventional or macroscale milling, as shown in Figure 1.4 [2]. This significantly increases the specific cutting forces, tool temperatures, and tool wear in comparison to macroscale milling [8-12]. An example of the specific cutting energy vs. uncut chip thickness, *t*, is shown in Figure 2.1. As the feed rate is reduced to the microscale, the specific energy increases drastically.

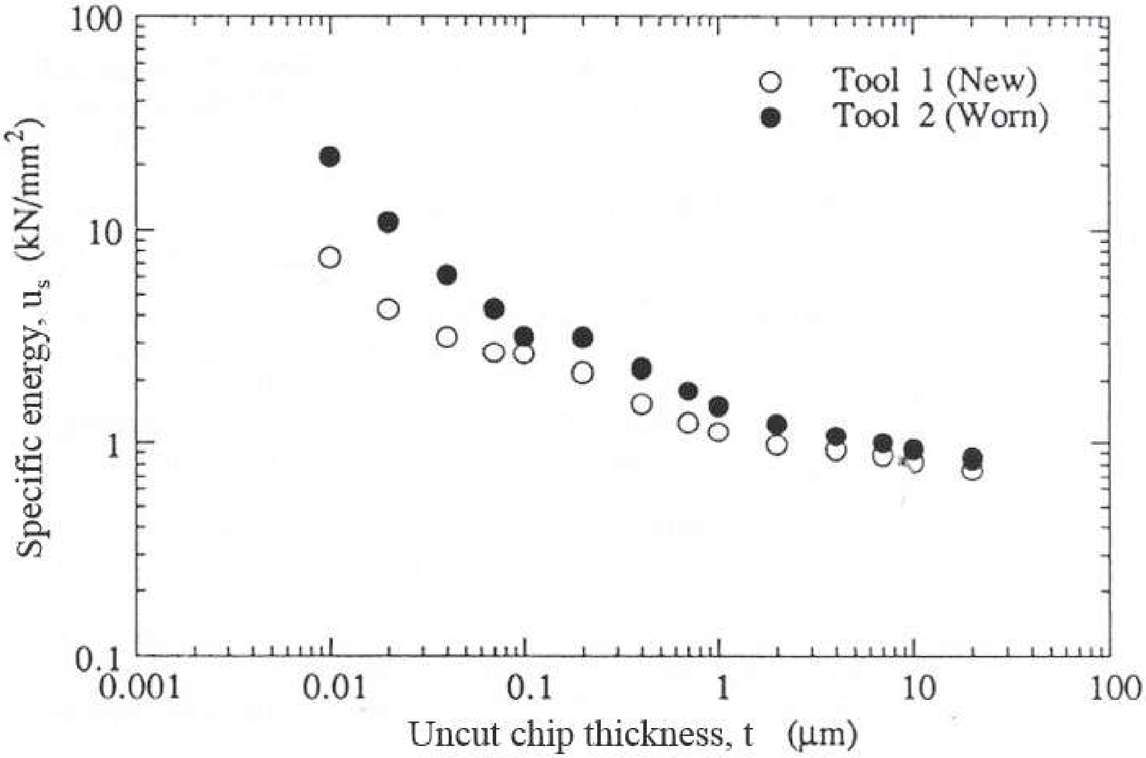

Figure 2.1: Specific energy vs. uncut chip thickness in single point cutting of copper; figure adapted from [12].

Several thorough reviews of micro milling have been presented in the last five years [1, 13-16]. Due to the size effect, several models have been developed to compute the cutting forces [17-20]. Figure 2.2 shows an FEA model [20] comparing stress due to different uncut chip thicknesses in micromachining of copper.

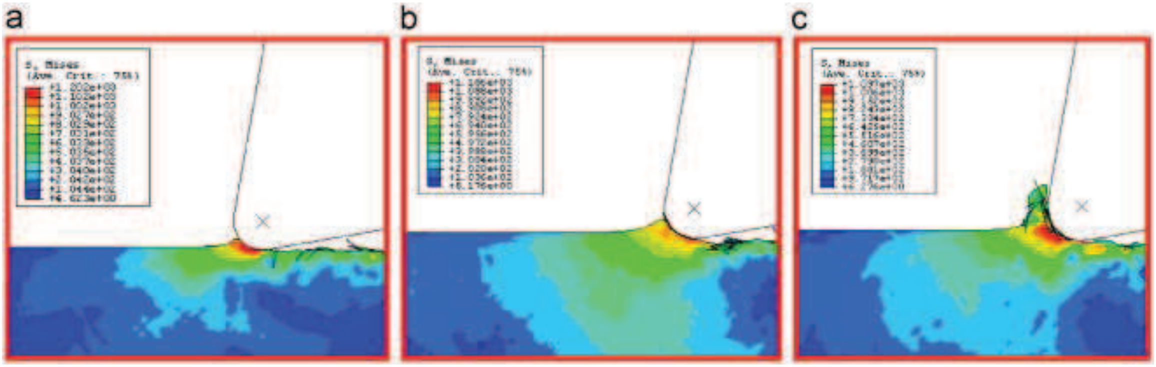

Figure 2.2: Chip formation process in orthogonal micromachining of copper. (a) t = 0.1 R (0.2 μm); (b) t = 0.2 R (0.4 μm); (c) t = 0.3 R (0.6 μm) [20].

Significant work has also been done to improve machine tool components such as high-speed, low run-out spindles, high precision stages, and better sensors for process monitoring [21-23]. Tool coatings for micro tools have been studied [24-29]. The effects of cutting parameters such as feed, speed, depth of cut, and tool path planning strategies have been studied to determine how they impact micromachinability as measured by part quality and tool life [8, 11, 29-32]. Attanasio et al. [33] showed how different grain sizes, microstructures, and work material hardness could greatly affect the micromachinability of Ti-6Al-4V material. Filiz et al. [11] investigated micro milling of copper and found that lower feed rates lead to more tool wear and burrs, which they attributed to the size effect. Wu [34] found that as the feed rate increased, the surface roughness initially decreased to a minimum and then increased. In micro milling of stainless steel [28] and inconel 718 [29], AlCrN and TiAlN tool coatings were found to be most effective, as shown in Figure 2.3.

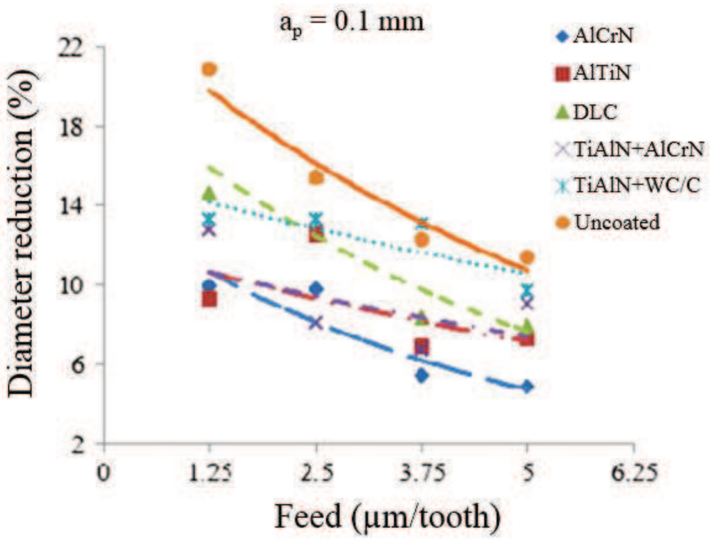

Figure 2.3: Effect of coating materials and feed on change in tool diameter in micro milling of Inconel; figure adapted from [29].

Due to challenges in micro milling of high strength materials such as stainless steels, titanium, and nickel superalloys, many solution approaches have been investigated to enhance micromachinability as quantified by part quality, tool life, and material removal rates. Some of these methods include conventional cooling and lubrication methods including flood cooling, minimum quantity lubrication (MQL), vortex tube cooling, and hybrid methods such as laser assisted micro milling (LAMM).

### 2.2.2 Flood cooling

Flood cooling, also referred to as wet assist in this thesis, is often used in machining to lubricate and remove heat from the tool-workpiece interface, as shown in Figure 2.4.

Figure 2.4: Example of flood cooling in conventional end milling (CNC Cookbook ®).

Wet assist is the most commonly used method to enhance tool life. Pei et al. [35] presented a review of wet assist methods. In micro drilling, Percin et al. [36] found wet assist to reduce surface roughness and produce a smaller heat affected zone. Vazquez et al. [37] found that the use of wet assist micro milling of several alloys leads to grooves with lower surface roughness, as shown in Figure 2.5, and causes less built-up edge formation.

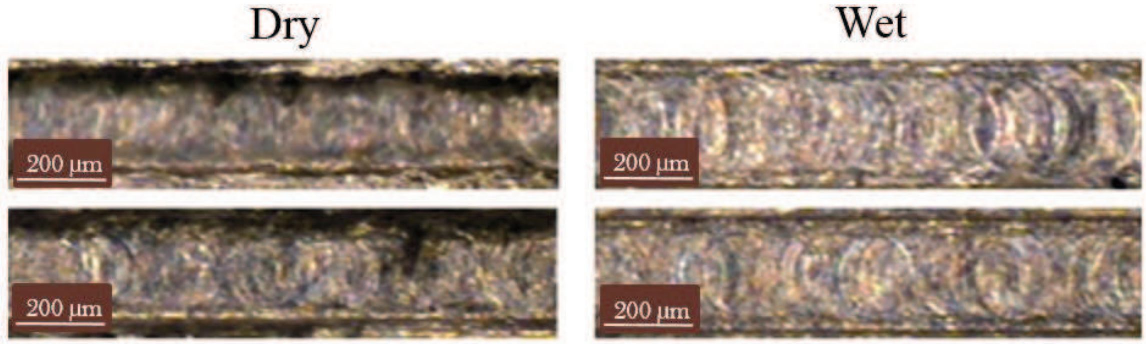

Figure 2.5: Top view of micro-channel in aluminum showing roughness optimization by coolant application; figure adapted from [37].

In conventional scale turning of high nickel content alloys, Wada et al. [38] found that use of wet assist at higher pressures leads to better chip breakage and lower tool wear. Al-Falahi et al. [39] observed in conventional scale milling of Hastelloy that at higher cutting speeds, wet assist was often unable to penetrate the tool-workpiece interface. When conventional scale milling superalloy M-77, Pei et al. [40] found that wet assist led to lower residual stresses and better surface finish. Wet assist has many benefits in macromachining, however at times it may be unsuitable for micro milling due to the force exerted by the liquid coolant stream on the relatively compliant tool, which can negatively impact the dimensional accuracy of the part feature being micromachined [4].

### 2.2.3 Minimum quantity lubrication (MQL)

Minimum quantity lubrication (MQL) uses air mixed with atomized oil droplets to better lubricate the tool-workpiece interface [3], as shown in Figure 2.6 and Figure 2.7.

Figure 2.6: MQL cooling of a micro end mill (Modern Machine Shop).

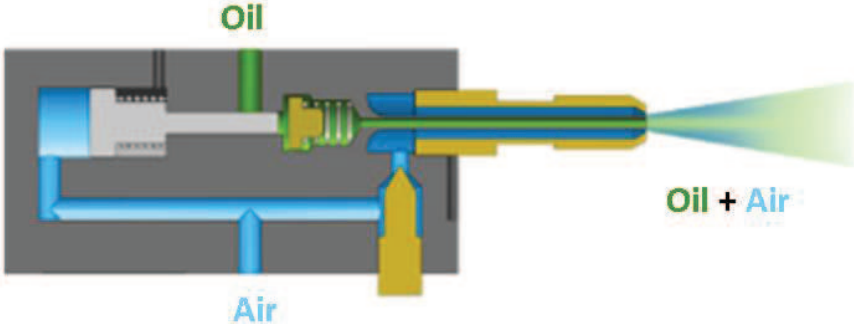

Figure 2.7: MQL schematic (Unist Inc.).

MQL is becoming more common due to its minimal oil usage, ~ 10 ml/hr, compared to conventional flood cooling methods where oil usage is ~ 1000 ml/hr. Nevala et al. [4] found that the use of MQL in micro milling of aluminum increased tool life by 100 times compared to dry micro milling. Kajaria et al. [41] found that MQL greatly reduced built-up edge and increased tool life significantly compared to dry and conventional flood cooling in micro milling of 316L stainless steel. In micro milling of Ti-6Al-4V, Vazquez et al. [42] found that, in comparison to conventional flood cooling, MQL yielded less tool wear, more accurate cuts, and less burr. They noted that the momentum of the coolant flow in conventional flood cooling caused the tool to vibrate. It was also suspected that, in flood cooling, the coolant was unable to penetrate the tool-workpiece interface. Vazquez et al. [43] also developed a computational fluid dynamics (CFD) model, which showed conventional flood cooling had much higher entropy and was, therefore, less likely to reach the tool-workpiece interface. The model, however, showed that the lubricant in MQL was able to easily penetrate the tool-workpiece interface and create a lubricant boundary layer. Ming et al. [44] created a CFD model to optimize the MQL parameters. It was found that optimal settings yielded the smallest oil droplet size, which can more easily penetrate through gaps, create a boundary lubricant film at the tool-workpiece interface. The droplet size was most dependent on the air flow rate. The higher the air flow rate, the smaller the droplet size. Li and Chou [45] experimentally found that higher air flow rates in MQL reduced tool wear, as shown in Figure 2.8.

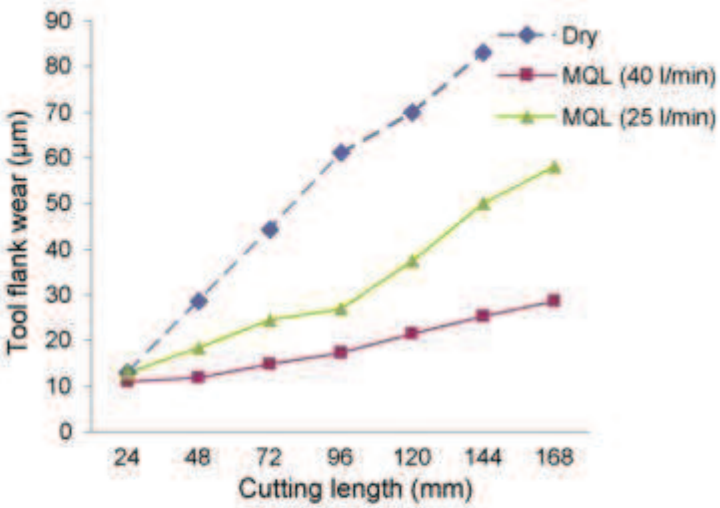

Figure 2.8: Tool wear progression in micro milling of SKD 61 steel at different air flow rates in MQL (spindle speed = 30,000 rpm, feed = 1 µm/rev and oil flow rate = 7.5 ml/h) [45].

### 2.2.4 Vortex tube cooling

Ranque-Hilsch vortex tubes and other forms of air cooling methods are also used to assist the cutting process with the goal of reducing tool wear and improving machinability. An example of a commercial vortex tube is shown in Figure 2.9.

Figure 2.9: Vortex Tube example (Cold Air Gun by Vortec Inc.).

Vortex tubes take in compressed air and make use of the Ranque-Hilsch phenomenon to direct a flow of cold air to the tool-workpiece interface [5] [6], as shown schematically in Figure 2.10.

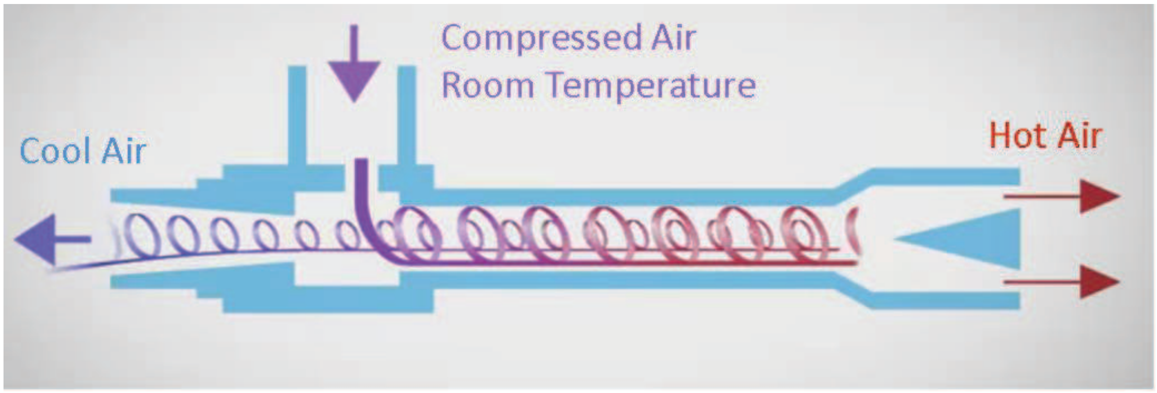

Figure 2.10: Vortex Tube schematic (Vortec Inc.).

Yalcin et al. [46] found that vortex tube cooling was able to reduce tool wear and built-up edge by almost as much as flood cooling in conventional scale machining of AISI

1050 steel. The surface roughness was also found to improve compared to dry cutting. Liu and Chou [47, 48], through modeling and experimentation, tried to determine the optimal vortex cooling parameters for conventional scale turning of Aluminum 390. Their results showed that there is a trade-off between the effects of air flow rate and air temperature. Less tool wear was observed at lower air flow rates and at lower air temperatures than at higher flow rates and at warmer air temperatures. Su et al. [49] used a cold air refrigeration method very similar to vortex cooling in macroscale milling of D2 tool steel. They found that cold air reduced tool wear as effectively as MQL. However, in micro milling of aluminum, Neevala et al. [4] found that vortex cooling was much less effective than MQL in improving tool life. Their work is the only one aimed at investigating the use of vortex cooling in micro milling.

### 2.2.5 Laser assisted micro milling (LAMM)

Another machinability enhancement method is laser assisted micro milling (LAMM). As shown in Figure 1.5, in this process a laser is focused in front of the tool's path of travel to preheat and thermally soften the workpiece, thereby lowering the cutting forces and subjecting the end mill to less wear.

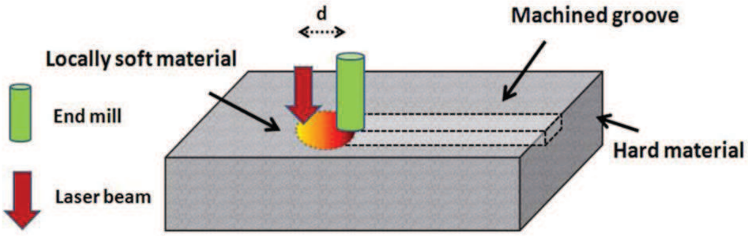

Figure 2.11: LAMM schematic [7].

The use of laser heating to enhance machinability has been researched thoroughly at the conventional or macroscale, where it is often termed Laser Assisted Machining (LAM) [50-54]. At the microscale, however, there is very little work on methods to enhance tool life and micromachinability in LAMM. Table 2.1 summarizes all known published work on LAMM.

Table 2.1: Summary of Literature on LAMM.

| Workpiece | Variables | Measurements | Control comparison |
|---|---|---|---|
| Ti6Al4V [55] | Feed, speed | Force, tool wear | Dry |
| Inconel 718 [56] | Feed, speed, depth of cut | Force, tool wear | Dry |
| Ti6Al4V, Inconel 718, AISI 422 [57] | Laser location, power | Force, wear, groove condition | Dry |
| Ti6Al4V, AISI 316, AISI 422 [58, 59] | Feed, speed, depth of cut, laser power | Acoustic emission, roughness | Dry |
| Al 6061, AISI 1018 [60] | Laser power | Force, roughness, burr | Dry |
| Al 6061, AISI 1018 [61] | Laser power | Specific energy | Dry |
| AISI 4340 [62] | Feed, speed | Force, burr | Dry |
| AISI A2 [63] | Tool coating | Tool wear | Dry |
| AISI A2 [64] | Feed, depth of cut | Force, tool wear, groove profile, roughness, burr | Dry |
| 52100 steel [65] | Feed, laser power | Force | Dry |

Mohid et al. [55, 56] showed that LAMM lowered the cutting forces and tool wear but increased chip adhesion and built-up edge when cutting Ti-6Al-4V. Ding et al. [57] found that LAMM reduced the wear rate significantly and was more effective when preheating the top surface than the side of the workpiece. Shelton et al. [58, 59] found that LAMM reduced the surface roughness and acoustic emission when micromachining 316 stainless steel. Pfefferkorn et al. [60-62] found that LAMM lowered the specific cutting energies and allowed for a higher feed rate (chipload), as shown in Figure 2.12. However, LAMM increased the burr size and surface roughness.

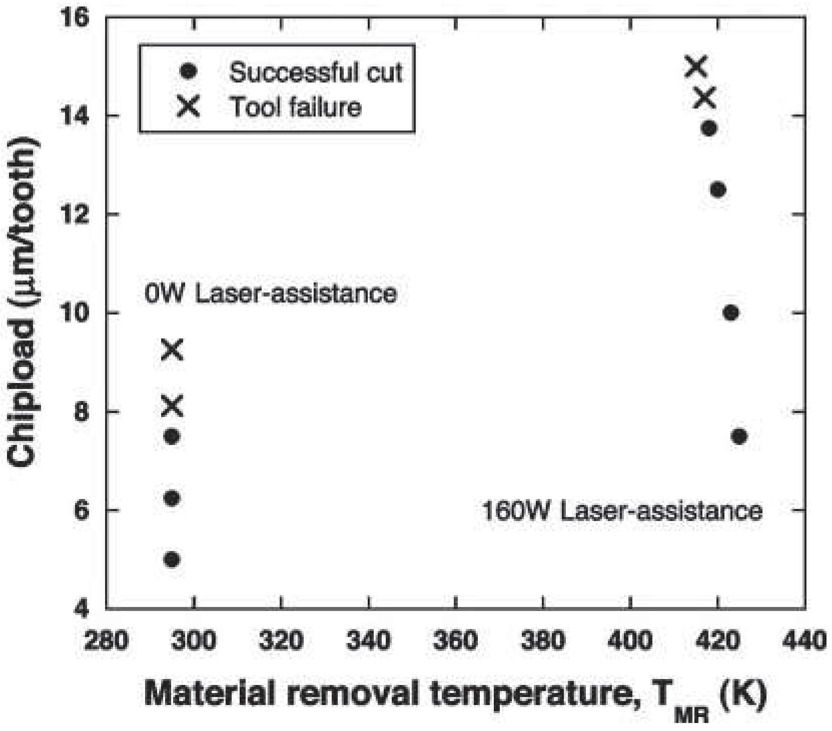

Figure 2.12: Chipload as a function of material removal temperature in laser assisted micro milling of Al 6061-T6 [60].

Other studies of LAMM [7, 63-65] found that the process yielded significant reductions in the cutting force, higher material removal rates, and improvements in tool life when cutting 62 $HR_c$ tool steel. As seen in Figure 2.13, without laser assist the TiAlN coated carbide tool has chipped significantly. However, with laser assist negligible rounding of the tool corner is evident after cutting through 203.2 mm of A2 tool steel [64].

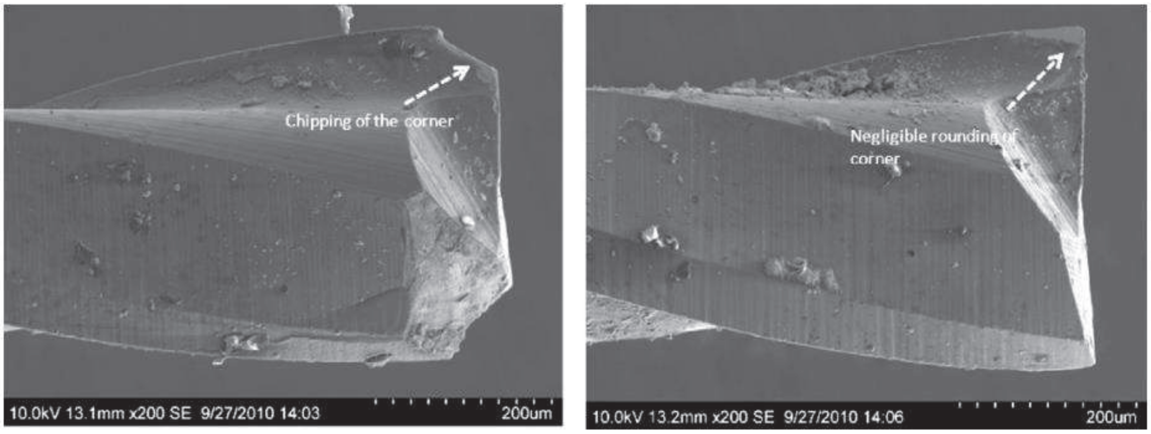

Figure 2.13: SEM images of 400 µm diam. tools after cutting 203.2 mm without (left) and with (right) laser assist (feed: 4.4 µm/flute, axial depth: 55 µm) [64].

As can be shown in Table 2.1, all studies on LAMM have only used dry cutting as the control process for purposes of comparison. Studies comparing LAMM with wet assist are lacking.

### 2.2.6 Combined processes

While MQL, vortex cooling, and laser heating have been used to improve machinability, very few studies have investigated the combined effects of laser assist, and cooling and/or lubrication methods simultaneously. Wang et al. [66] combined plasma enhanced machining (PEM) and cryogenic cooling to thermally soften the workpiece and to cool the tool, respectively, in macroscale turning of Inconel 718. Tool life in the combined process was found to increase significantly in comparison to PEM alone. Similarly, in macroscale turning of Ti-6Al-4V, Dandekar et al. [54] combined LAM with cryogenic cooling and found that tool life in the combined process increased significantly compared to LAM alone, as shown in Figure 2.14.

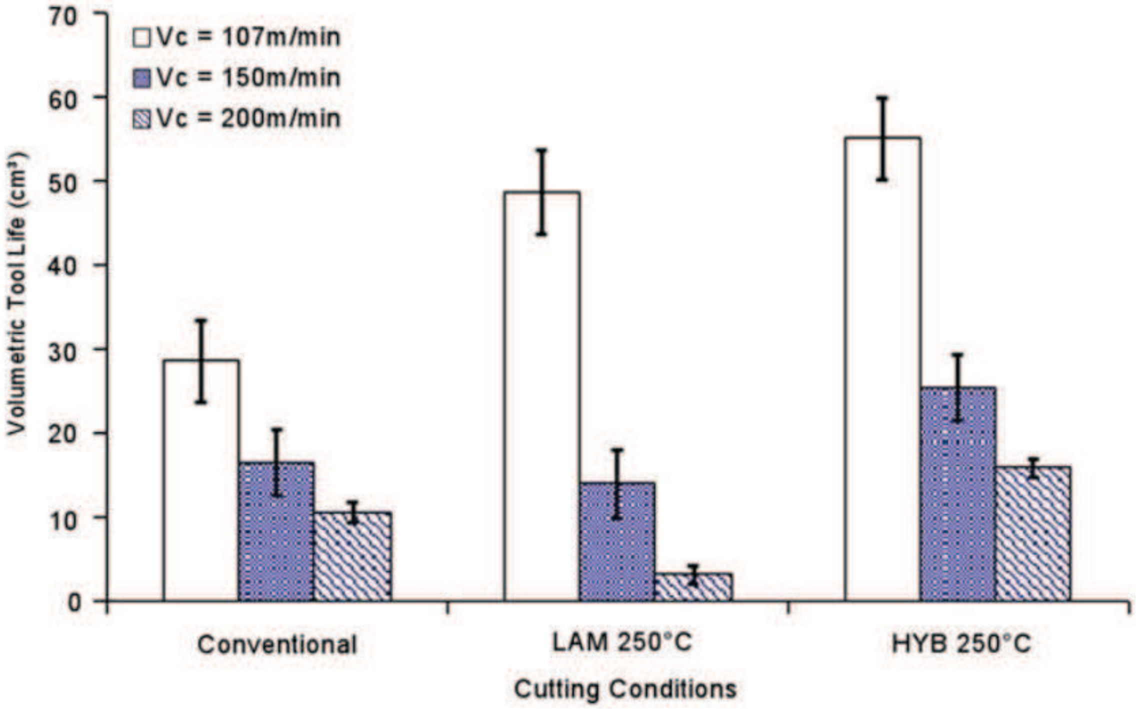

Figure 2.14: Comparison of tool life at various cutting speeds, feed of 0.075 mm/rev, and a depth of cut of 0.76 mm in laser assisted micro milling of Ti-6Al-4V [54].

Bermingham et al. [53] found that the use of laser heating in macroscale milling of Ti-6Al-4V was detrimental to tool life when compared to dry milling. As in previous studies, LAM tended to increase adhesion and built-up edge leading to accelerated tool notch wear. On the other hand, by combining LAM with MQL, tool life was greatly increased. It was however also shown that at low cutting speeds MQL alone was just as effective as the combined process. This showed that MQL was the dominant assist method in the combined process. Tool wear results for the combined process are shown in Figure 2.15.

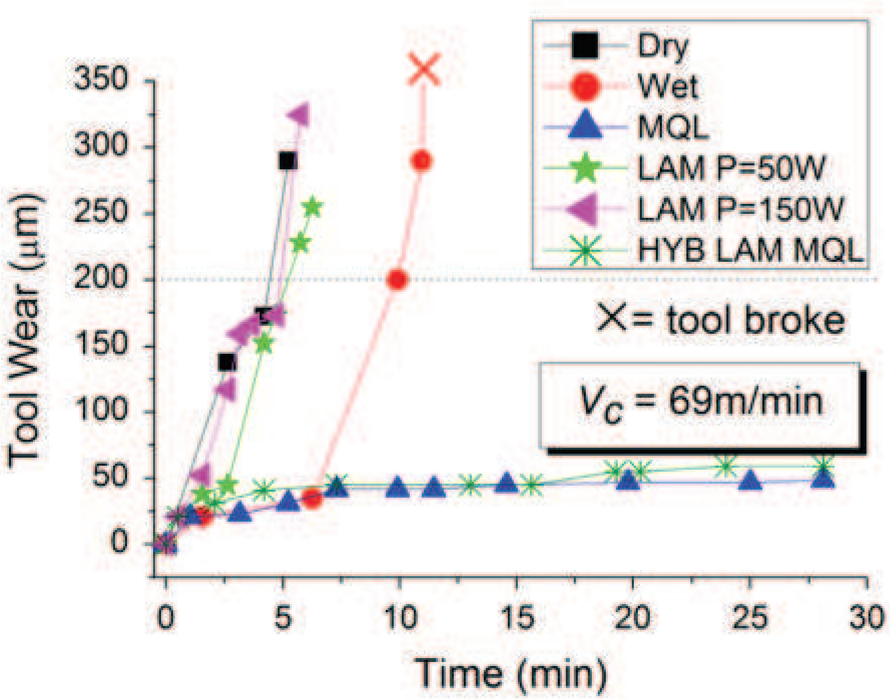

Figure 2.15: Flank wear for various combined assist methods in macroscale machining of Ti-6Al-4V [53].

Their work is the only work to combine laser assist and MQL at the macroscale. However work combining laser assist and MQL at the microscale is lacking. In addition, no work has been reported on the combined effect of laser assist and cooling and lubrication methods such as MQL and vortex cooling in micro milling of difficult-to-cut metals.

## 2.3 Motivation for this thesis

A thorough literature review on micro milling and assistive heating, cooling and/or lubrication methods to enhance micromachinability was completed. There is, however, insufficient knowledge of micro milling of difficult-to-machine materials such as high nickel content steels. For instance, there are no reported studies of laser assisted micro milling of A-286 steel, a material of interest in this thesis, which is widely used in aerospace and gas turbine applications. Current LAMM work presents laser assisted micromachining as a hypothetical alternative to conventional wet techniques, but as seen in Table 2.1, there is no work that compares conventional wet assist methods to LAMM. This thesis (Chapter 4) compares the micromachinability of dry, wet, and LAMM in micro milling of a difficult-to-cut high nickel content steel (A-286) used in aerospace applications.

In addition, as noted earlier, there is no prior work that compares the relative effects of MQL and vortex cooling on micromachinability in LAMM. Therefore, this thesis (Chapter 6) investigates the effects of MQL and vortex cooling on micromachinability in laser assisted micro milling of a difficult-to-cut high nickel content steel (A-286) used in aerospace applications. Specifically, the effects of MQL and vortex cooling on various aspects of micromachinability of A-286 steel such as the machined surface condition, burr formation, tool condition including wear and built-up edge, dimensional accuracy of the cut grooves, surface finish, and cutting forces are evaluated. The performance of LAMM+MQL and LAMM+Vortex cooling are also compared with dry cutting and LAMM.

## 2.4 Summary

This chapter reviewed prior research on micro milling and several heating, cooling and/or lubrication methods used to improve micromachinability. This chapter also described where research was lacking. Specifically, there is no work that systematically compares the micromachinability of conventional wet assist methods to LAMM. In addition, there is no work that investigates the benefits and limitations of combining MQL with LAMM and vortex cooling with LAMM in micro milling of difficult-to-cut metals.

The remainder of the thesis describes experimental work aimed at addressing the aforementioned lack of knowledge.

# CHAPTER 3: EXPERIMENTAL DESIGN AND SETUP

## 3.1 Introduction

It is well-known that difficult-to-cut materials such as A-286 alloyed steel undergo thermal softening, which makes them easier to cut [67]. The tensile yield strength, $F_{ty}$, and the ultimate strength, $F_{tu}$, of A-286 as a function of temperature are shown in Figure A.1. Proper design of the LAMM experiments (e.g. selection of laser and cutting parameters) to cut a difficult-to-cut material such as A-286 requires an understanding of the temperature rise in the workpiece material due to laser irradiation. Consequently, this chapter seeks to model and understand the influence of different laser and machining parameters on the temperature rise in A-286 steel. Previously developed thermomechanical models for LAMM were employed to analyze the workpiece temperature rise due to laser irradiation and due to plastic deformation during cutting. The laser power, spot size, and the laser-tool distance between centers of the laser spot and the cutting tool were established from the model-based analysis. In addition, this chapter describes the physical design of the LAMM experimental setup, the properties of the A-286 workpiece material, and the cutting tools used throughout this thesis.

## 3.2 Thermal analysis

### 3.2.1 Temperature rise due to laser heating

To understand how different laser parameters affect temperature rise in the workpiece material, a thermal analysis of the temperature rise due to laser irradiation was conducted using previously developed thermo-mechanical models of the LAMM process

[7, 65]. The thermal model accounted for the laser parameters such as laser power, spot size, scan speed, and the laser-tool distance between the centers of the laser spot and tool. The thermal model provides the *in situ* temperature distribution, $T(x,y,z)$, in the workpiece due to laser heating. Special attention was given to the temperature rise in the workpiece at the moment it comes into contact with the tool. Figure 3.1 shows a schematic of the laser and tool configuration assumed in the model. A laser spot size of diameter, $d_s$, is focused in front of the tool at a center-to-center laser-tool distance, $d$. The temperature distribution, $T(x,y,z)$, along the leading edge of the tool, represented by arc $AB$, is of interest since the workpiece material in this region first sees the cutting tool.

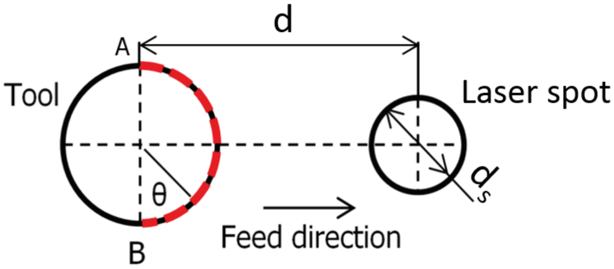

Figure 3.1: Tool and laser configuration during LAMM experiments. The highlighted portion (red) of the tool periphery represents the region of interest in the thermal analysis.

The analytical model used to calculate the temperature distribution $T(x,y,z)$ along $AB$ is based on Jaeger's model [68] of a moving heat source acting on a semi-infinite body, as given below:

$$T(x,y,z) = \alpha \int\int \frac{q(x',y')}{2\pi K s} e^{\frac{-U}{2\kappa}(s-(x-x'))} dx'dy' \tag{3.1}$$

$$s = \sqrt{(x-x')^2 + (y-y')^2 + z^2}. \tag{3.2}$$

Where $\alpha$ is the laser absorptivity, $q$ is the heat intensity (W/m$^2$), $K$ is the thermal conductivity (W/m·K), $\kappa$ is the thermal diffusivity (m$^2$/s), and $U$ is the heat source velocity (m/s). The thermal diffusivity (m$^2$/s), $\kappa$, is defined by:

$$\kappa = \frac{K}{\rho C} \tag{3.3}$$

where $\rho$ is the density. The thermal conductivity $K$ and specific heat $C$ for A-286 were modeled as a linear function of temperature as follows [69]:

$$K = 0.0192T + 12.18 \tag{3.4}$$

$$C = 0.6431T + 468.6 \tag{3.5}$$

Due to the temperature dependence of the thermal conductivity and specific heat, the temperature rise due to laser heating was solved iteratively. The laser heating was modeled as a Gaussian distributed heat source characterized by a diameter, $d_s$, of 300 μm as given by the following equation:

$$q(x,y) = q_0 e^{(x^2+y^2)} \tag{3.6}$$

where $q_0$ was the average heat intensity in the center of the laser spot.

The temperature rise along the arc AB was calculated Eqs. 3.1 – 3.6 at 60 angular positions using in each of six evenly spaced axial planes along the axial depth of cut as shown schematically in Figure 3.2. Since no significant temperature variation was seen along the six planes in the Z direction, the temperatures corresponding to the same angular position in the six planes were averaged.

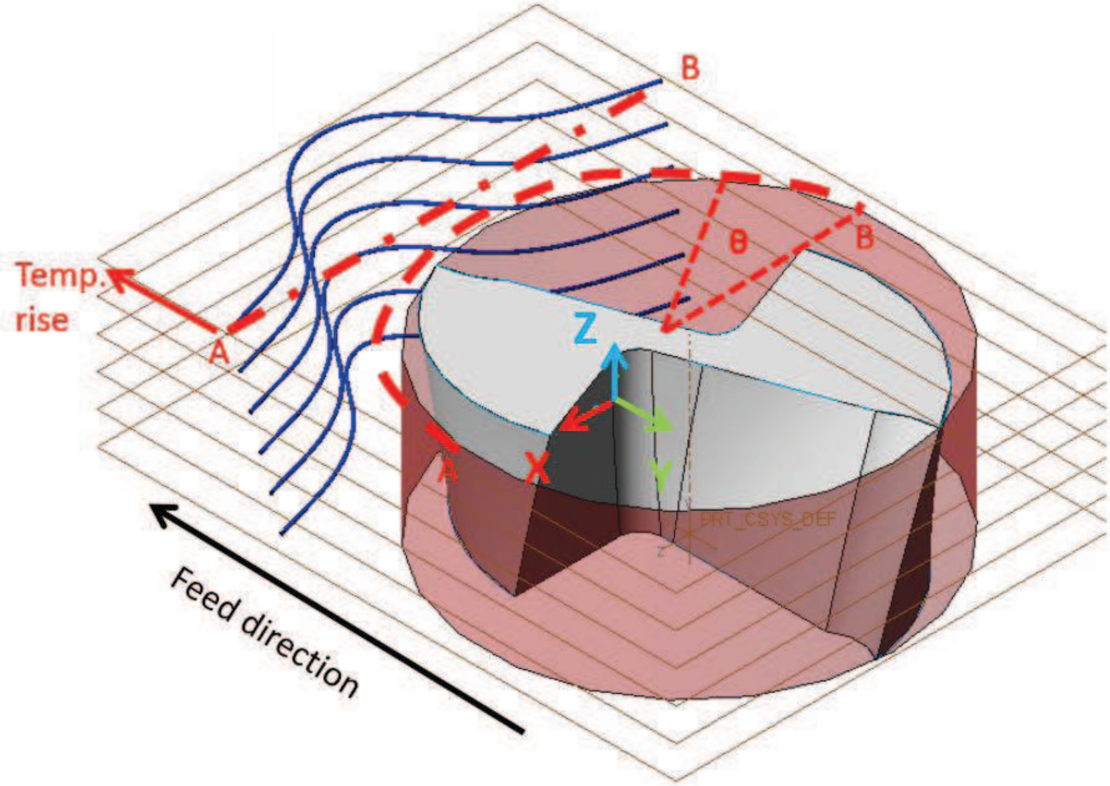

Figure 3.2: Temperature distribution on the leading edge of the tool.

The laser parameters were selected to maximize the temperature rise along arc *AB* but without reaching the oxidation temperature of the tool coating (600°C). Machining parameters such as cutting speed, feed, and depth of cut were chosen from a survey of other micro milling literature [8, 29, 56]. Cutting speeds, feed, and depth of cut were varied and were seen to have a minimal effect on the temperature rise. For example, the feed, which determines $U$, showed a minimal effect on the temperature rise over the ranges examined, seen in Figure 3.3. As expected, the temperature rise was observed to increase with reduction in the laser-tool distance, $d$. The laser power, which determines $q_0$, had the most significant effect on the temperature distribution as shown in Figure 3.5.

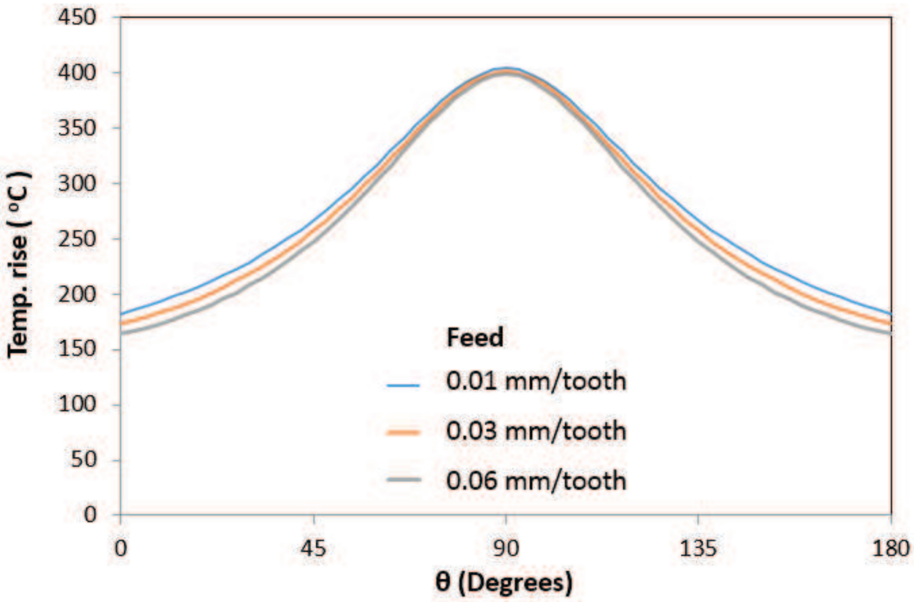

| Cutting speed | Depth of cut | Spot size | Laser-tool distance | Laser power |
|---|---|---|---|---|
| 19 m/min | 0.02 mm | 300 µm | 450 µm | 20 W |

Figure 3.3: Effect of feed on the mean temperature rise along AB.

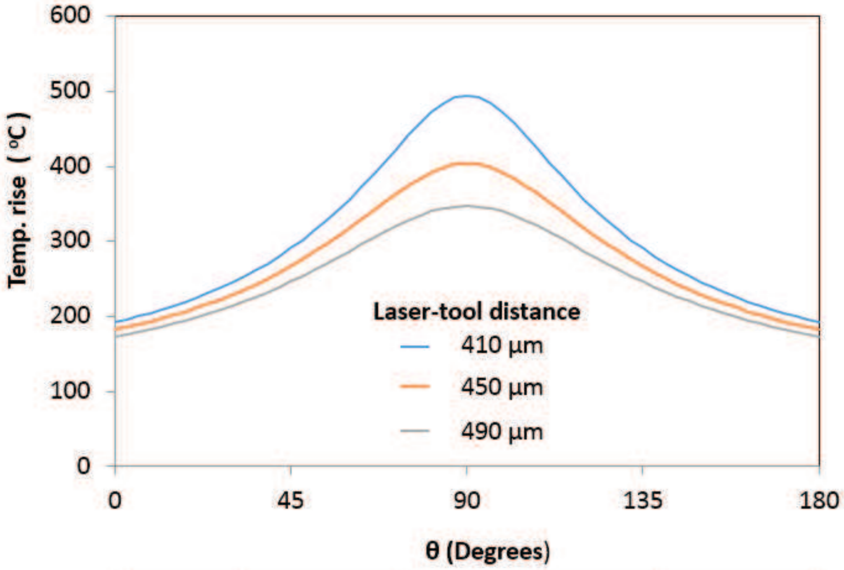

| Cutting speed | Feed | Depth of cut | Spot size | Laser power |
|---|---|---|---|---|
| 19 m/min | 0.01 mm/tooth | 0.02 mm | 300 µm | 20 W |

Figure 3.4: Effect of laser-tool distance on the mean temperature rise along AB.

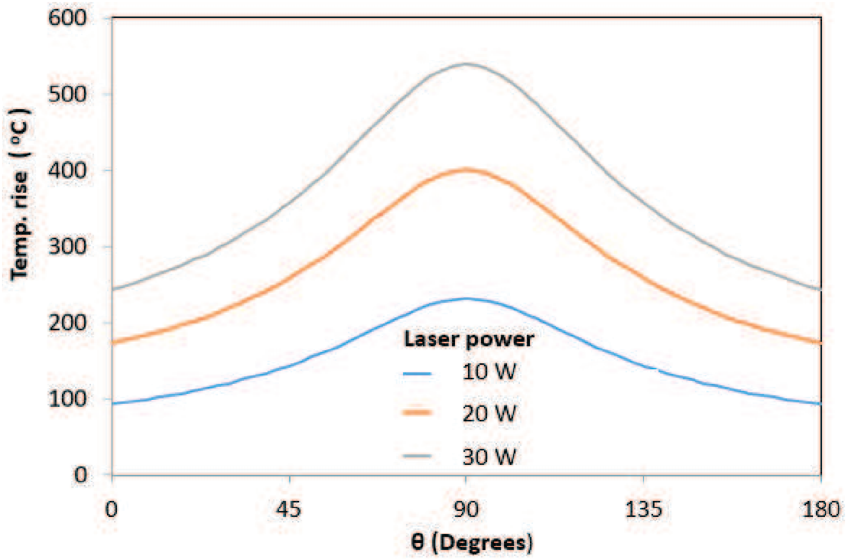

| Cutting speed | Feed | Depth of cut | Spot size | Laser-tool distance |
|---|---|---|---|---|
| 19 m/min | 0.01 mm/tooth | 0.02 mm | 300 µm | 450 µm |

Figure 3.5: Effect of laser power on the mean temperature rise along AB.

Based on the above model simulations, it was decided to use laser powers of 12 W and 18 W in the LAMM experiments presented in the next chapter. The laser-tool distance between the centers of the laser spot and tool was set to 450 µm and the laser spot size was fixed at 300 µm.

### 3.2.2 Temperature rise due to plastic deformation

Loewen and Shaw's model [70] was used to model the temperature rise at the tool surface due to plastic deformation of the material during the cutting process. Assuming an orthogonal cutting process at each point of the cut periphery, the temperature rise due to shear was calculated using the following equations:

$$\theta_s = \frac{R_1 u_s}{C\rho J} + \theta_0 \tag{3.6}$$

$$R_1 = \frac{1}{1 + 1.328\left[\frac{\kappa\gamma}{V_c t}\right]^{0.5}} \tag{3.7}$$

$$u_s = k_0 \gamma \tag{3.8}$$

$$\gamma = \cot(\phi_0) + \tan(\phi_0 - \alpha_r) \tag{3.9}$$

$$k_0 = \frac{F_{ty}}{\sqrt{3}} \tag{3.10}$$

Where:

$R_1$ - fraction of heat conducted into the chip,

$\kappa$ - thermal diffusivity,

$\gamma$ - shear strain,

$V_c$ - cutting speed (19 m/s)

$t$ - instantaneous uncut chip thickness (0.01mm)

$u_s$ - specific cutting energy,

$k_0$ - shear yield stress,

$\phi_0$ - shear angle [71],

$J$ - mechanical equivalent of heat (4.18 Nm/Js$^2$),

$\alpha_r$ - radial rake angle (0.070 radians)

The temperature rise due to plastic deformation when cutting dry and without laser assist are shown in Figure 3.6. During dry micro milling, the maximum temperature rise due to plastic deformation was almost 160 °C at the midpoint of the tool periphery. With laser assist, the temperature rise due to plastic deformation was drastically reduced to around 60 °C. This drastic decrease was due to thermal softening of A-286, which enables it to shear at a substantially lower stress. As shown by Kumar et al. [65] and seen in Figure 3.6, the maximum plastic deformation induced temperature rise in LAMM is not at $\theta = 90°$. This is because of increased thermal softening of the material at $\theta = 90°$ due to the maximum temperature rise at that location produced by the Gaussian distributed laser heat source.

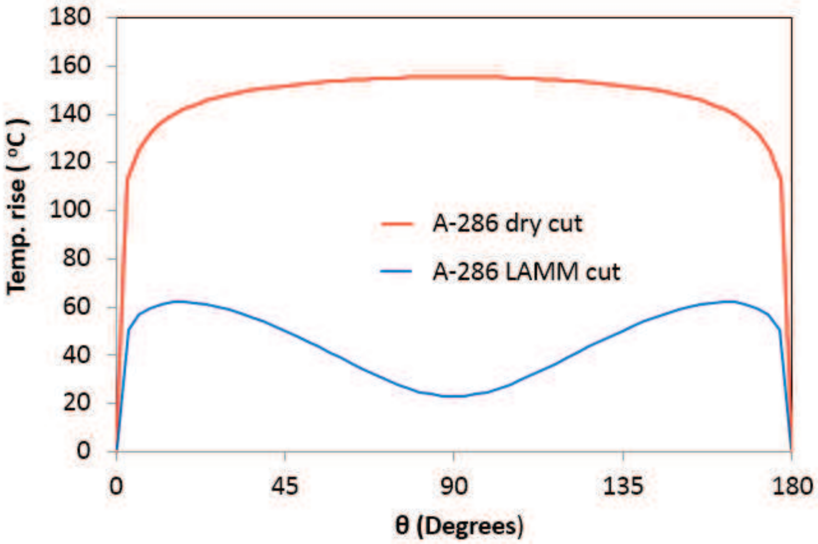

| Cutting speed | Feed | Depth of cut | Spot size | Laser-tool distance | Laser power |
|---|---|---|---|---|---|
| 19 m/min | 0.01 mm/tooth | 0.02 mm | 300 µm | 450 µm | 18 W |

Figure 3.6: Temperature rise due to plastic deformation during dry micro milling and LAMM.

A decrease in temperature rise due to plastic deformation implies that material is being removed with less mechanical energy input by the tool, thereby reducing tool stresses. The result in Figure 3.6 indirectly validates that LAMM reduces the mechanical energy input by the tool when laser parameters are set to a spot size of 300 µm, a laser-tool distance of 450 µm, and a power of 18W.

## 3.3 Experimental setup and procedure

### 3.3.1 LAMM setup

The LAMM setup shown in Figure 3.7 was used to conduct the experiments described in Chapters 4 and 5.

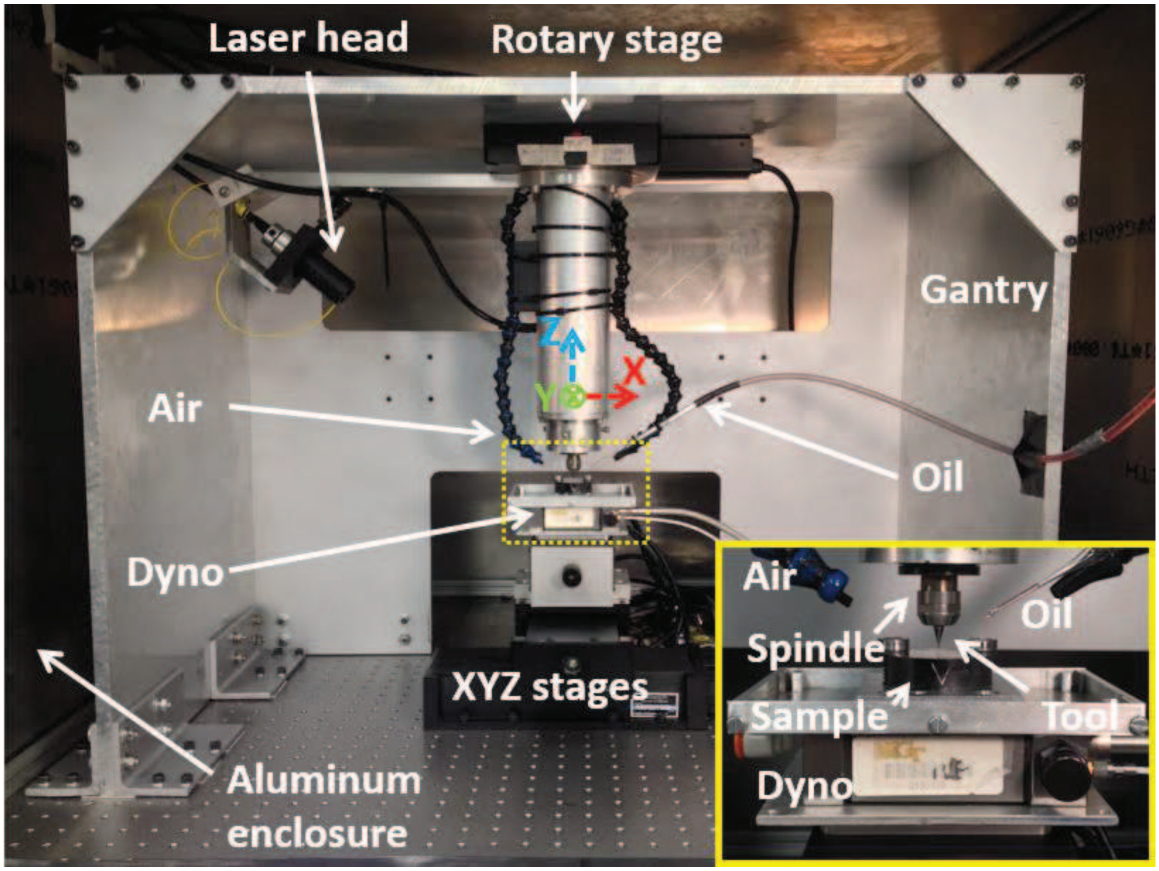

Figure 3.7: Experimental setup.

The laser head was mounted on a rotary stage fixed to the top of the gantry structure, and it enables the laser beam to rotate 360° around the Z-axis. A Ytterbium-doped continuous wave fiber laser (IPG Photonics – YLM 30) with a Gaussian beam and a near infra-red nominal wavelength of 1070 nm was focused down to a 300 μm diameter spot size located in front of the tool at center-to-center laser-tool distance of 450 μm. The tool cutting speed was derived from a variable high-speed electric spindle with a maximum spindle speed of 60,000 revolutions per minute (rpm). Three stacked linear motion ball screw stages (Aerotech ATS-125 and AVS-105) were fixed to an anti-vibration table and provided the workpiece feed motions. A piezoelectric force dynamometer (Kistler Minidyne® 9256C2) was mounted on the stacked stages. In order to detect tool-workpiece contact, a uniaxial accelerometer (Kistler Model 8636C50, ±50g range, 6KHz frequency range) was attached to the side of the dynamometer [72]. The workpiece was fixtured to the dynamometer. For wet assist experiments presented in Chapter 4, flood cooling with oil (Hangsterfer's Hard Cut NG cutting oil) was gravity fed at a flow rate of 12 ml/min and was directed to the cutting zone with a glass pipette. Air flow at a pressure of 0.3 MPa was directed at the tool to blow chips and excess oil away from the tool.

The LAMM setup was modified to include MQL and vortex cooling to conduct the experiments described in Chapter 6, as shown in Figure 3.8.

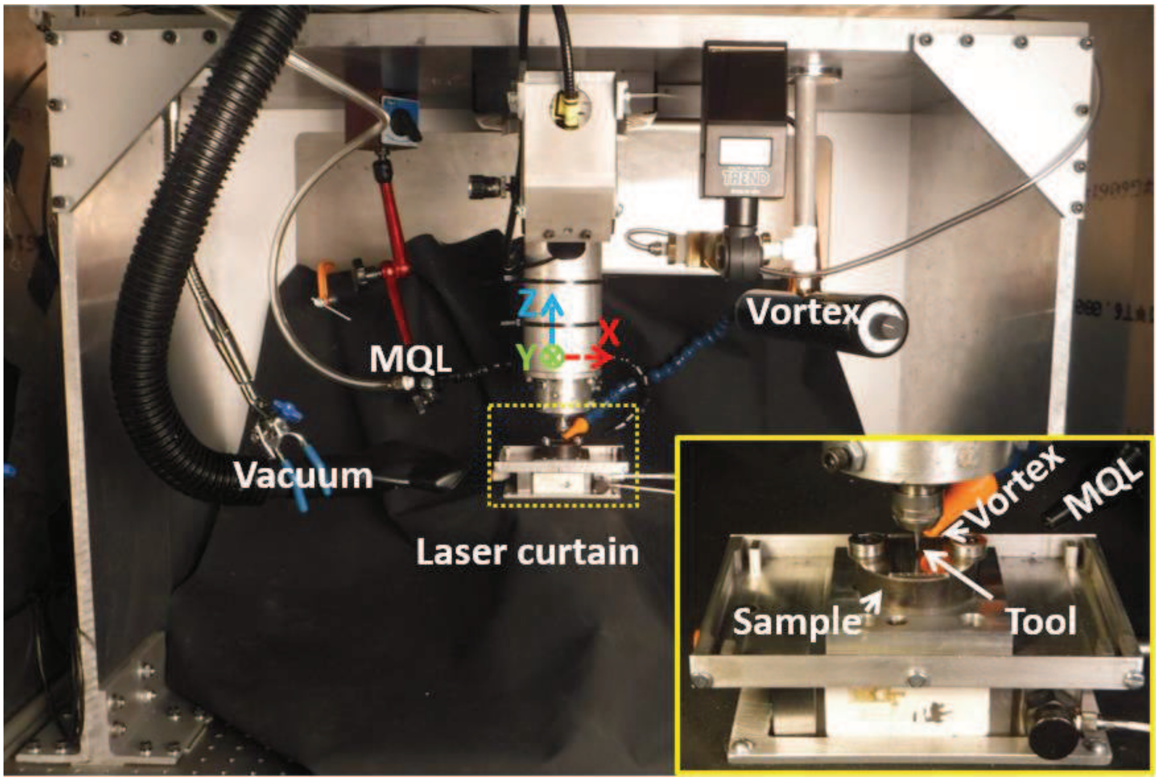

Figure 3.8: Modified experimental setup including MQL and vortex cooling systems.

An MQL system (UNIST Coolubricator) was incorporated into the LAMM setup for use in the MQL only and LAMM + MQL experiments presented in later chapters. The

MQL system outputs an atomized mixture of compressed air and oil (Coollube 2210EP) through a nozzle. A vortex tube system (Vortec 610 Cold Air Gun) was fixed to the top of the gantry for use in the vortex cooling and LAMM + Vortex cooling experiments presented in later chapters. The vortex tube takes in compressed air and outputs cold air through a nozzle.

### 3.3.2 Workpiece and tool material

The workpiece material used in the experiments was a cold reduced round bar of precipitation hardened A-286 (41.8 ± 0.6 $HR_c$), commonly used in the production of aerospace parts. Precipitation hardening was preformed by heating samples at 720 °C for 16 hours and air cooling afterwards. A-286 is a high nickel content steel alloy with high tensile strength (1455 MPa), good corrosion resistance (oxidation resistance up to 700 ºC), and good high temperature creep resistance . It is composed of (by wt%) 56.8% Fe, 24.5% Ni, 14.1% Cr, 2.2% Ti, and small traces of other metals. The presence of abrasive hard carbide phases in the steel make it difficult-to-machine, particularly at the microscale where ploughing is prevalent and is, therefore, an ideal material for LAMM. The cutting tools used in all experiments were 500 μm diameter, two flute, square end, TiAlN coated tungsten carbide end mills (Mitsubishi MStar MS2SSD0050).

## 3.4 Summary

In this chapter, analytical thermal and thermo-mechanical models were used to understand the influence of different laser and machining parameters on the temperature rise in the workpiece. Based on the analysis, the laser parameters such as laser power, laser spot size, and laser spot to tool distance were established. In addition, this chapter presented details of the experimental setup and the workpiece material (A-286) used in this thesis.

# CHAPTER 4: COMPARISON OF DRY CUTTING, WET ASSIST, AND LAMM

## 4.1 Introduction

Machinability of high nickel content steels (e.g. stainless) is known to be challenging. This chapter presents an experimental study of the micro-machinability of A-286 (42.8 $HR_c$), a precipitation-hardened high nickel content steel. Micro milling experiments are carried out under dry, wet, and laser assisted conditions, and the resulting surface morphology, burrs, part feature depth, tool wear, and cutting forces are analyzed. It is found that laser-assist consistently yields the best results characterized by minimal chip adhesion to the workpiece surface, low cutting forces, good feature depth accuracy, low tool wear, and acceptable burrs.

## 4.2 Experimental setup and procedure

### 4.2.1 Experiment design

The A-286 nickel base alloy (composed by weight of 56.8% Fe, 24.5% Ni, 14.1% Cr, 2.2% Ti, and small traces of other metals) was obtained as a cold reduced round bar, and precipitation age hardened to $42.8 \pm 0.2$ $HR_c$. The tools used were square end, tungsten carbide, two flute, 500μm diameter, and TiAlN coated end mills (Mitsubishi MS2SSD0050). A new tool was used for each test. The tool path in each test consisted of six parallel 25.4 mm long grooves created on a pre-machined workpiece surface for a total cutting length of 152.4 mm, as shown in Figure 4.1.

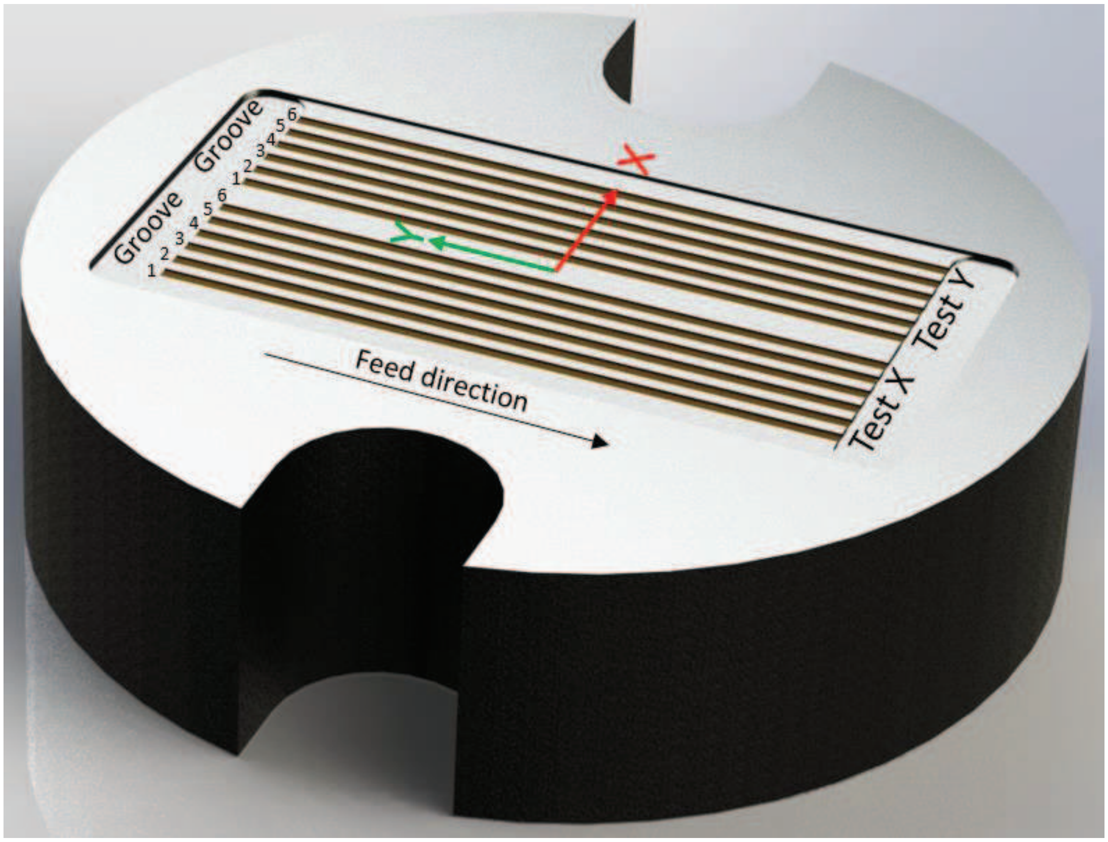

Figure 4.1: Workpiece geometry and tool path.

The cutting parameters used in the experiments are listed in Table 4.1 and were chosen from a survey of other micro milling literature [8, 29, 56]. The eight cutting conditions were applied to each of the four assist mechanisms: dry, wet, and two LAMM cases, yielding a total of 32 tests.

Table 4.1: Machining conditions.

| **Condition** | **Cutting speed (m/min)** | **Feed (mm/tooth)** | **Depth of cut (mm)** |
|---|---|---|---|
| | $V_c$ | $f_t$ | $a_p$ |
| 1 | 19 | 0.01 | 0.02 |
| **2** | 19 | 0.01 | 0.04 |
| **3** | 19 | 0.03 | 0.02 |
| **4** | 19 | 0.03 | 0.04 |
| **5** | 41 | 0.01 | 0.02 |
| **6** | 41 | 0.01 | 0.04 |
| **7** | 41 | 0.03 | 0.02 |
| **8** | 41 | 0.03 | 0.04 |

Air flow at a pressure of 0.3 MPa was directed at the tool in the dry and LAMM experiments to blow away chips. Wet assist experiments consisted of flood cooling with oil (Hangsterfer's Hard Cut NG cutting oil) applied at 12 ml/min. As discussed in the previous chapter, the laser parameters were chosen by analyzing the theoretical temperature distribution in the workpiece material via a thermal model [63]. The center of the 300 μm diameter laser spot was focused in front of the tool at a laser-tool distance of 450 μm. Two laser powers, 12 W and 18 W, corresponding to peak intensities of 340 W/mm$^2$ and 510 W/mm$^2$, respectively, were used to investigate the effect of laser power on the process.

### 4.2.2 Measurement methods

The grooves produced in the tests were imaged by an optical microscope (Nikon Microphot-FXL) to analyze burr formation, chip adhesion, and surface morphology, as shown in Figure 4.2. Tool condition was also evaluated by optical microscopy, as shown in Figure 4.2. Tool diameter was measured before and after the tests to quantify tool wear, as shown in Figure 4.3.

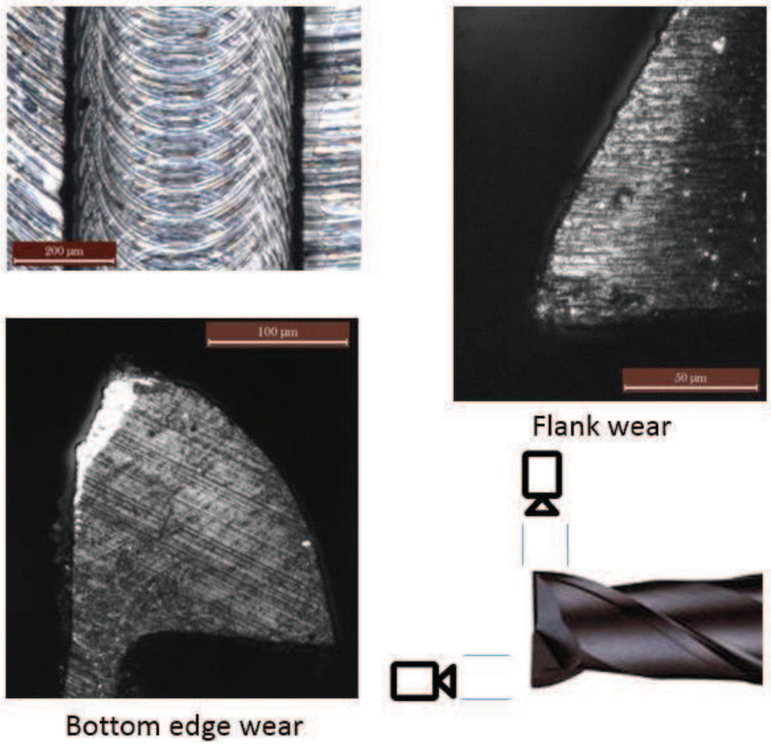

Figure 4.2: Representative images of the groove and of the tool images.

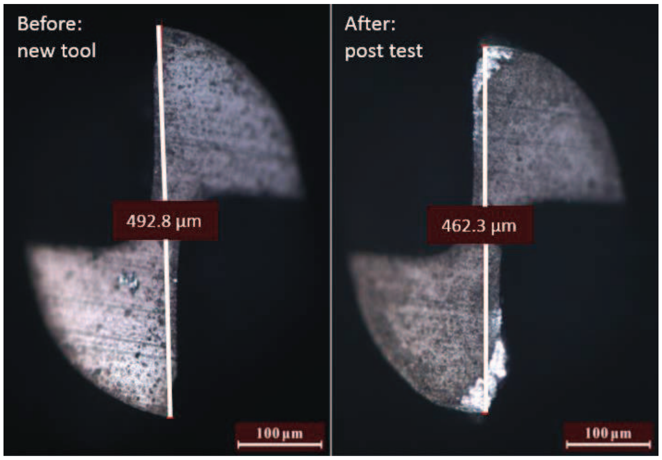

Figure 4.3: Representative tool diameter measurement before and after the test.

A stylus surface profilometer (Taylor Hubson Talysurf) was used to measure the groove cross-sectional profile to evaluate the groove depth, as shown in Figure 4.4. The calculated groove depth is the difference between the average heights of the top and bottom surfaces (denoted by green dots) of each groove evaluated over the data ranges indicated by the red dots.

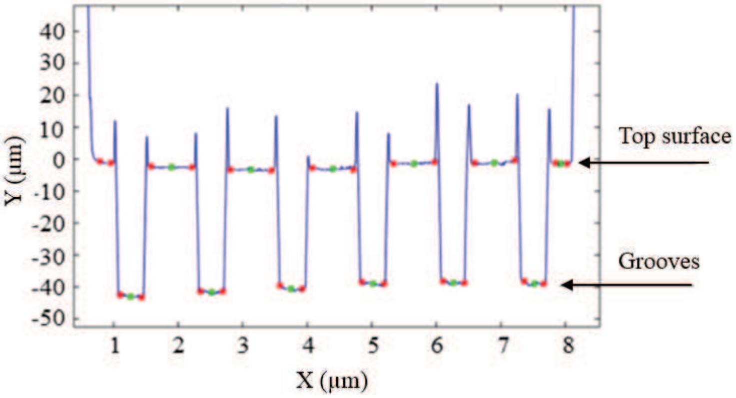

Figure 4.4: Groove depth measurement example.

Finally, the mean resultant forces for the first and last grooves were computed from the dynamometer data.

## 4.3 Results and discussion

### 4.3.1 Groove condition

The first groove in all the tests typically showed little to no burr or surface defects, because the tool was still new. However, by the sixth groove (~150 mm length of cut) the groove condition was affected by the cutting conditions and the assist method, as shown in Figure 4.5.

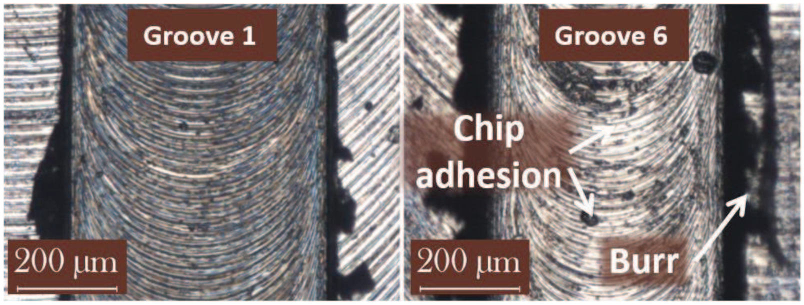

Figure 4.5: Groove 1 and 6 comparison for dry test cutting condition 6 (downward feed direction).

Figure 4.6 shows optical images of the sixth groove for the dry cutting tests for machining conditions 1 through 8. Note that the dry tests at the higher depth of cut (0.04 mm), i.e. conditions 2, 4, 6, and 8, exhibit larger burrs and chip adhesion. For the dry tests at the lower depth of cut (0.02 mm), i.e. conditions 1, 3, 5, and 7, far less burr and chip adhesion was observed.

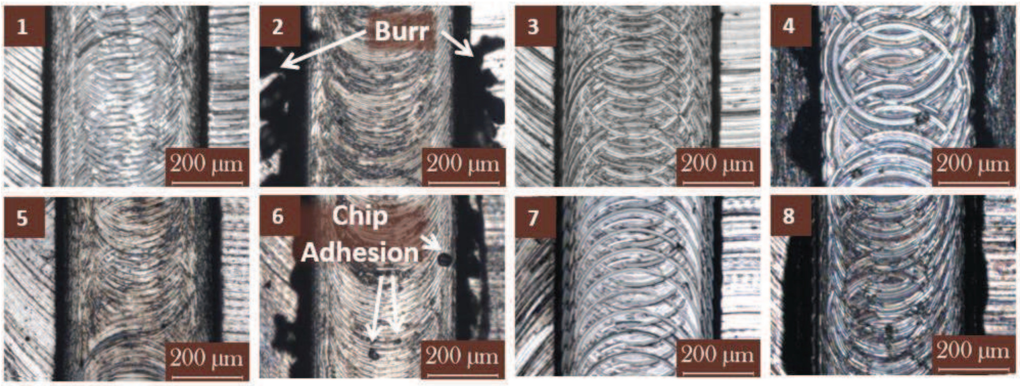

Figure 4.6: Surface morphology and burrs in dry cutting; cutting conditions 1-8 (6th groove shown).

Figure 4.7 compares grooves produced by machining condition 2 for the dry, wet, 12 W and 18 W LAMM cases. As can be seen, there is significantly less burr in the wet test than in the dry test. In addition, compared to the dry case, there is little or no chip adhesion on the groove surface in the wet test. As seen in Figure 4.7, the LAMM tests yielded better quality grooves than the dry and wet tests. Of the four assist methods investigated, the least amount of burr was produced in the 12 W LAMM test. The wet condition, however, had the least chip adhesion. Thicker and more burrs were created in the 18 W LAMM test than the 12 W LAMM test. The 18 W test produced even higher temperatures causing the material to soften even more, which led to more burrs.

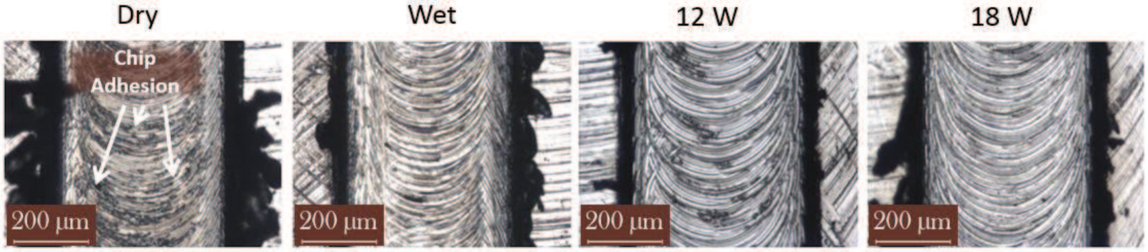

Figure 4.7: Comparison of grooves for dry, wet, 12 W, 18 W; machining condition 2.

Figure 4.8 shows how the groove depth is affected by the four assist mechanisms along the entire length of cut for machining condition 3. As seen from the figure, the 12 W LAMM test was the most accurate while the dry test was the least accurate. In the dry and wet tests, as the tool wore, less material was removed in the axial depth of cut direction. It should be noted that in the LAMM tests, the axial depth of cut is generally higher than the programmed (or target) depth of cut due to the thermal expansion of the workpiece, which can be easily compensated. This is plausible given the thermal expansion coefficient of A-286 (16 μm/m-°C) and the temperature distribution in the workpiece as shown by the thermal model presented in the previous chapter.

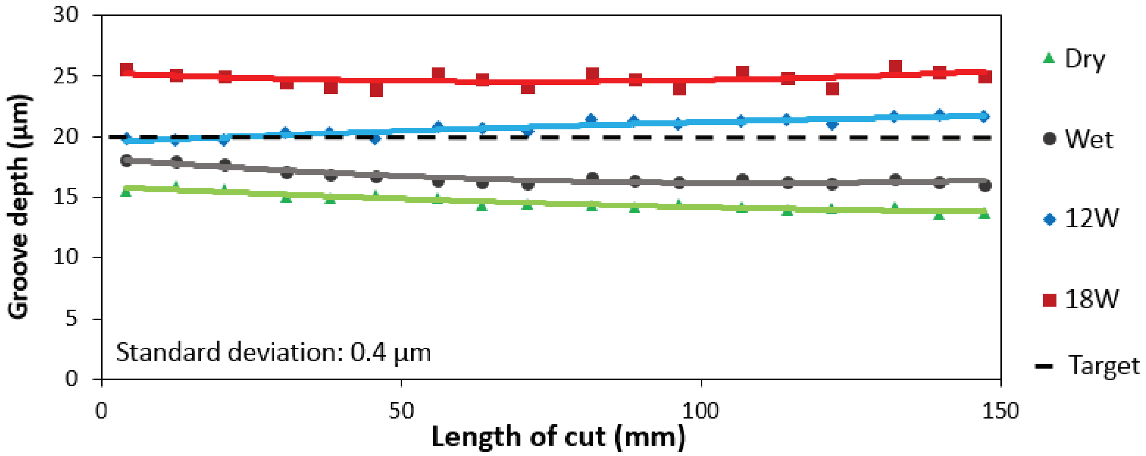

Figure 4.8: Comparison of groove depths for dry, wet, 12 W, 18 W cases; machining condition 3.

## 4.4 Tool condition

Figure 4.9 and Figure 4.10 show representative images of the tool bottom edge wear and tool flank wear, respectively, for the dry test performed under machining conditions 1, 2, 3, and 5. Machining condition 3 had the least amounts of bottom edge wear and flank wear. In condition 1, the tooth chipped. In condition 2 and 5 there was some rounding of the cutting edge and a large amount of flank wear. Machining condition 3 had a larger feed of 0.03 mm/tooth than conditions 1, 2, and 5, which had a feed of 0.01 mm/tooth. The lower wear observed in machining condition 3 can be attributed to the higher feed rate, which improved material removal through shear deformation and reduced the amount of ploughing and rubbing.

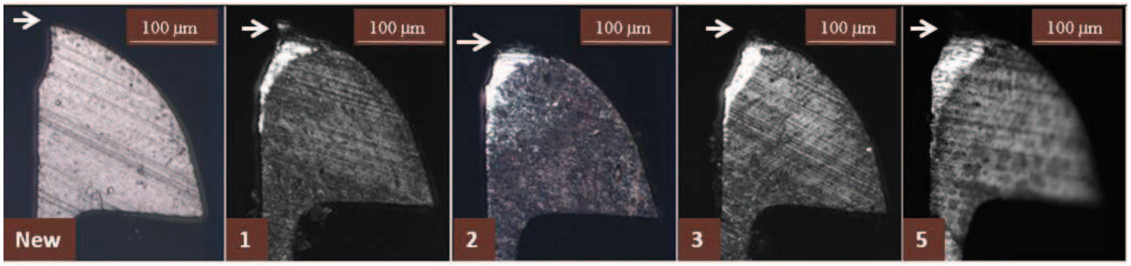

Figure 4.9: Bottom edge wear for dry test under machining conditions 1,2,3, and 5.

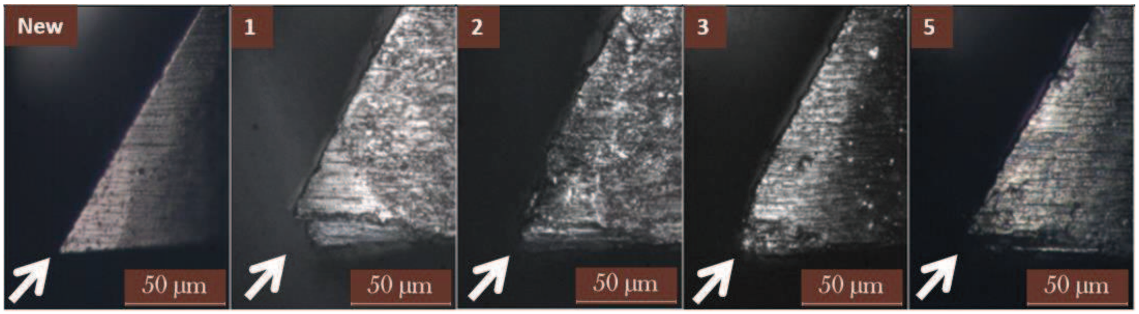

Figure 4.10: Flank wear for dry test under machining conditions 1,2,3, and 5.

Figure 4.11 shows representative images of the tool bottom edge for the tests carried out using machining condition 6. Note that the tool in the dry test exhibits a noticeably rounded tooth profile. The wet assist case showed better preservation of the tooth profile. The 12 W and 18 W LAMM tests preserved the tooth profile very well compared to the dry and wet tests. Some material adhesion to the tool was observed in the 12 W and 18 W LAMM tests.

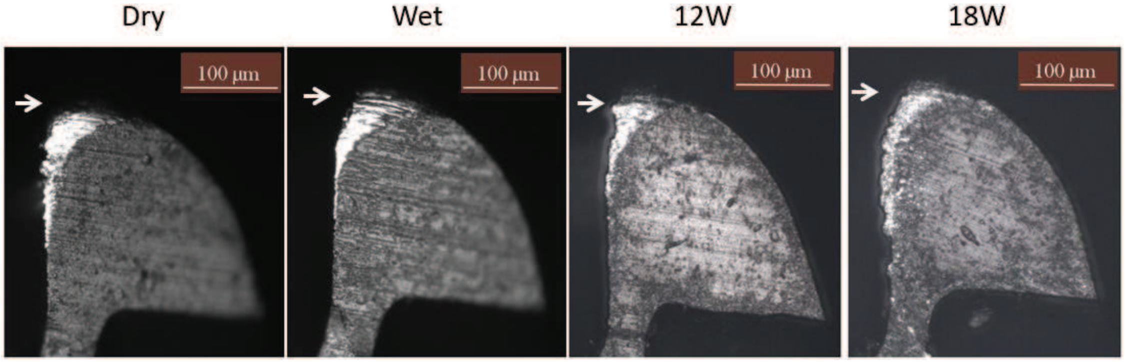

Figure 4.11: Tool bottom edge wear for dry, wet, 12 W, 18 W cases; machining condition 6.

Figure 4.12 shows representative images of the tool flank for the tests conducted using cutting condition 1. Note that while the tool chipped in the dry test, there was no chipping in the wet test, which showed a marginal reduction in flank wear. The flank wear in the 12 W and 18 W LAMM tests is significantly reduced compared to that in the dry and wet tests for the same cutting conditions. As seen in Figure 7, the tool edge is relatively clean and sharp for the 12 W case but shows some flank wear. The 18 W case shows less wear than the 12 W case but shows more material adhesion. It is clear from these results that laser assist helps to reduce tool flank wear.

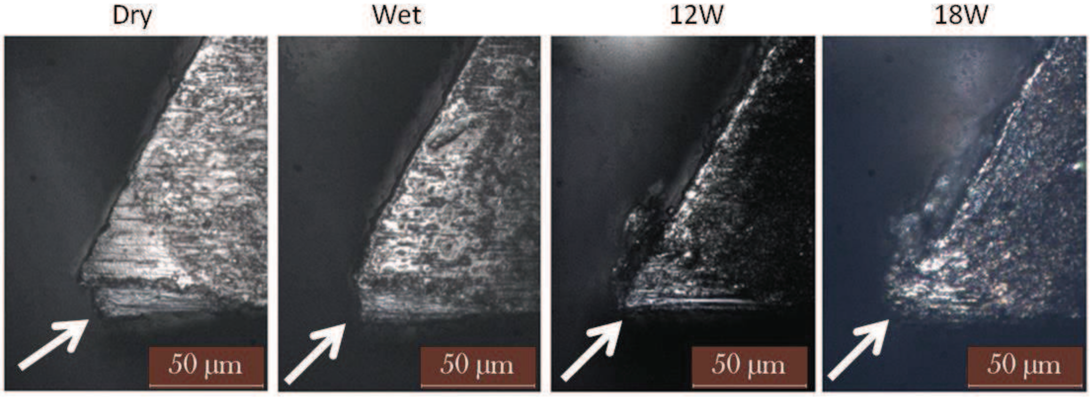

Figure 4.12: Flank wear for dry, wet, 12 W, 18 W cases; machining condition 1.

For each test condition, the tool diameter was measured both when the tool was new and after cutting six grooves. The change in tool diameter due to wear for all 32 tests is shown in Figure 4.13. In the dry tests, cutting conditions 3 and 7, which had a higher feed (0.03 mm/tooth) and a lower depth of cut (0.02 mm), produced the least wear–only 30 and 35 µm, respectively–compared to more than 40 µm wear or chipping observed in all the other tests. The higher feed is thought to have reduced ploughing thereby decreasing tool wear. In the wet tests, marginal improvement in tool wear was seen compared to the dry tests under the same conditions. The change in tool diameter due to wear for the 12 W LAMM case under all cutting conditions was less than in the dry and wet tests. It can be seen in Figure 4.13 that most of the 18 W LAMM tests produced less change in tool diameter than in the 12 W case. The higher laser power produces greater thermal softening of the workpiece, which permits improved shearing of the material. The 18 W LAMM tests, however, did produce more adhesion of the work material to the tool surfaces. Nevertheless, in the majority of the 18 W tests, the benefits of thermal softening appear to outweigh the harm caused by built-up-edge. Compared to dry cutting, the 18 W LAMM case produced, on average, 29% less change in tool diameter. The maximum reduction in tool diameter change (40%) in the 18 W case was observed for machining condition 7.

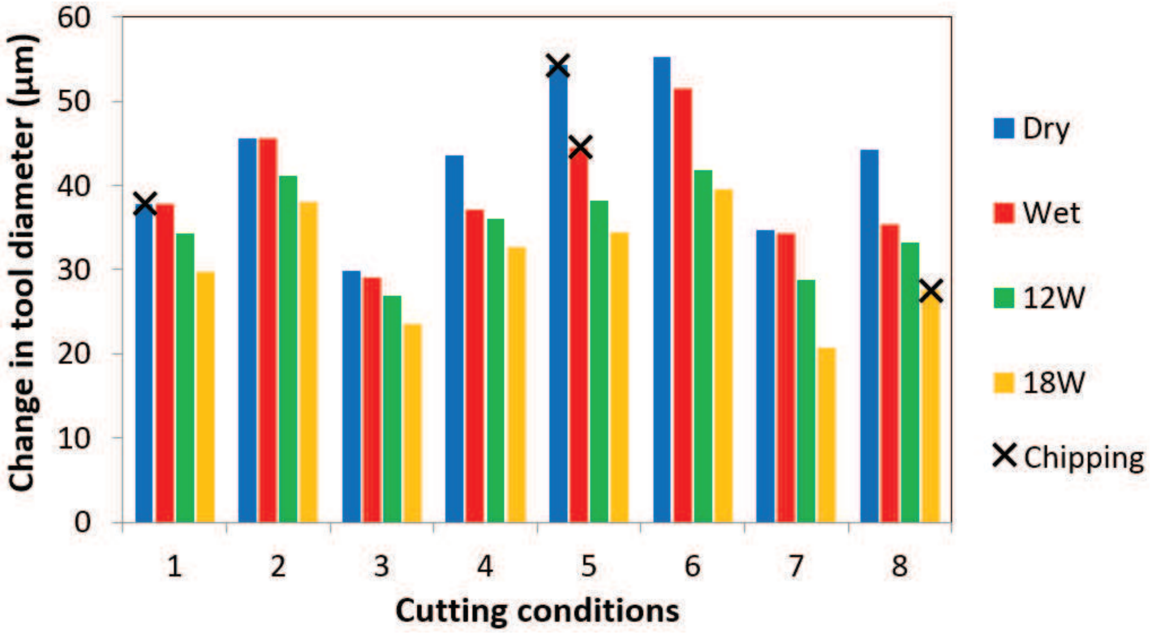

Figure 4.13: Change in tool diameter due to wear.

## 4.5 Cutting forces

The mean resultant forces for the first and last grooves produced in all 32 tests are shown in Figure 4.14. The forces were always lower for the first groove when the tool was new but tended to increase by groove 6 due to wear.

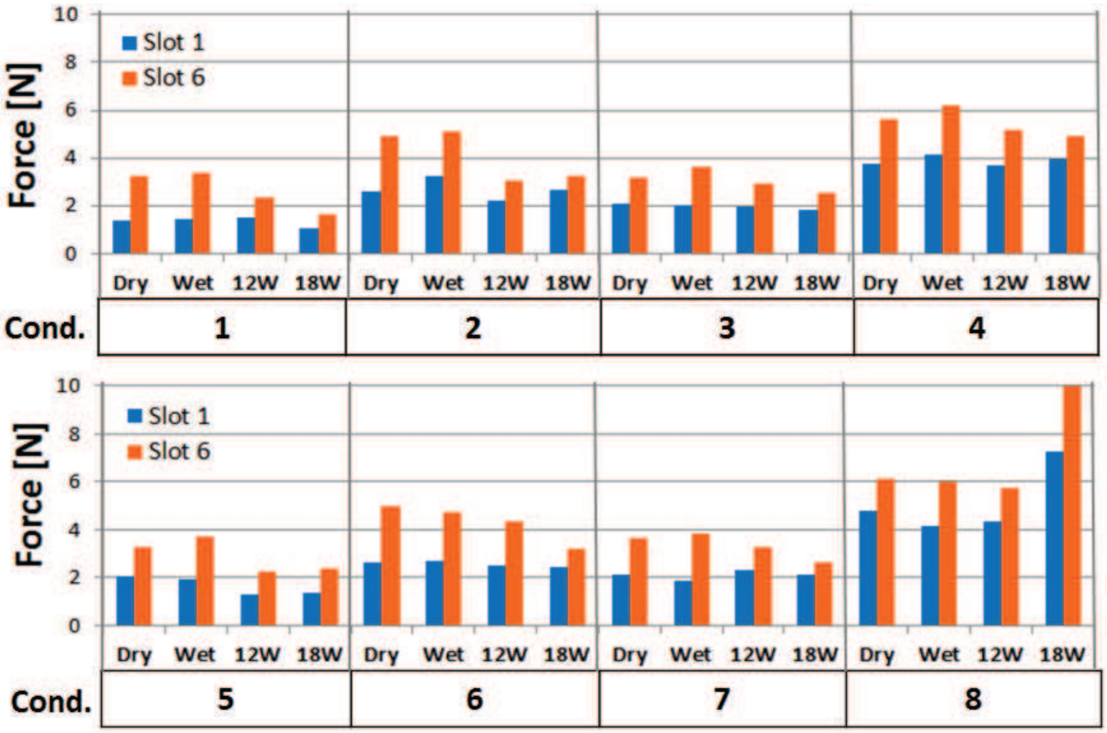

Figure 4.14: Mean resultant force for the first and sixth grooves for all eight machining conditions used.

For the higher depth of cut (0.04 mm) cases, i.e. machining conditions 2, 4, 6, and 8, higher forces were obtained irrespective of the assist mechanism used. An interesting observation is that, for all assist mechanisms, when the feed rate was tripled, i.e. machining conditions 3, 4, and 7, there was only a marginal increase in the forces compared to conditions 1, 2, and 5, respectively. At the higher feed rate, the material is able to shear easily with less ploughing and rubbing. Most notably, for the same machining conditions and in comparison to the dry tests, the 18 W LAMM tests yielded mean resultant forces that were, on average, 10% lower. The wet experiments typically showed higher forces than the dry tests, but this is primarily due to the additional weight of the cutting oil that accumulates on the top face of the dynamometer.

### 4.6 Overall comparison

To better understand which combination of assist method and machining condition are optimal from the standpoint of micromachinability, a *qualitative* comparison of all the data was made. The experimental results were evaluated by groove condition, shown in Figure 4.15, and tool condition, shown in Figure 4.16, which is broken into three subcategories each scored from one to five, with one being the worst and five being the best. The scores in each subcategory, described below, were then summed up and are presented in Table 4.2.

1. Condition of groove 6:
    - A. Burr formation based upon burr size (1 to 5)
    - B. Surface quality based upon chip adhesion and scarring (1 to 5)
    - C. Precision of depth of cut (1 to 5)
2. Tool condition:
    - A. Bottom edge wear (1 to 5)
    - B. Flank wear (1 to 5)
    - C. Change in tool diameter (1 to 5)

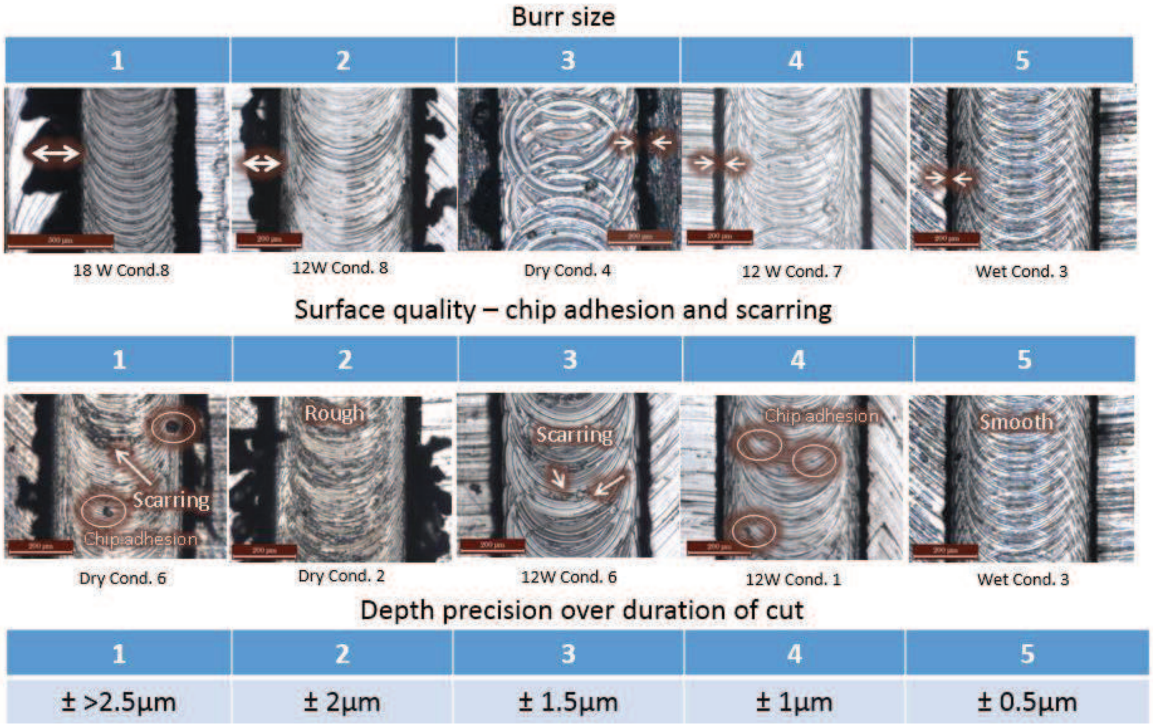

Figure 4.15: Groove condition.

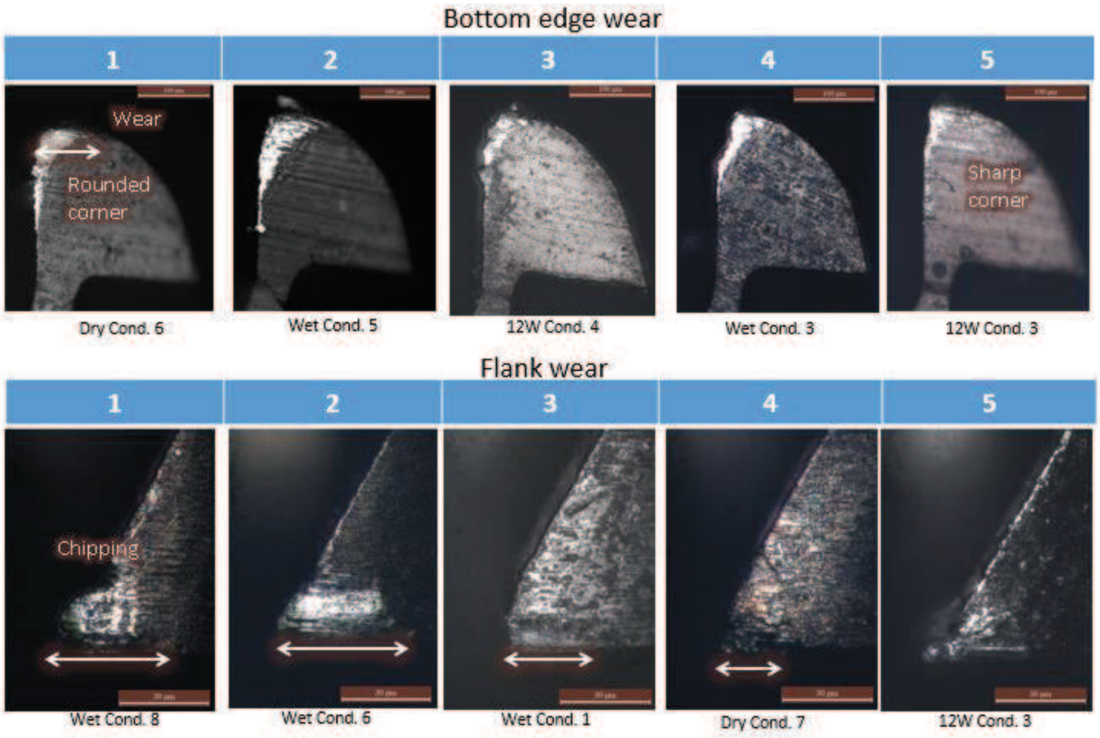

Change in tool diameter

| 1 | 2 | 3 | 4 | 5 |
|---|---|---|---|---|
| <45 µm | < 40 µm | < 35 µm | < 30 µm | < 25 µm |

Figure 4.16: Tool condition.

Table 4.2: Optimum assist method and cutting condition analysis.

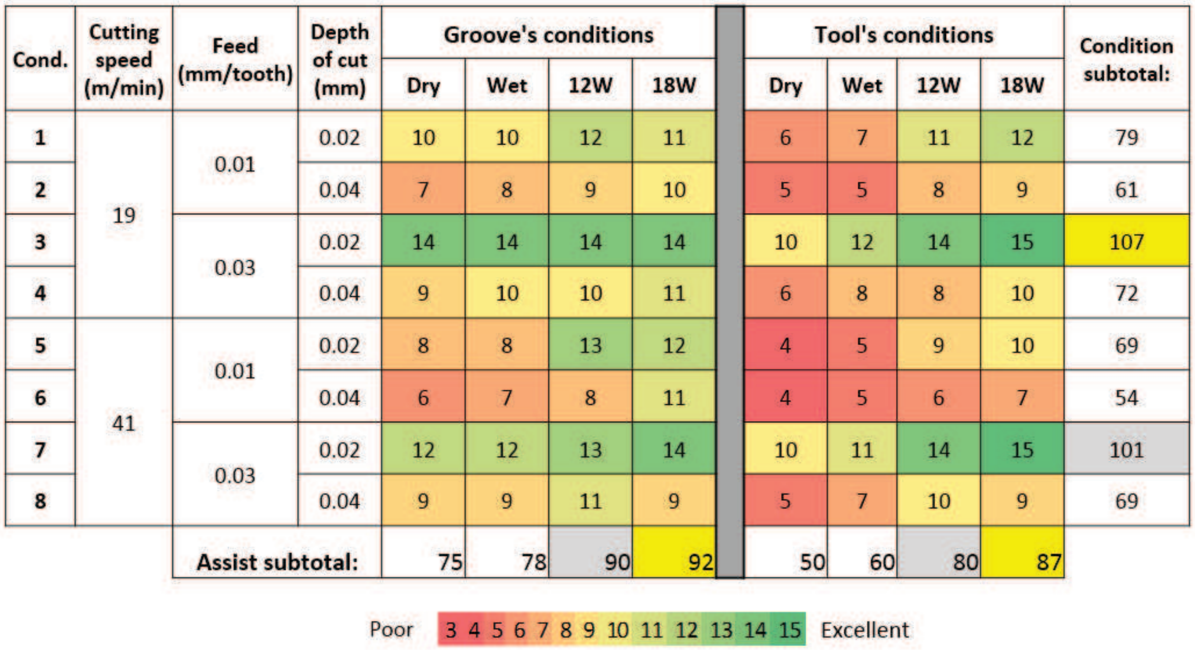

| Cond. | Cutting speed (m/min) | Feed (mm/tooth) | Depth of cut (mm) | Groove's conditions | | | | Tool's conditions | | | | Condition subtotal: |
|---|---|---|---|---|---|---|---|---|---|---|---|---|
| | | | | Dry | Wet | 12W | 18W | Dry | Wet | 12W | 18W | |
| 1 | 19 | 0.01 | 0.02 | 10 | 10 | 12 | 11 | 6 | 7 | 11 | 12 | 79 |
| 2 | | | 0.04 | 7 | 8 | 9 | 10 | 5 | 5 | 8 | 9 | 61 |
| 3 | | 0.03 | 0.02 | 14 | 14 | 14 | 14 | 10 | 12 | 14 | 15 | 107 |
| 4 | | | 0.04 | 9 | 10 | 10 | 11 | 6 | 8 | 8 | 10 | 72 |
| 5 | 41 | 0.01 | 0.02 | 8 | 8 | 13 | 12 | 4 | 5 | 9 | 10 | 69 |
| 6 | | | 0.04 | 6 | 7 | 8 | 11 | 4 | 5 | 6 | 7 | 54 |
| 7 | | 0.03 | 0.02 | 12 | 12 | 13 | 14 | 10 | 11 | 14 | 15 | 101 |
| 8 | | | 0.04 | 9 | 9 | 11 | 9 | 5 | 7 | 10 | 9 | 69 |
| | | **Assist subtotal:** | | 75 | 78 | 90 | 92 | 50 | 60 | 80 | 87 | |

The qualitative scoring analysis presented above yielded the highest score for machining condition 3, which was then taken to be the optimum cutting condition. Condition 3 was characterized by low cutting speed (19 m/min), high feed (0.03 mm/tooth) and a low axial depth of cut (0.20 mm). The 18 W LAMM assist method scored the highest for all cutting conditions. Based on this analysis, the combination of 18 W LAMM and test condition 3 was determined to be the best cutting condition.

## 4.7 Summary

In this chapter, micro milling experiments were run with dry, wet, and laser assist methods under a wide range of cutting conditions. Compared to the dry and wet methods, LAMM was found to yield the best results overall. The following specific conclusions related to LAMM can be drawn from the results presented in this chapter:

- LAMM improved the groove condition and maintained a more precise depth of cut.
- LAMM reduced tool diameter wear by 29% on average and preserved tool condition better than the wet assist case.
- LAMM decreased the mean resultant force on average by 10% when compared to the dry case.
- The 18 W LAMM case combined with machining condition 3 (cutting speed of 19 m/min, feed of 0.03 mm/tooth, axial depth of cut of 0.02 mm) was found to be the optimum combination of assist mechanism and machining condition to cut A-286.

# CHAPTER 5: TOOL LIFE IN LAMM

## 5.1 Introduction

### 5.1.1 Tool life test

The previous chapter showed that in comparison to conventional wet assist, LAMM greatly enhanced the cutting process when removing a small volume of material (1.52 $mm^3$) over a short duration ($\leq$ 30 seconds). However, to be economical in an industrial environment, a single tool has to machine far longer than 30 seconds, usually on the order of tens of minutes to hours. Having found suitable LAMM parameters in the previous chapter, this chapter details the tool life testing of a single micro end mill over a longer duration of cutting (25 minutes). The micromachinability of LAMM in the tool life test is characterized by monitoring the groove condition, burr formation, tool wear, and cutting forces.

### 5.1.2 Motivation

In the previous chapter, it was demonstrated that the LAMM 18W test under cutting condition 3 yielded the best results in limited duration cutting. For the tool life test discussed in this chapter, cutting parameters similar to those used in cutting condition 3 were employed; the only difference was that the cutting speed was decreased from 19 m/min to 16 m/min. This was motivated by the economics of the practical application of the LAMM process where longer tool life is desirable to minimize tool change costs. Previous studies [53, 73, 74] have shown that decreasing cutting speeds drastically increases tool life and reduces tooling costs.

### 5.1.3 Experiment design

The tool life test parameters are shown in Table 5.1.

Table 5.1: Tool life test parameters.

| **Laser power (W)** | **Spot size (µm)** | **Laser-tool distance (µm)** | **Cutting speed (m/min)** | **Feed (mm/tooth)** | **Depth of cut (mm)** |
|---|---|---|---|---|---|
| $P$ | $d_s$ | $d$ | $V_c$ | $f_t$ | $a_p$ |
| 18 | 300 | 450 | 16 | 0.03 | 0.02 |

The machining parameters listed in Table 5.1 correspond to a material removal rate of 6 $mm^3$/min. Since the tool life test was run for 25.3 minutes, it corresponds to a total cutting length of 15,300 mm or 153 $mm^3$ of material removal.

Similar to the previous chapter, the workpiece material was A-286 steel age hardened to 41.8 ± 0.6 $HR_c$ and the cutting tool used was a square end, tungsten carbide, two flute, 500 µm diameter, TiAlN coated end mill (Mitsubishi MStar MS2SSD0050). The tool life test consisted of micro milling 14 grooves that were each 0.5 mm wide and 28.4 mm in length. The total depth of each groove varied depending on the number of passes used for each groove. Over the 25 minutes duration of the tool life test, 42 grooves were cut in three separate workpiece samples with a single tool.

An example of the tool path for the grooves on the first workpiece sample is shown in Figure 5.1. The first groove is a shallow groove (indicated in green). Each shallow groove consists of a single tool pass to yield a groove depth of 20 µm. From left to right, the second groove (indicated in orange) is produced using 5 tool passes to yield a total groove depth of 100 µm. The third groove is also a shallow groove. The fourth groove is a deep groove (indicated in red) produced by 18 tool passes to yield a total groove depth of

360 µm. The remainder of the 42 grooves were machined as either a shallow or a deep groove as shown in Figure 5.1 and Table A.1. Shallow grooves served as locations to monitor the tool wear, cutting forces and groove dimensions. Tool wear was measured prior to cutting the shallow grooves. The deep and medium grooves primarily served to induce tool wear. Groove dimensions were also measured on a select few deep grooves as well.

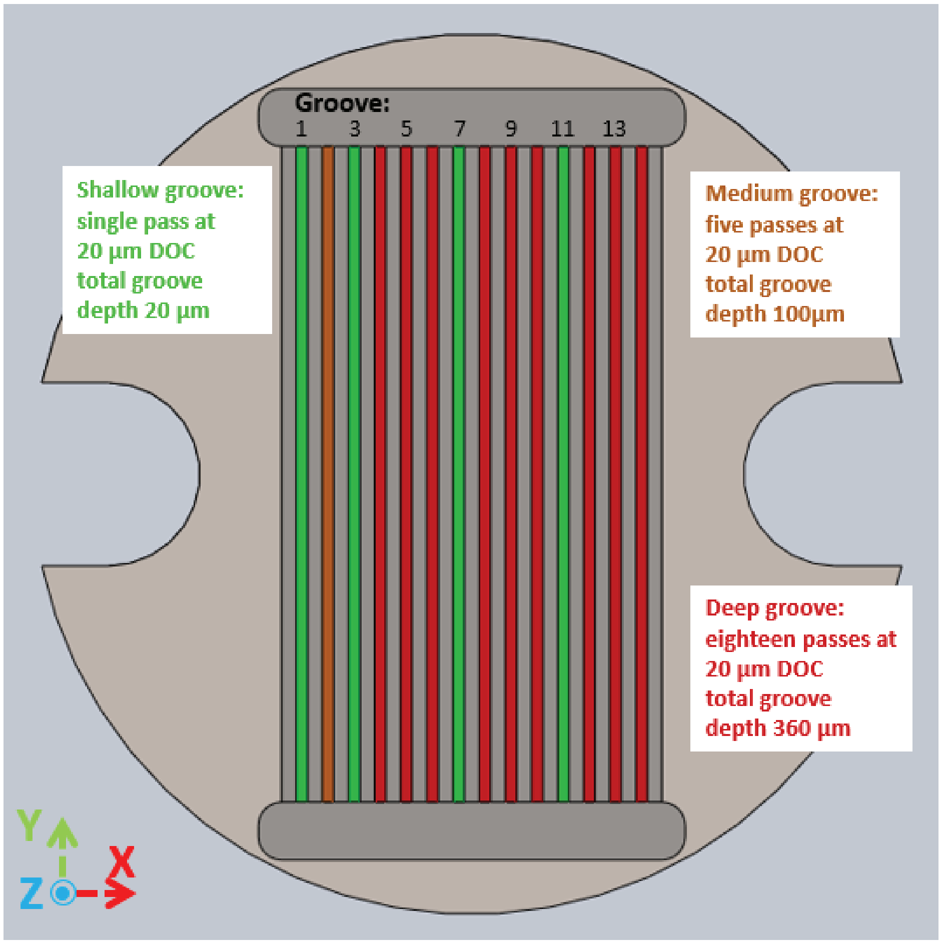

Figure 5.1: Tool path used in the tool life test.

### 5.1.4 Measurement techniques

Groove quality measurements were taken on select shallow and deep grooves. The measurements were made using a confocal microscope (Olympus LEXT) and consisted of optical images and cross-sectional profiles of the selected grooves. Groove dimensions such as groove depth and groove width were evaluated from the cross-sectional profiles. Tool diameter wear was measured using an optical microscope (Mitutoyo toolmaker's 510-D). Tool wear on the bottom edge of the end mill was imaged using the confocal microscope. Peripheral tool flank wear was imaged using a scanning electron microscope (Hitachi S-3700N VP-SEM). Tool wear measurements were periodically taken as shown in Table A.1. Cutting forces were measured using a piezoelectric force dynamometer (Kistler Minidyne® 9256C2) at a sampling rate of 30 kHz.

## 5.2 Groove condition

### 5.2.1 Shallow groove

The optical images of selected shallow groove surfaces over the duration of the test are shown in Figure 5.2. Below each image is a representative cross-sectional profile of the groove. Some noteworthy features are emphasized for illustration. Since the first groove was machined with a sharp new tool, the groove has minimal chip adhesion and a relatively square cross-section. In addition, because of the new tool,the groove bottom surface exhibits distinct cutter teeth marks. By groove 15, the tool had removed 48.9 mm$^3$, i.e. 8 minutes, and the tool had experienced some wear, which is discussed later. Due to progressive wear of the tool cutting edge and corner radius, the surface of groove 15 is characterized by more non-uniform burrs, and more tapered and rounded corners as seen by the groove cross-sectional profiles. Tool wear causes a burnishing action, which leads to cutter marks that are less distinct compared to those in the first groove. With increased material removal, groove 29 and groove 40 showed more burnishing of the surface, rounding at the bottom corner, and burrs along the groove edges.

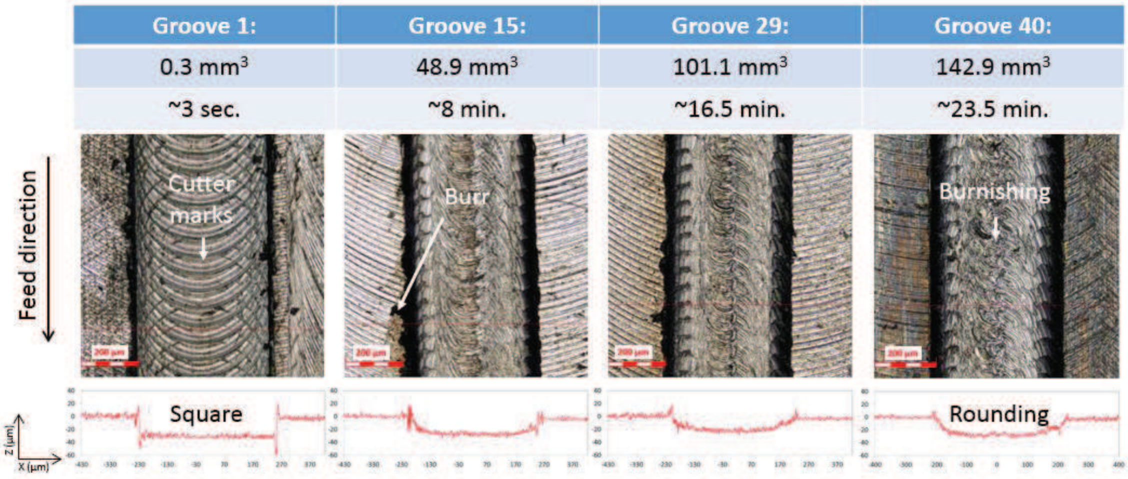

Figure 5.2: Images of selected shallow grooves and their cross-sectional profiles. For each groove, the elapsed volumes of material removed and the machining times are also listed.

Measurements of the groove width and depth groove cross-sections were obtained from the groove cross-sections as illustrated in Figure 5.3. The groove width was measured at five different cross-sections per selected shallow groove and averaged. The groove depth was measured 500 times per cross section at three different cross-sections per selected shallow groove and averaged.

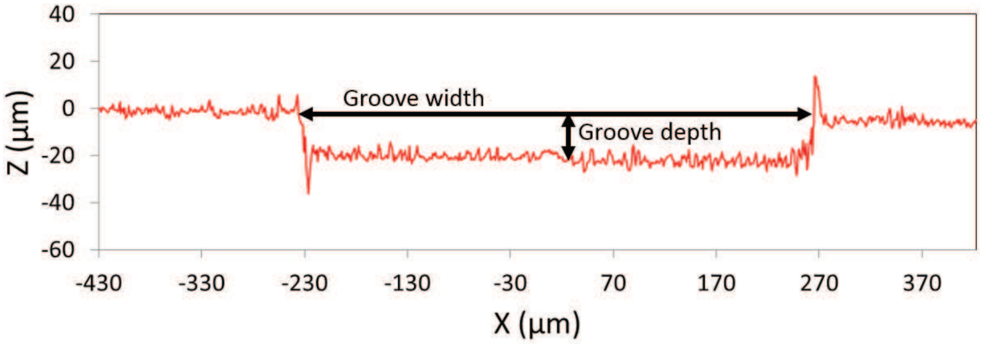

Figure 5.3: Example of groove width and depth measurements from the groove cross-sectional profile.

Shown in Figure 5.4 is the progression of the groove depth over the duration of the test. The programmed or target depth of cut was 20 µm as indicated by the black dashed line. The measured groove depths overshoot the target depth by an average of 6.3 µm. This overshoot is attributed to the thermal expansion of the workpiece surface due to laser heating. This overshoot can easily be compensated for by selecting the target depth of cut to be less by the amount of thermal expansion, which can be estimated from the calculated temperature rise in the workpiece due to laser heating. Also, theoretically, the shallow groove depth should decrease with tool wear. However, since the tool was periodically removed to measure tool wear, reinserted, and re-zeroed to the workpiece surface, tool wear was systematically compensated for in the axial (Z) direction.

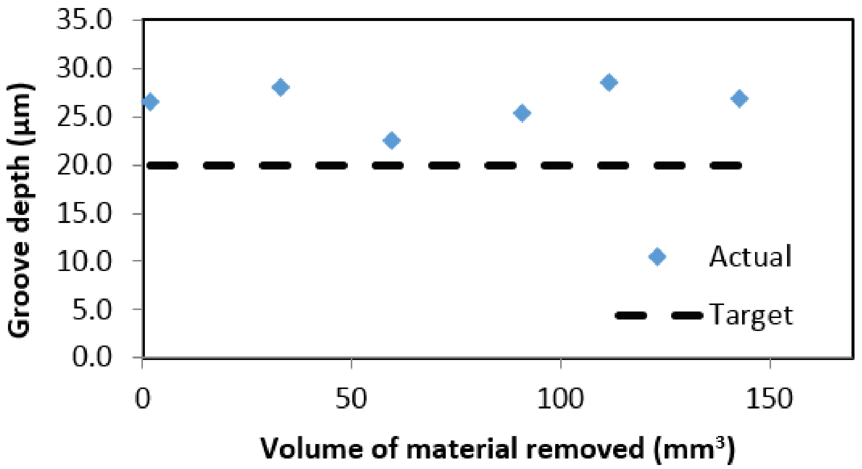

Figure 5.4: Shallow groove depth (95% confidence interval of ± 0.3 µm) over the test duration. The dashed target line represents the programmed axial depth of cut for each of the grooves.

The change in groove width over the test duration is shown in Figure 5.5. It can be seen that the initial groove width was 481 µm, similar to the initial tool diameter. As more material was removed, the tool wore and the groove width decreased rapidly in the first 50 $mm^3$, but subsequently reached steady state. This decrease in groove width can also be seen in Figure 5.2.

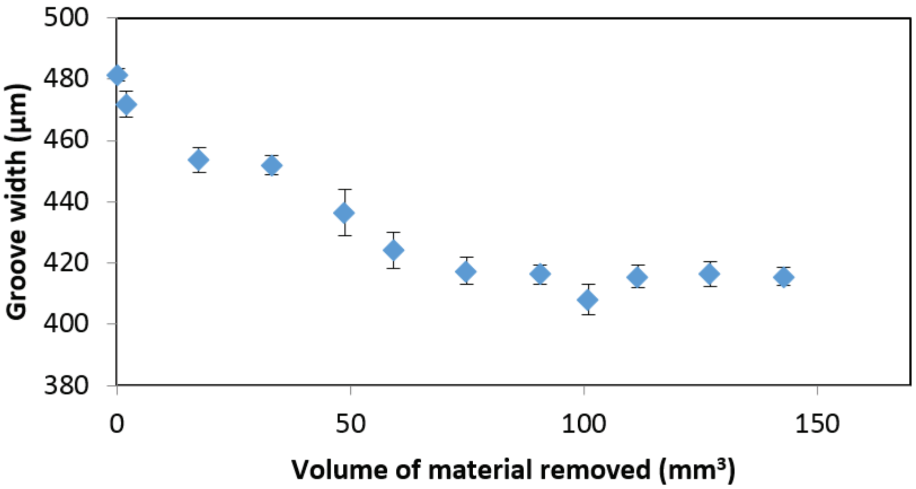

Figure 5.5: Shallow groove width over the test duration. Error bars denote the 95% confidence interval.

A comparison of three shallow groove cross-sectional profiles at different times in the tool life test is shown in Figure 5.6. As more material was removed, the grooves became less square and more rounded. The grooves also receded inward as the groove width decreased. It can be clearly seen that there is a significant difference between the profiles corresponding to the 0.3 $mm^3$ and 48.8 $mm^3$ cases. However, the difference between the 48.8 $mm^3$ and 142.9 $mm^3$ cases is marginal.

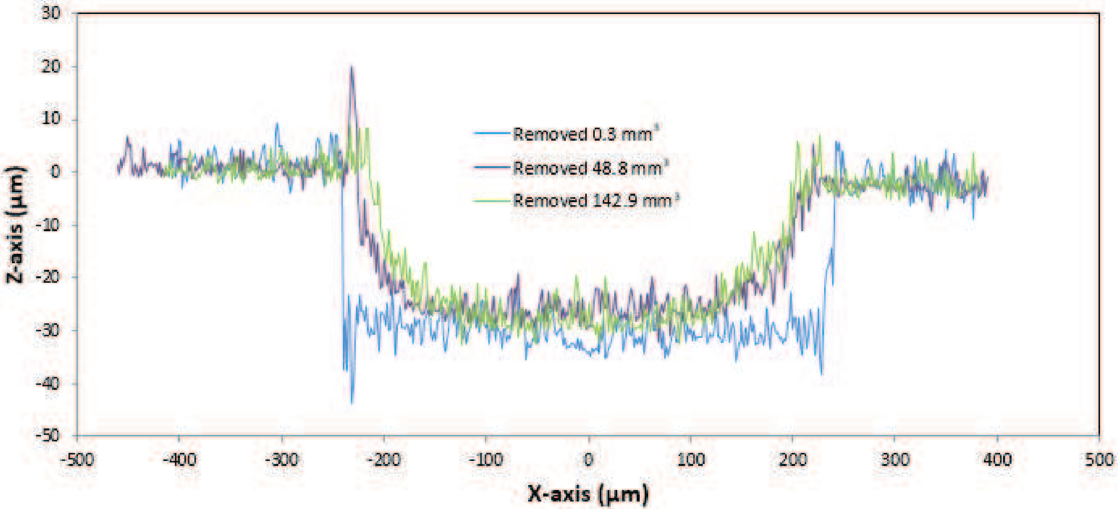

Figure 5.6: Comparison of shallow groove cross-sectional profiles with elapsed volume of material removed.

### 5.2.2 Deep groove condition

Similar to the shallow grooves, optical images of selected deep groove surfaces over the test duration are shown in Figure 5.7. The results correlate well with the results for the shallow grooves above. Since groove 4 was cut with a tool that was relatively new and sharp, the groove has minimal chip adhesion and has a relatively square cross-section. Also, since the tool is new, the groove has very distinct cutter teeth marks on the bottom surface. By groove 13 the tool had removed 43.5 $mm^3$ of material (~7 minutes), and the tool had worn some. Compared to groove 4, the surface of groove 13 is characterized by more non-uniform burrs and more tapered and rounded corners as seen in the cross-sectional profile.

As more material was removed, groove 33 and groove 42 showed more burnishing of the surface, rounding of the groove bottom corner, and burrs along the groove edges. These results seem to be consistent with the shallow groove observations. However, one significant difference is that the deep grooves involved multiple passes, and therefore the overall grooves were more square than the shallow grooves attributed to the multiple passes going downward along the Z axis.

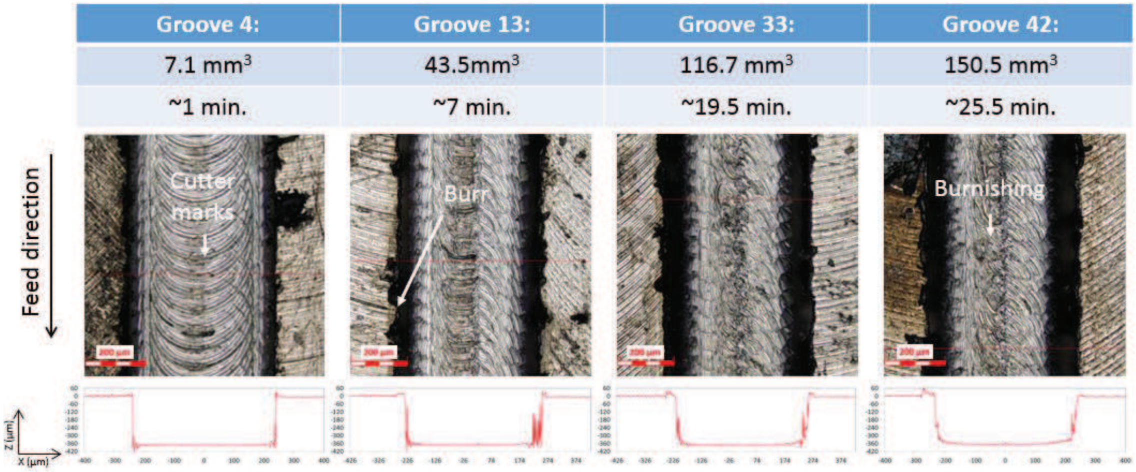

Figure 5.7: Images of deep grooves and their cross-sectional profiles. For each groove, the elapsed volumes of material removed and the machining times are also listed.

Similar to the shallow groove case, the groove widths and depths of selected deep grooves were measured. The groove widths reported for the deep groove case are averages of the groove widths measured at the top and middle (180 µm below the top surface) of the groove cross-section.

Figure 5.8 shows the change in the average depth of selected deep grooves over the test duration. The groove depth overshot the target depth by an average of 6.9 µm. This is consistent with the 6.3 µm overshoot seen in the shallow grooves and is again attributed to thermal expansion of the workpiece surface due to laser heating.

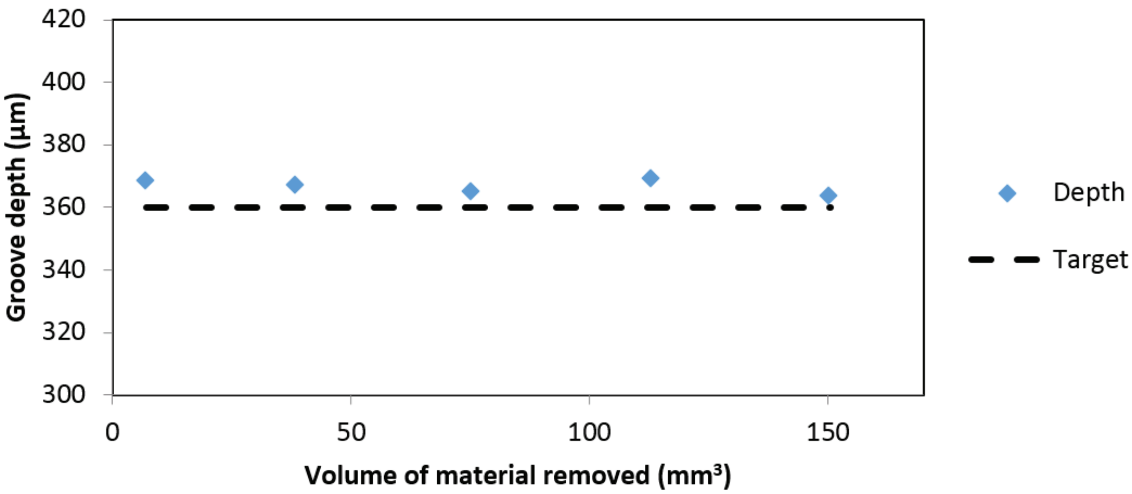

Figure 5.8: Deep groove depth (95% confidence interval of ± 0.3 µm) over the test duration.

The change in groove widths measured at the top and middle of the groove over the test duration is shown in Figure 5.9. It can be seen that both the top and middle groove widths started around the 481 µm, which is close to the nominal tool diameter. The middle groove width was always slightly less than the top groove width, indicating that there was a mild taper in the groove. Compared to the shallow groove results shown in Figure 5.5, the deep groove widths only marginally decreased as the tool wore. This effect is attributed to the multiple passes of the tool path. As the tool wore, the diameter at the very bottom of the tool decreased rapidly. However, since the deep grooves were produced using multiple tool passes,any uncut material after a tool pass was removed in the subsequent pass by the less worn upper part of the tool.

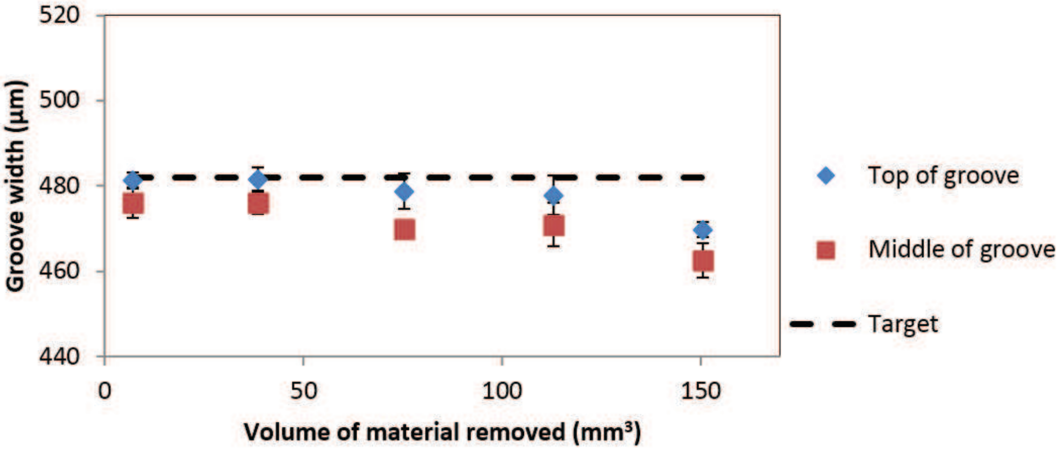

Figure 5.9: Deep groove width over the test duration. Error bars denote the 95% confidence interval.

Figure 5.10 shows a side-by-side comparison of three deep groove cross section profiles at different times in the tool life test. As more material was removed, the grooves became slightly more rounded and receded marginally inward as the groove width decreased. There is no significant difference between the 7.1 mm$^3$ and 153.1 mm$^3$ cases. Burr formation is visible at the top. However, this could easily be removed using a post-machining deburring process.

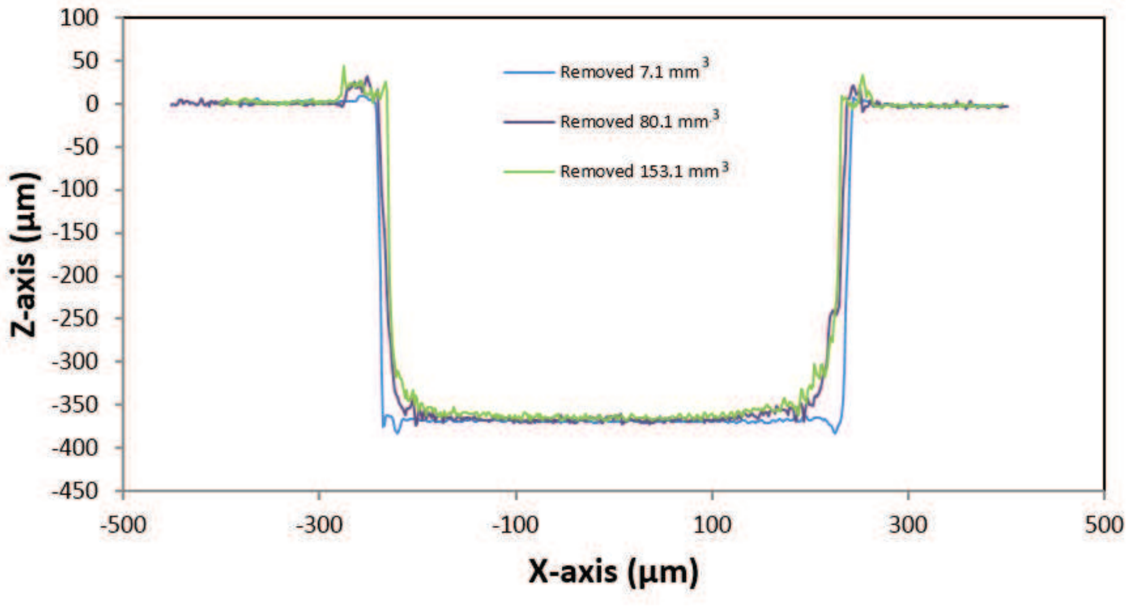

Figure 5.10: Comparison of deep groove cross-sectional profiles with elapsed volume of material removed.

## 5.3 **Tool condition**

The tool condition during the tool life test was evaluated using optical, confocal, and scanning electron microscopy (SEM). The conditions of the bottom and peripheral cutting edges of the tool were imaged from two camera positions as shown schematically in in Figure 5.11.

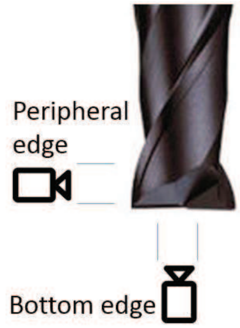

Figure 5.11: Schematic of optical evaluation of the tool condition.

Confocal microscope images of the bottom edges of the tool taken at select intervals during the tool life test are shown in Figure 5.12. It can be seen from the figure that a small built-up edge is formed by groove 15, and, by groove 29 and groove 42, the built-up edge is quite large. The images also show that the tips of the cutting edges at the bottom of the tool wear progressively.

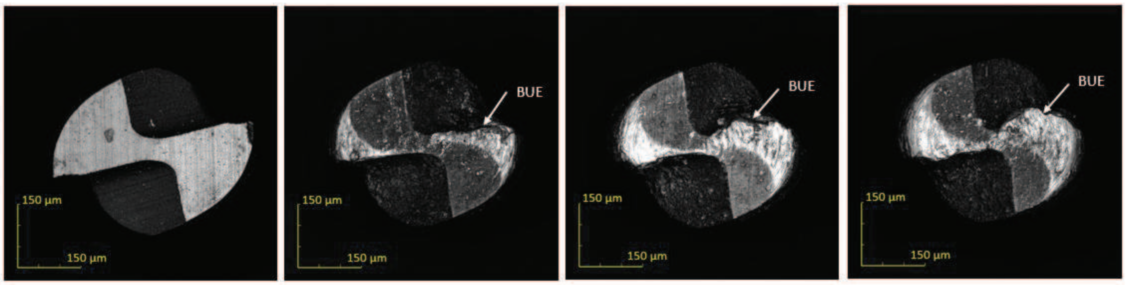

| New: | Pre-groove 15: | Pre-groove 29: | Post-groove 42: |
|---|---|---|---|
| 0 mm$^3$ | 48.6 mm$^3$ | 100.8 mm$^3$ | 153.1 mm$^3$ |
| 0 min. | ~8 min. | ~16.7 min. | ~25.5 min. |

Figure 5.12: Bottom edge of the tool over the test duration.

SEM images of the peripheral edges of the tool, taken at selected intervals during the tool life test, are shown in Figure 5.13. It can be seen from the figure that a small amount of built-up edge is formed by groove 15, and by groove 29 and groove 42, the amount of built-up edge is quite large. Workpiece adhesion is also observed to the right of the cutting edge. Tool flank wear was observed to increase progressively as more material was removed.

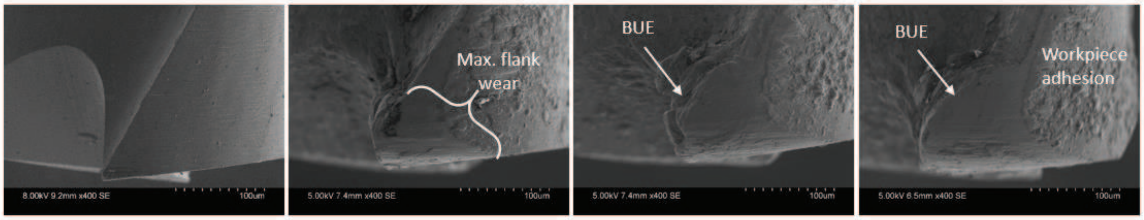

| New: | Pre-groove 15: | Pre-groove 29: | Post-groove 42: |
|---|---|---|---|
| 0 mm$^3$ | 48.6 mm$^3$ | 100.8 mm$^3$ | 153.1 mm$^3$ |
| 0 min. | ~8 min. | ~16.7 min. | ~25.5 min. |

Figure 5.13: Representative peripheral cutting edge and flank of the tool over the test duration.

Notwithstanding the formation of built-up edge in LAMM, the better groove quality and lower cutting forces presented in the previous chapter outweigh the negatives of the process. However, built-up edge is still a concern. Built-up edge, once formed, will eventually break off taking with it some of the coating and possibly the tool material. This can lead to a reduction in tool life. Possible solutions to the built-up edge problem are investigated in the next chapter.

In addition to flank wear, the change in tool corner radius and change in tool diameter due to wear were also measured as illustrated in Figure 5.14. The tool corner radii of both teeth on the tool were measured. The tool diameter was measured at 0, 10, 20, and 60 µm from the tool end along the tool axis.

Since the target axial depth of cut for each tool pass was 20 µm, the tool diameter was measured where the wear was the most prevalent i.e. 0, 10, and 20 µm from the tool end. The widths of the deep groove were defined by the tool diameter higher up the tool axis. Therefore, the tool diameter was also measured at 60 µm from the tool end. For illustration purposes, SEM images are shown in Figure 5.14. However, actual measurements were made using an optical microscope.

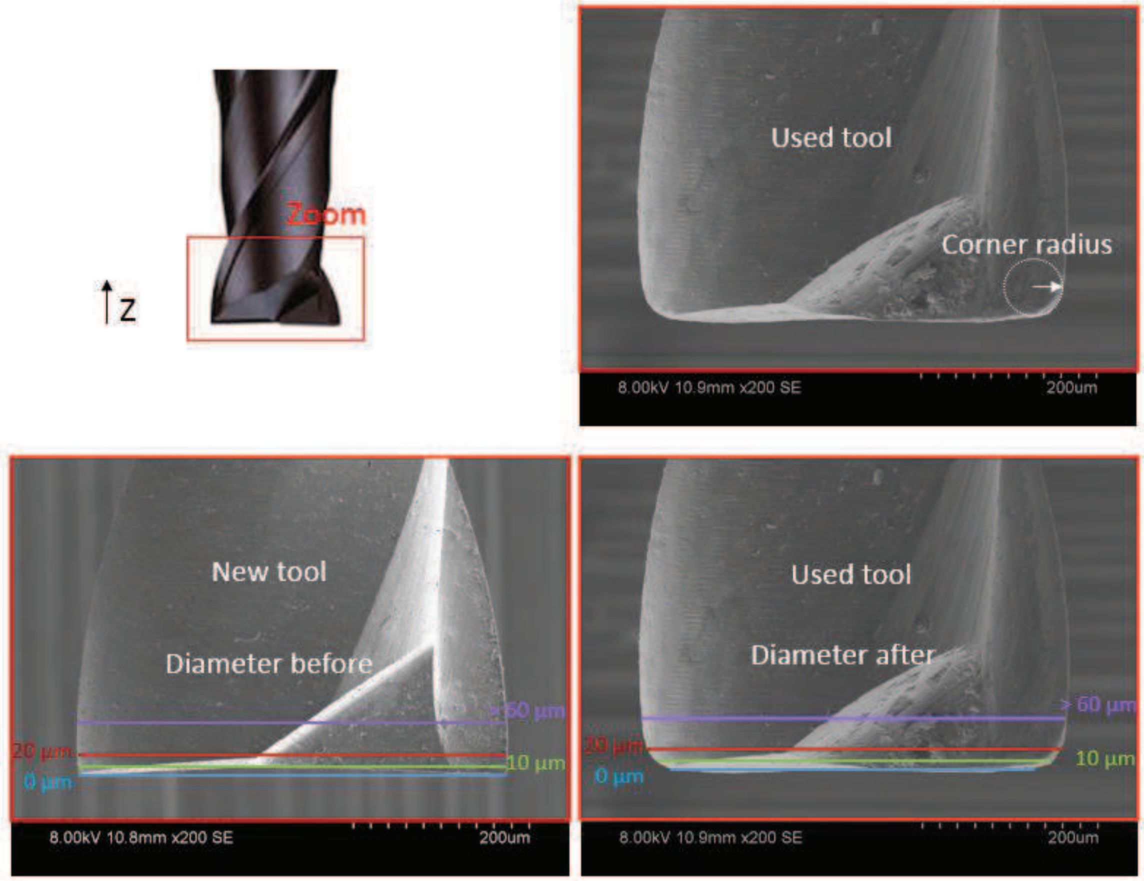

Figure 5.14: Measurement procedure for the tool corner radius and tool diameter wear.

The change in the tool corner radius and the tool diameter over the test duration are shown in Figure 5.15 and Figure 5.16, respectively. As seen in Figure 5.15, the tool corner radius increased rapidly in the first 20 mm$^3$ of material removal but increased gradually thereafter. This increase in the corner radius is the main cause for the rounding of the groove corners in the cross-sectional profiles shown in Figure 5.6. As seen in Figure 5.16, the tool diameters at all axial locations start at 483 µm but decreases rapidly within the first 20 mm$^3$ due to wear. Thereafter, it decreases slowly. The rapid tool wear rate within the first 20 mm$^3$ followed by a slow wear rate is consistent with the running-in and progressive tool wear stages reported in the literature [75]. The most significant change in tool diameter due to wear was seen at the tool end (0 µm) due to increase in the tool corner radius. The least significant diameter wear was seen at 60 µm up the tool axis. As described earlier, the first 20 µm of the tool length did most of the cutting while the upper part of the tool was responsible for minimal cutting and therefore experienced less wear.

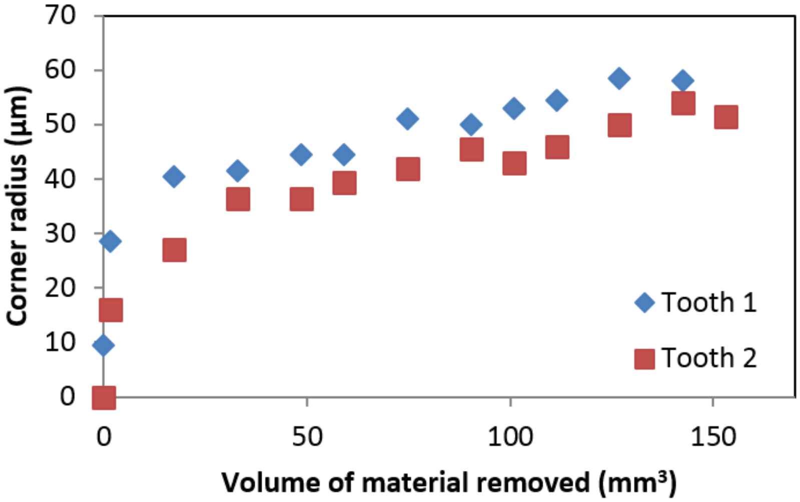

Figure 5.15: Change in tool corner radius over the test duration.

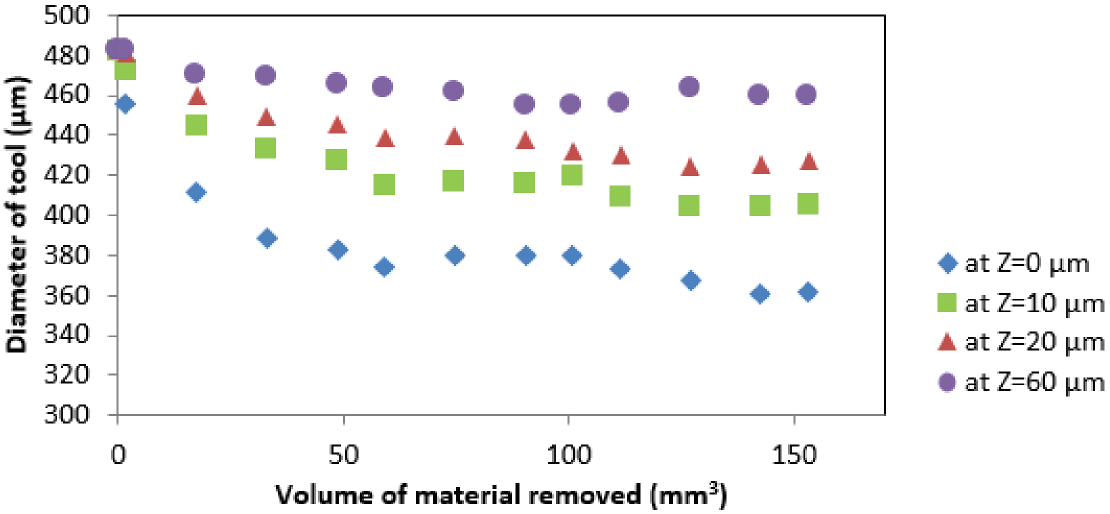

Figure 5.16: Tool diameter at different axial locations over the test duration.

As seen in Figure 5.17, a flank wear scar can be observed along the flank of the peripheral cutting edge. For each test, the maximum flank wear ($V_{b\_max}$) was measured on both teeth of the tool per the ISO 8688-2 standard. An example of the flank wear measurement made in a confocal microscope is shown in Figure 5.17. The confocal measurements were verified also using a SEM.

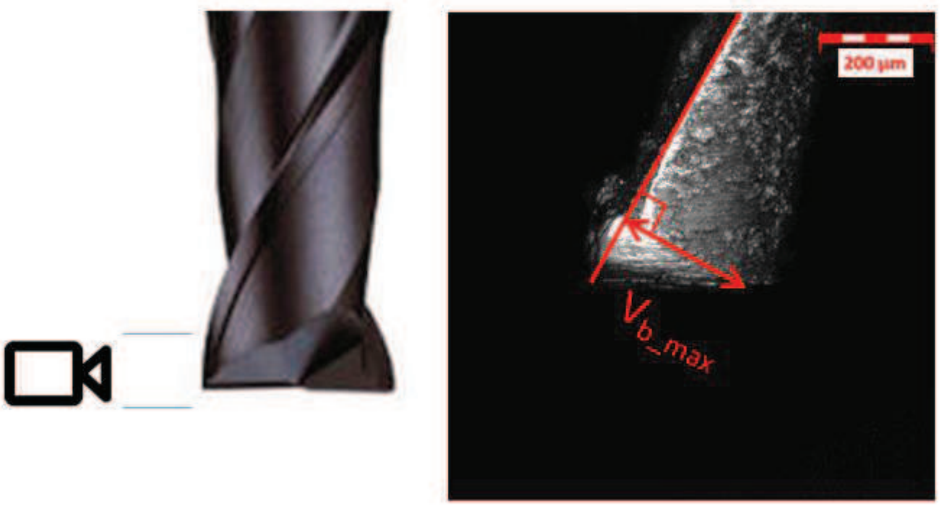

Figure 5.17: Peripheral flank wear measurement example.

The maximum flank wear of each cutting tooth over the test duration is shown in Figure 5.18. The flank wear trends observed are similar to the trends seen earlier for the tool corner radius and tool diameter.

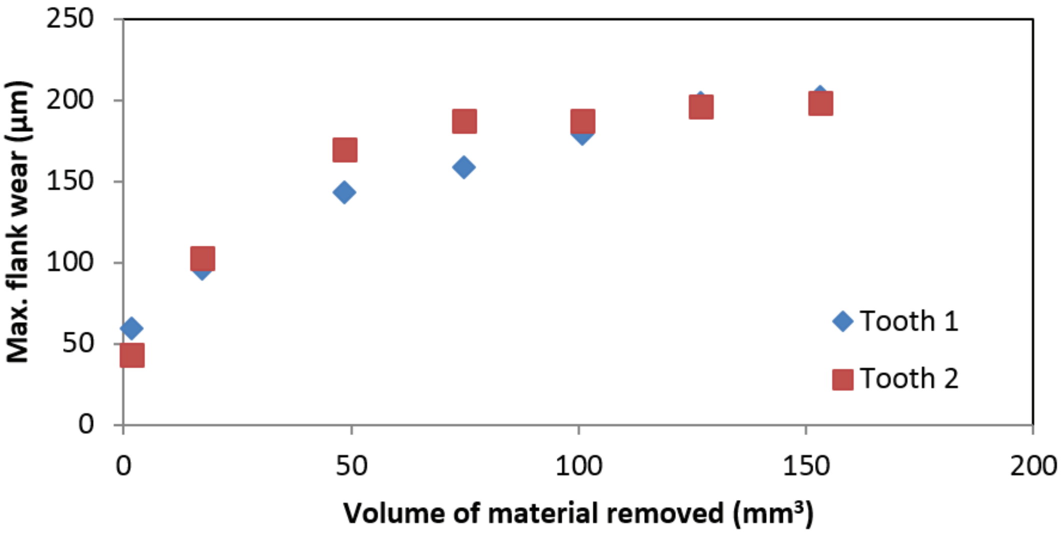

Figure 5.18: Maximum flank wear over the duration of the test.

## 5.4 Cutting forces

The cutting forces were measured on all shallow grooves. Forces were measured when cutting was in a steady state for a duration of 0.3 seconds or 50 tool revolutions. The resultant cutting force in each test was computed from the measured steady state X, Y, Z forces over a 0.3 seconds (50 tool revolutions) duration:

$$Resultant\ Force = \sqrt{{F_x}^2 + {F_y}^2 + {F_z}^2} \tag{5.1}$$

A representative resultant force profile consisting of 5 tool revolutions is shown in Figure 5.19. The average resultant force is the average of the resultant force data over 50 tool revolutions. The peak resultant force is the average of the maximum peak resultant force during each tooth pass, represented by black dots.

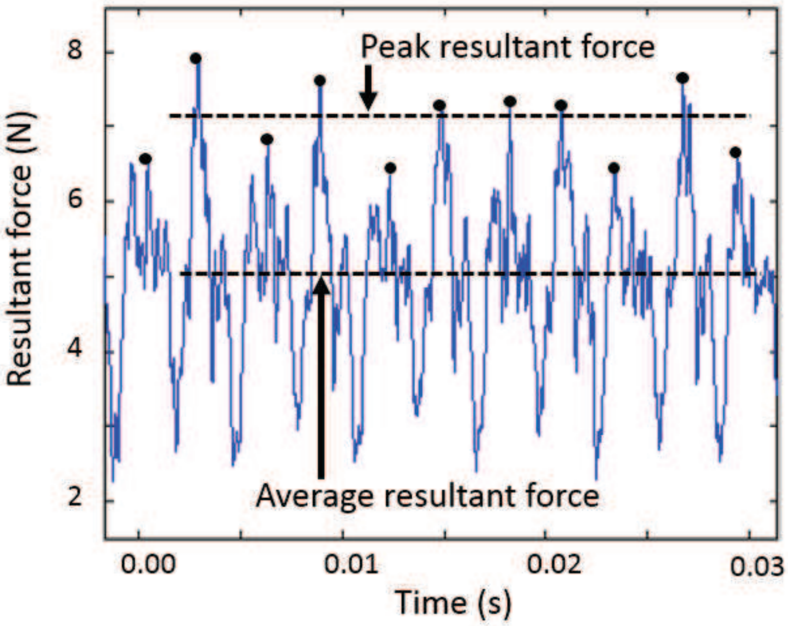

Figure 5.19: Representative resultant force measurement.

Shown in Figure 5.20 is the average resultant force and the peak resultant force over the test duration. The average resultant force for the first groove was initially 2.9 N but increased at almost linearly to 15.9 N for the final shallow groove. Between the first and last shallow grooves, the resultant force increased by a factor of 5. Similarly, the peak resultant force increased from 4.9 N for the first shallow groove to 21.8 N for the last shallow groove. This is an increase by a factor of 4. The observed force increases are primarily due to tool wear.

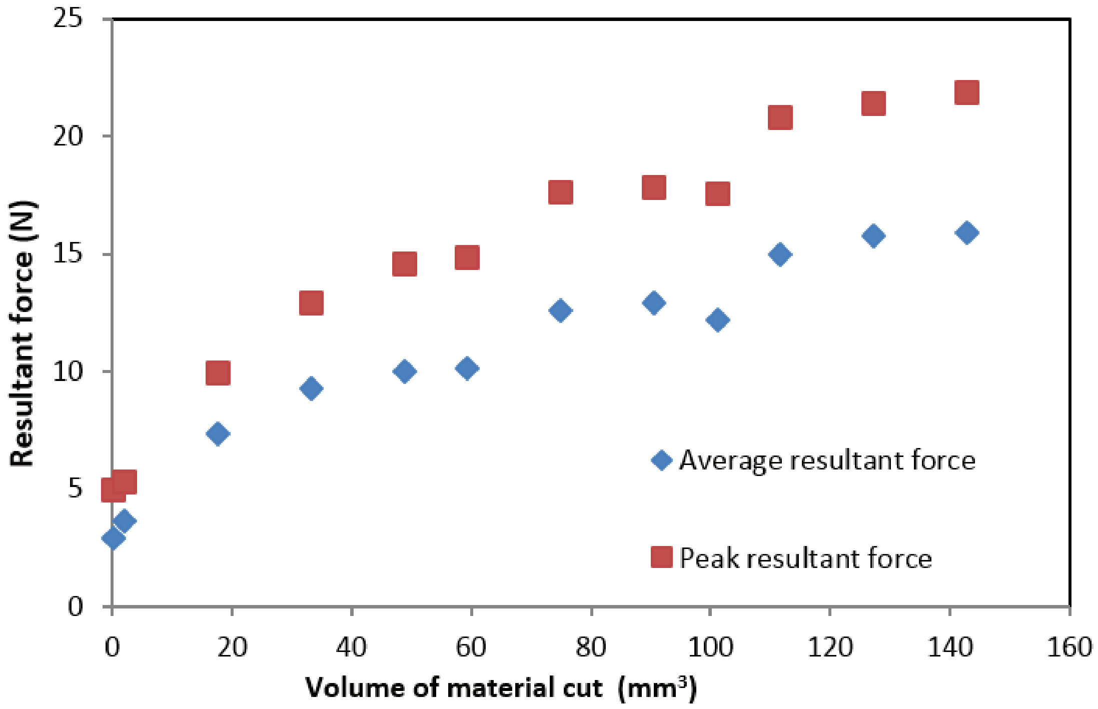

Figure 5.20: Resultant forces over the test duration.

## 5.5 Summary

This chapter presented the results of an extended duration (25 minutes) LAMM tool life test carried out using the previously identified cutting conditions for micromachining of hardened A-286 (41.8 $HR_c$). The groove condition, tool wear, and cutting forces were monitored during the test. The main conclusions of this chapter are:

- When the tool was new and sharp, the initial shallow groove had a square cross-section and its bottom surface showed distinct cutter marks. As the tool wore, the shallow grooves developed a tapered and rounded cross section, and a burnishing effect could be seen on the bottom surface of the groove. Non-uniform burrs on the groove edges became more prevalent over the test duration.

- Throughout the test, the shallow groove depth was quite consistent and overshot the programmed or target depth by an average of 6.3 µm. This is attributed to the thermal expansion of the workpiece due to laser heating.
- As more material was removed, the tool wore, and the shallow groove width decreased rapidly in the first 50 mm3, but reached a steady state thereafter.
- Similar to the shallow grooves, the initial deep groove had distinct cutter marks, but as time progressed, burnishing of the groove surface became more prevalent, and burrs were observed along the edges of the groove. As the tool wore, the deep grooves exhibited mild tapering and rounding of the cross-sectional profile, which was not as significant as seen in the shallow grooves. This was due to the groove being cut by multiple passes.
- Built-up edge formation was prevalent and tended to increase over the test duration.
- The tool corner radius and tool diameter exhibited rapid changes in the first 20 mm3 of material removal, after which they changed gradually.
- The average and peak resultant forces increased linearly due to tool wear over the test duration.

# CHAPTER 6: EFFECT OF MQL AND VORTEX COOLING ON MICROMACHINABILITY IN LAMM

## 6.1 Introduction

In the previous chapters, it was shown that LAMM is a promising micromachining process for difficult-to-cut materials and thermal softening benefitted dimensional accuracy and reduced tool wear. However, thermal softening caused the workpiece material to adhere to the tool and form a built-up edge. To mitigate this problem and to enhance the micromachinability of the workpiece material, this chapter investigates the following two lubrication and cooling methods: (i) minimum quantity lubrication (MQL), and (ii) vortex cooling. As noted in Chapter 3, there is no prior work that compares the relative micromachinability performance of MQL and vortex cooling in combination with LAMM. LAMM experiments assisted by MQL and vortex cooling are carried out on a difficult-to-cut high content nickel base alloy steel (A-286) and various aspects of micromachinability including surface morphology, tool condition, burr formation, groove dimensional accuracy, surface finish, cutting forces are analyzed. The performance of LAMM+MQL and LAMM+Vortex cooling are compared with dry cutting and LAMM. Possible physical reasons for the experimental observations are given.

## 6.2 Experimental setup and procedure

### 6.2.1 Experiment design

The experiments in this chapter were run on the setup described in Chapter 3, shown in Figure 3.7 with the modifications shown in Figure 3.8.

Similar to the experiments discussed in Chapters 4 and 5, the workpiece material used in the current experiments was a cold reduced round bar of precipitation hardened A-286 (41.8 ± 0.6 $HR_c$) and the cutting tools used in the experiments were 500 μm diameter, two flute, square end, TiAlN coated tungsten carbide end mills (Mitsubishi MStar MS2SSD0050). Each test was performed with a new tool.

As shown in Figure 6.1, four slots (grooves) were machined in each test. The first groove (indicated in green) is a shallow groove produced by a single pass of the tool at a depth of cut of 20μm. The second and third grooves (indicated in red) are deep grooves produced by 18 tool passes, with each pass made at a depth of cut of 20 μm to yield a total groove depth of 360 μm. The fourth and last groove is a shallow groove. The overall tool path in each test consisted of 38 tool passes, each 28.4 mm long and a depth of cut 20μm, for a total cutting length of 1079.2 mm and total material removal volume of 10.8 $mm^3$. All reported measurements were made on the first and fourth grooves. The purpose of the second and third deep grooves was to induce tool wear.

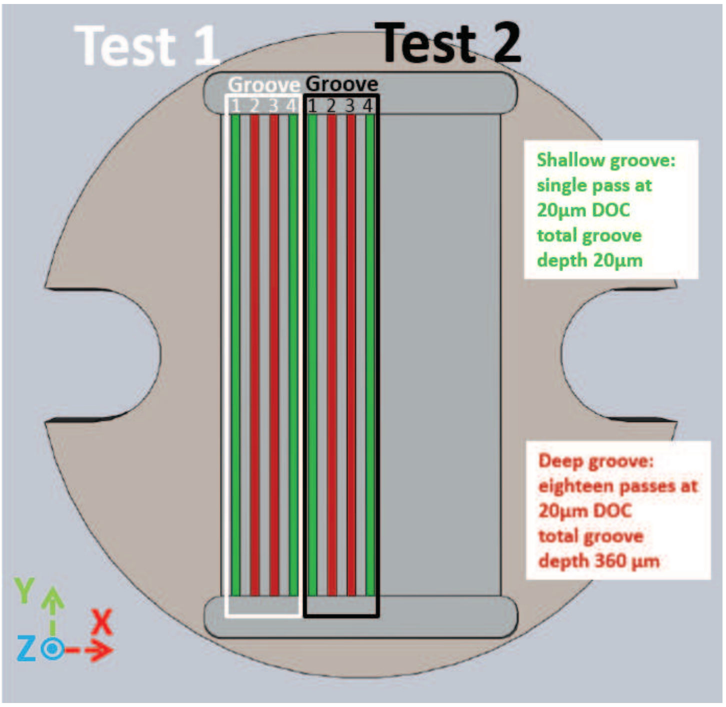

Figure 6.1: Tool path.

A total of ten (10) test combinations, listed in Table 6.1, were executed as part of the experimental campaign in this chapter.

Table 6.1: Test combinations.

| Test # | Test type |
|---|---|
| 1 | Dry |
| 2 | LAMM |
| 3 | MQL I |
| 4 | LAMM + MQL I |
| 5 | MQL II |
| 6 | LAMM + MQL II |
| 7 | Vortex I |
| 8 | LAMM + Vortex I |
| 9 | Vortex II |
| 10 | LAMM + Vortex II |

Machining and laser parameters were selected and fixed based on previous work shown in Chapter 4. The center of the laser spot was located 450 μm from the tool center. The laser power was set to 18 W with a corresponding peak intensity of 510 W/mm$^2$. The two sets of MQL parameters, MQL I and MQL II, were selected based on prior work reported in the literature [45] and based on recommendations of the MQL system provider. The two vortex cooling tests, Vortex I and Vortex II, were based on the maximum flow rate and maximum temperature concept [47, 48]. The specific parameters selected for the MQL and vortex cooling conditions are listed in Table 6.2.

Table 6.2: Test parameters.

| | **Cutting speed** | **Feed** | **Axial depth of cut** |
|---|---|---|---|
| Micro mill | 16 m/min | 0.03 mm/tooth | 0.02 mm |

| | **Power** | **Spot size** | **Laser-tool distance** |
|---|---|---|---|
| LAMM | 18 W | 300 μm | 450 μm |

| | **Oil flow rate** | **Air flow rate** | **Air temperature** |
|---|---|---|---|
| MQL I | 10 ml/hr | 30 l/min | 21° C |
| MQL II | 10 ml/hr | 50 l/min | 21° C |
| Vortex I | - - - | 200 l/min | -12° C |
| Vortex II | - - - | 400 l/min | 0° C |

Using a simple cylinder in cross air flow to model an end mill subjected to vortex cooling, the Nusselt numbers for the flows represented by Vortex I and Vortex II were computed to be 17.2 and 23.3, respectively. Interestingly, Vortex II, which is characterized by a warmer but higher air flow rate, has the ability to remove more heat as shown by the Nusselt numbers. For comparison, the air flow in MQL I and MQL II only had a Nusselt number of 6.8 and 8.6, respectively. This signifies that the air in the MQL technique had a negligible cooling effect and was predominantly used to transport atomized oil to the tool-workpiece surfaces to lubricate the cutting process.

Figure 6.2 schematically shows the orientation of the MQL and vortex cooling nozzles relative to the tool and laser spot. The nozzle was located approximately 10 mm from the tool tip at a yaw angle of 135° and a pitch angle of 60° from the direction of tool travel. Both MQL spray and vortex flow had a diameter of 10 mm or larger, and consequently, they not only impinged on the tool but also impacted much of the surrounding workpiece, as indicated by the wavy blue lines.

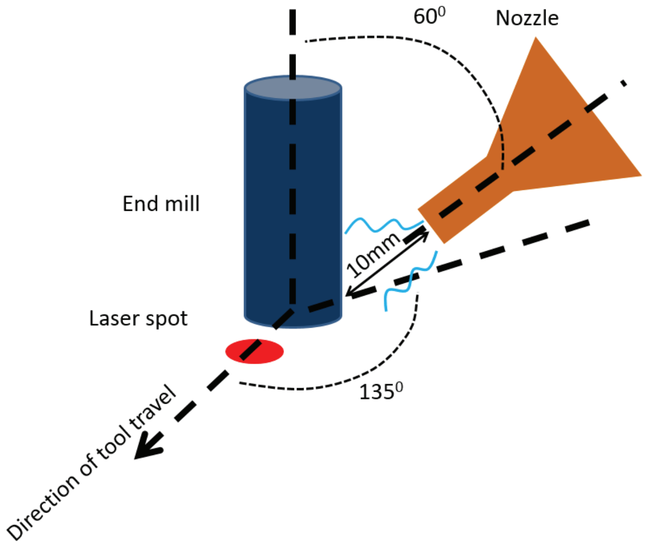

Figure 6.2: Schematic of tool, laser, and MQL/Vortex cooling nozzle locations.

### 6.2.2 Measurements methods

All groove quality measurements were made on the shallow grooves 1 and 4 shown in Figure 6.1. Groove quality measurements were made using a confocal microscope (Olympus LEXT) and consisted of the groove dimensions, burr dimensions, and surface roughness. Tool diameter wear was measured using a toolmaker's microscope. Tool wear at the bottom of the end mill was imaged in the confocal microscope. Peripheral tool flank wear was imaged using a scanning electron microscope (Hitachi S-3700N VP-SEM). Built-up edge on the tool was analyzed using electron dispersive spectroscopy (EDS) performed in the SEM. Cutting forces were measured using the Kistler dynamometer at a sampling frequency of 30 KHz.

## 6.3 Results and discussion

### 6.3.1 Groove condition

The optical images of the groove surfaces at the beginning of the tests (groove 1) produced in all ten tests are shown in Figure 6.3. Below each image is a representative cross-sectional profile of the groove. Since the first pass of each test was made with a tool that was new and sharp, the grooves have minimal chip adhesion, and their cross-sections are relatively square. In addition, since the tool is new, the groove floor surfaces have very distinct tool marks. In the LAMM + Vortex I and LAMM + Vortex II experiments, a dark vertical streak is visible along the center of the groove. The dark streak suggests the presence of a heat affected zone (HAZ) that was confirmed by hardness measurements, which yielded a hardness of 20.1 $HR_c$ in the dark region compared to ~42 $HR_c$ closer to the groove walls. The vortex cooling caused the tool not to engage the full programmed axial depth of cut as will be shown later in this chapter. Since the tool did not engage the full depth, it did not remove all of the thermally softened material. Consequently, a thermally softened HAZ was left on the cut surface. The reason the HAZ is confined to the center of the groove is the Gaussian distribution of the laser irradiation, which produces the highest temperature in the center of the groove and much lower temperatures closer to the groove walls. It can be seen that the surfaces produced by LAMM + MQL I and LAMM + MQL II also appear to exhibit HAZs. In the LAMM + MQL I and LAMM + MQL II cases, the MQL created a very thin layer of oil film on the top surface of the workpiece prior to machining. This is attributed to increased the absorptivity of the surface to laser irradiation in the presence of the layer of oil, which led to more heat penetrating into the workpiece than there was in LAMM alone. Previous studies have shown that, in the presence of olive oil, the infra-red laser absorption of stainless steels can increase anywhere from 37% [76] to 55% [77]. The oil used in the MQL experiments in this study (Coollube 2210EP) is a natural vegetable oil similar to olive oil.

The optical images of the groove surfaces at the end of the tests (groove 4) are shown in Figure 6.4. Due to progressive wear of the tool cutting edge and corner radius, the groove surfaces are characterized by chip adhesion and have more tapered and rounded corners as seen in the groove cross-sectional profiles shown. Tool wear results in a burnishing action, which leads to cutter marks that are less distinct compared to those in the first groove. The HAZ streaks are more pronounced in groove 4 than in groove 1 of the LAMM + MQL I, LAMM + MQL II, LAMM + Vortex I, and LAMM + Vortex II tests. This is attributed to less material being removed by the worn tool, which leaves behind more of the HAZ on the surface. The MQL tests exhibit larger burrs along the groove edges.

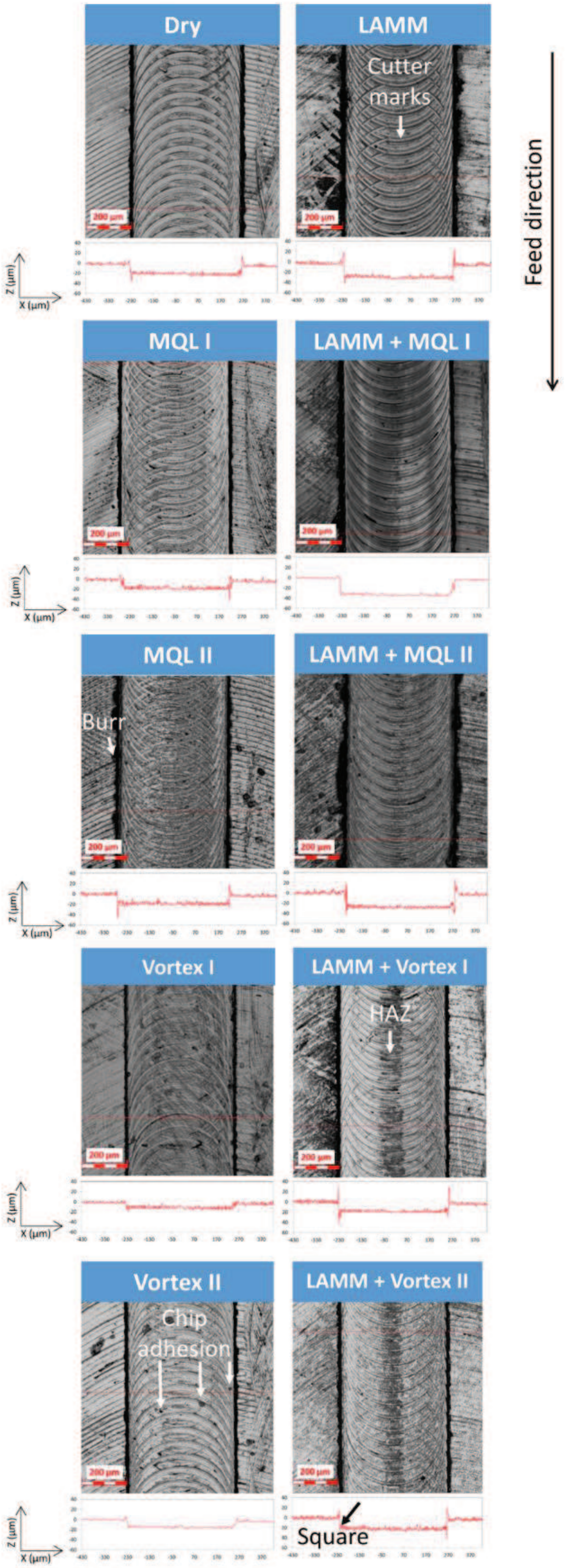

Figure 6.3: Surfaces of groove 1 and cross-sectional profiles.

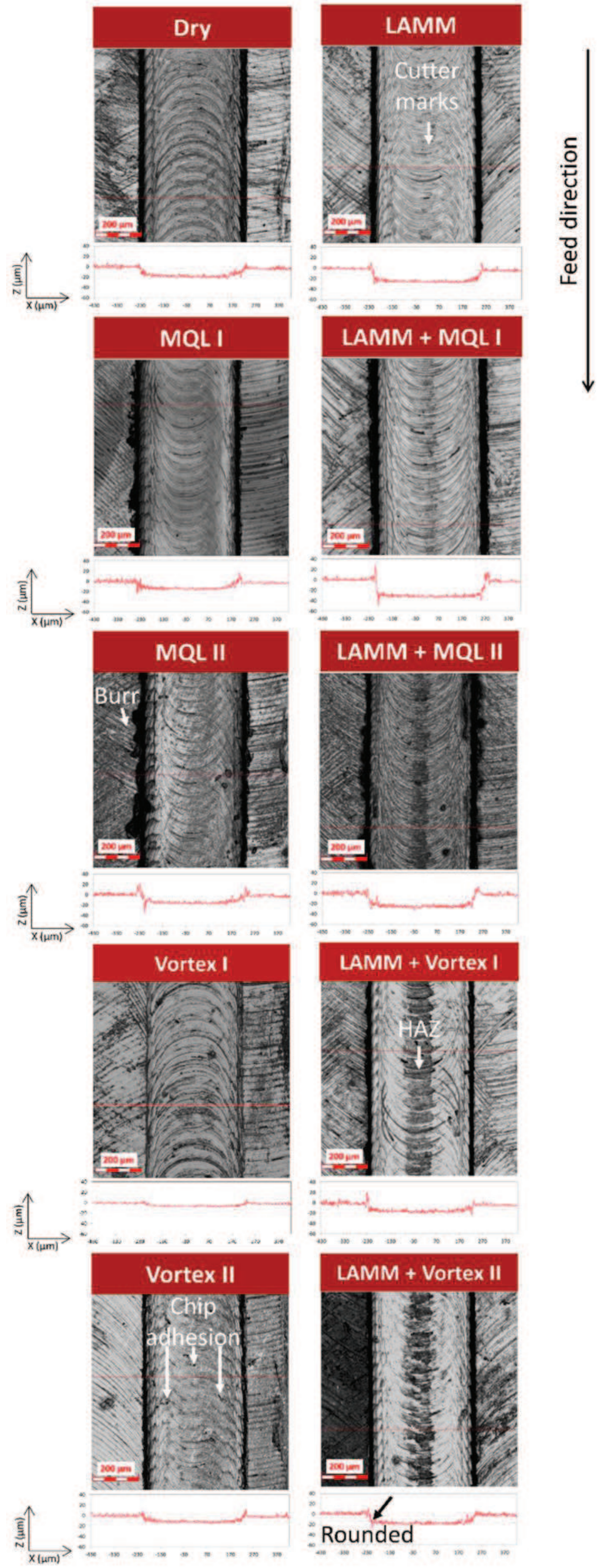

Figure 6.4: Surfaces of groove 4 and cross-sectional profiles.

A sample measurement of the groove width and groove depth is shown in Figure 6.5. The groove width was measured along the top of the groove at 10 different cross-sections per groove per test condition. The groove depth measurements reported here are the average of 500 depth measurements made along three different cross-sections per groove per test condition.

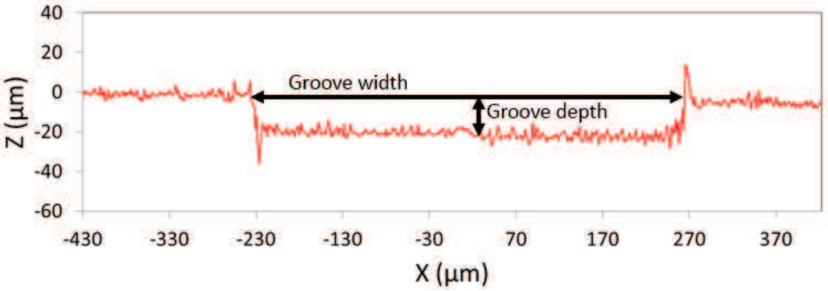

Figure 6.5: Measured groove dimensions.

Shown in Figure 6.6 are the average depths of groove 1 and groove 4 for each test condition. Due to tool wear, the groove depth decreased from groove 1 to groove 4 in all test cases. For tests without laser heating, i.e., dry, MQL I, MQL II, Vortex I, and Vortex II, the groove depths were under the programmed depth of cut by a few microns. This is attributed to the elastic deformation of the tool and workpiece due to the cutting forces. Interestingly, compared to the dry test, the depth of cut was smaller for Vortex I and Vortex II. The actual groove depths for the LAMM, LAMM + MQL I, and LAMM + MQL II tests were found to be greater than the programmed depth. As discussed in prior work [63, 64, 78], this is due to the thermal expansion of the tool and workpiece, which causes an increase in the depth of cut. Surprisingly, the depths of cut in LAMM + MQL I and LAMM + MQL II are greater than in LAMM alone. It is hypothesized that with the addition of MQL oil to the workpiece surface, the workpiece was able to absorb more of the laser's energy and reach higher temperatures, thus undergoing greater thermal expansion. Compared to Vortex I and Vortex II, LAMM + Vortex I and LAMM + Vortex II were characterized by higher depths of cut. On the other hand, compared to LAMM, LAMM + Vortex I and LAMM + Vortex II were characterized by lower depths of cut. These results suggest that vortex cooling causes a systematic reduction in the depth of cut. This is attributed to the thermal contraction of the workpiece and tool caused by vortex cooling. Given the thermal expansion coefficient of A-286 and the temperature gradient in the workpiece caused by vortex, it can be shown that there is a measurable contraction of the workpiece in the height direction, which impacts the depth of cut. It should be noted that the vortex cooling spot was approximately 10 mm in diameter, and therefore it cooled the tool and a large volume of the workpiece as well. LAMM + Vortex II yielded a groove depth that was closest to the target depth. It should be noted that the under- or over-shoot in the depth of cut can be easily compensated for.

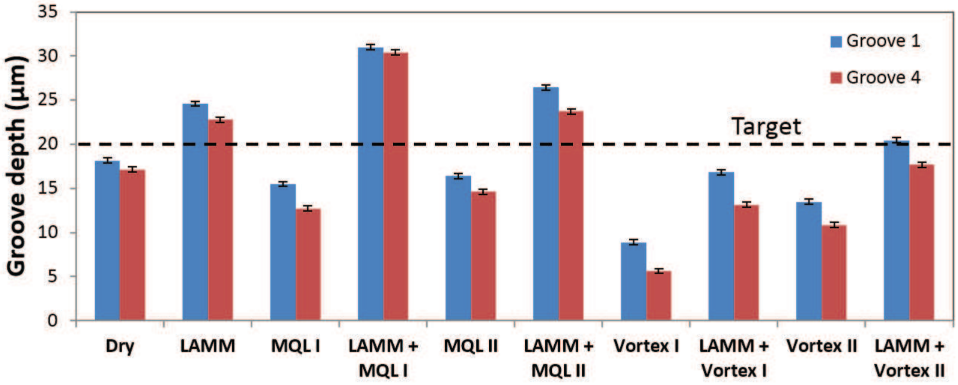

Figure 6.6: Groove depth measurements (error bars represent 95% confidence interval). Dashed line indicates the programmed (20 µm) axial depth of cut.

Comparing the widths of groove 4 and groove 1, the change in groove widths for the different test cases is shown in Figure 6.7. Among the tests without laser heating, MQL II had the smallest change in groove width. Compared to the dry test, the change in groove width in the LAMM test was 64% less. Similar results were observed for LAMM + MQL I and LAMM + MQL II compared to MQL I and MQL II, respectively. Though MQL II did help, laser heating seems to be the dominant assist mechanism in the LAMM + MQL II test condition. Compared to the LAMM test, the LAMM + MQL II test yielded a 41% smaller change in groove width. This is due to the beneficial impact of MQL on tool wear and built-up edge, as will be shown later in this chapter. Interestingly, when compared to LAMM, LAMM + Vortex I and LAMM + Vortex II produced larger changes in groove width, but this is attributed to the reduced thermal expansion of the tool and workpiece due to vortex cooling.

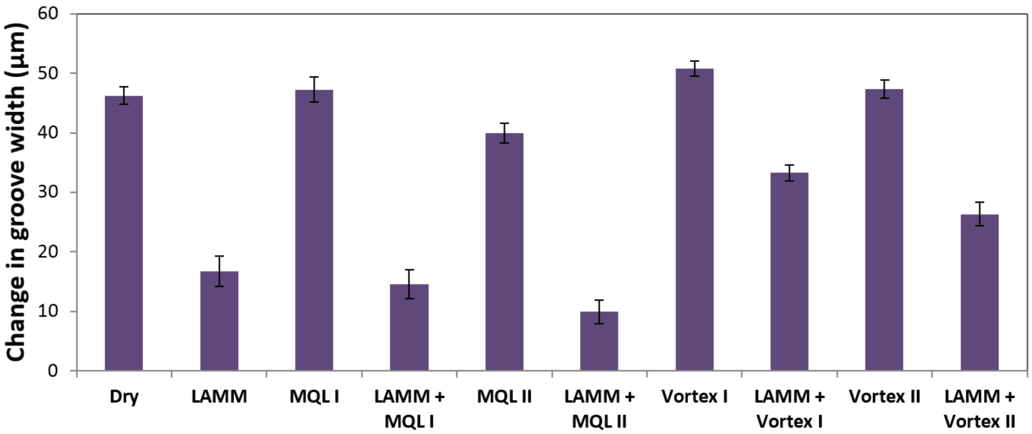

Figure 6.7: Change in groove width (error bars represent 95% confidence interval).

Burr size was measured using the Schäfer burr measurement method [79]. As shown in Figure 6.8, the burr height was measured from the top plane of the workpiece surface to the highest point of the burr. The burr root thickness was characterized by the burr width at the base of the burr. For each test condition, burr measurements were made at five different cross-sections on the left and right edges of the groove for a total of 10 measurements per groove for grooves 1 and 4. The resulting average burr root thickness is shown in Figure 6.9, and the average burr height is shown in Figure 6.10. Burr formation is fairly stochastic, but some trends can be seen. Compared to the dry test condition, LAMM produced larger burrs in groove 1 but not in groove 4. The use of vortex cooling generally produced the smallest change in burr dimensions as a function of tool wear. In the presence of MQL, the burr dimensions in most cases increased with tool wear (groove 1 to groove 4) with or without LAMM.

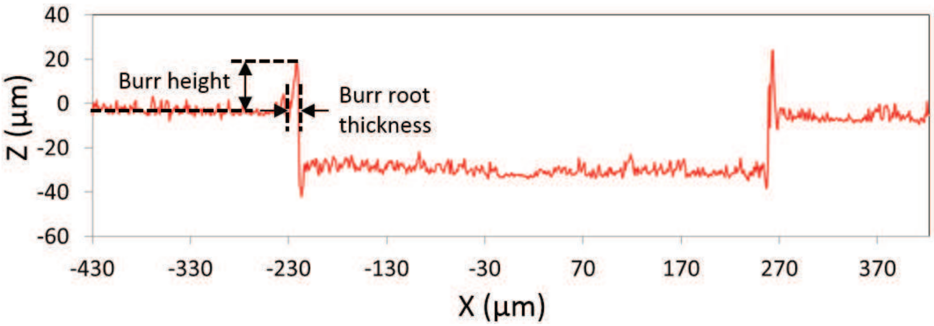

Figure 6.8: Sample groove burr root thickness and height measurements.

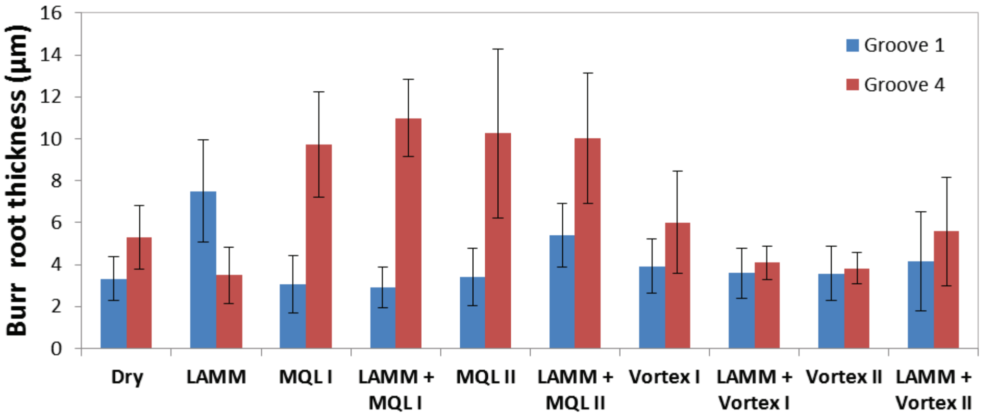

Figure 6.9: Burr root thickness results (error bars represent 95% confidence interval).

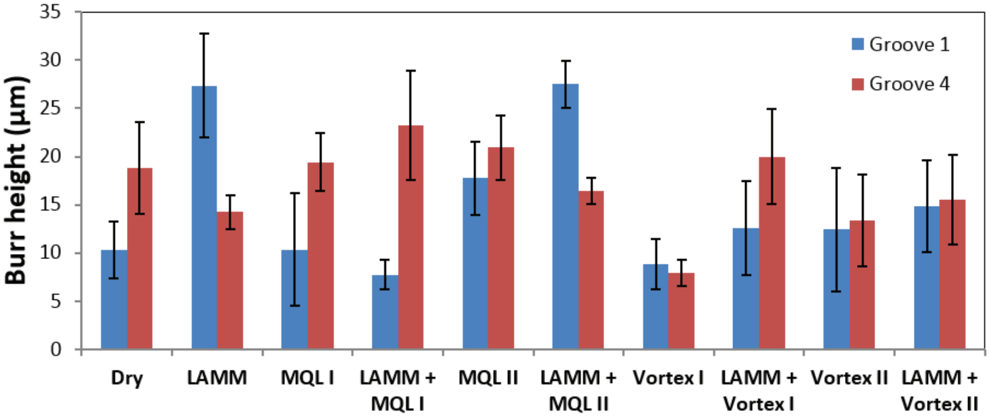

Figure 6.10: Burr height results (error bars represent 95% confidence interval).

The average areal surface roughness ($S_a$) of the groove floor for each test condition is shown in Figure 6.11. It can be seen that in most cases the surface roughness of groove 1 was greater than groove 4. When the tool was new and sharp, it left distinct cutter marks on the surface. But as the tool corner radius and cutting edge wore, the burnishing action of the tool tended to reduce the roughness. This also can be seen from the optical images of the cut surfaces in Figure 6.3 and Figure 6.4. With laser assist, the surface roughness tended to increase in all cases. This is attributed to the ability of LAMM to reduce tool wear thereby maintaining the sharpness of the tool which causes less burnishing and hence a rougher surface.

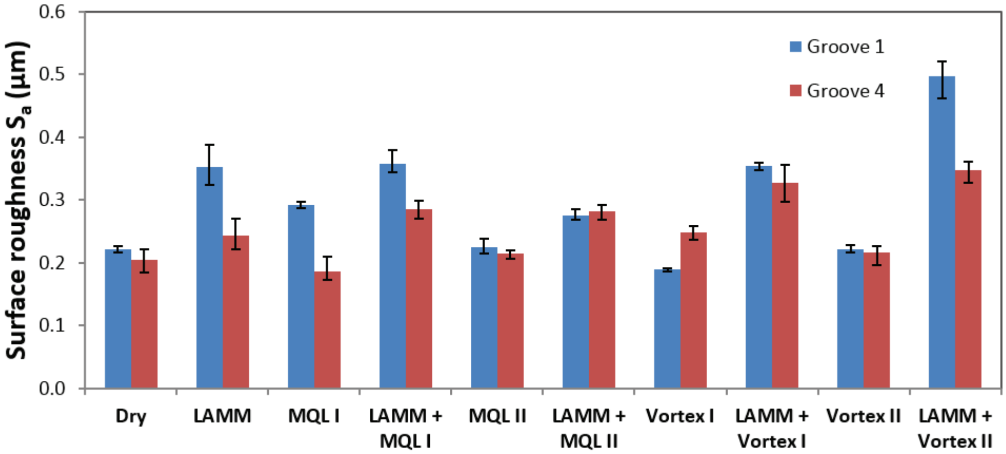

Figure 6.11: Areal surface roughness $S_a$ (error bars represent range).

### 6.3.2 Tool condition

The tool condition was evaluated using optical, confocal, and scanning electron microscopy (SEM). Figure 6.12 shows an example of how the tool corner radius and tool diameter were measured. The average of the corner radii measurements on the two teeth of the tool are reported for each test condition. The tool diameter was measured at the axial depth of cut i.e. 20 μm along the tool axis measured from the tool tip.

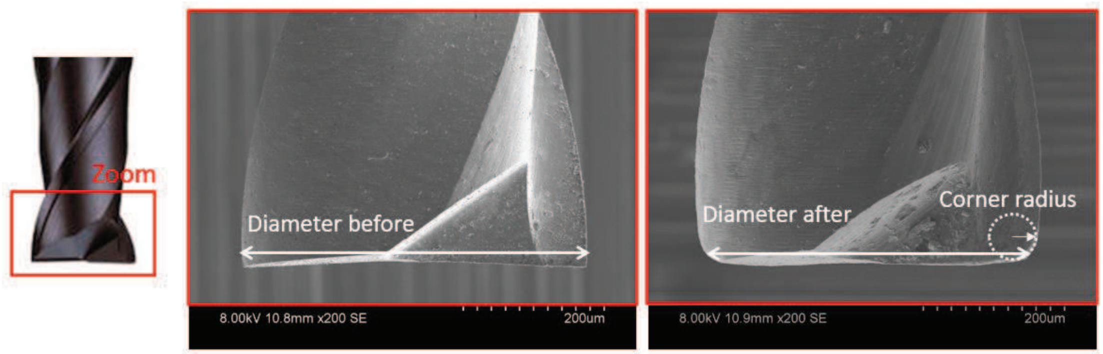

Figure 6.12: Tool diameter and corner radius measurements.

The tool corner radius and the tool diameter results are shown in Figure 6.13 and Figure 6.14, respectively. In the tests without laser assist, the corner radius was best preserved in the Vortex II test. Compared to the dry cutting test, MQL II and Vortex I were only marginally better. Vortex II yielded a sharper corner radius compared to the Vortex I and MQL II tests. This is attributed to the lower tool temperatures produced by the higher air flow rate used in Vortex II, which also helped to aggressively clear chips away from the cutting zone. MQL II did better than MQL I due to the higher air flow rate, which helped to create smaller oil droplets that tend to better penetrate the tool-workpiece interface and adhere to the tool surface. This is consistent with other MQL studies reported in the literature [44] [45]. Interestingly, the change in tool corner radius in the LAMM test was significantly less than in the tests without laser assist. Compared to the dry test, the tool corner radius in LAMM was 31% lower, indicating less tool wear. Among the tests with laser assist, LAMM + MQL II was best able to preserve the tool corner radius. Compared to LAMM, LAMM + MQL II had 27% smaller tool corner radius, indicating less tool wear. The LAMM + Vortex II test also yielded tool corner radius results similar to LAMM + MQL II. It can be seen from Figure 18 that the changes in tool diameter follow trends similar to the tool corner radius trends. Overall, from a standpoint of tool geometry, the LAMM + MQL II test condition yielded the best results.

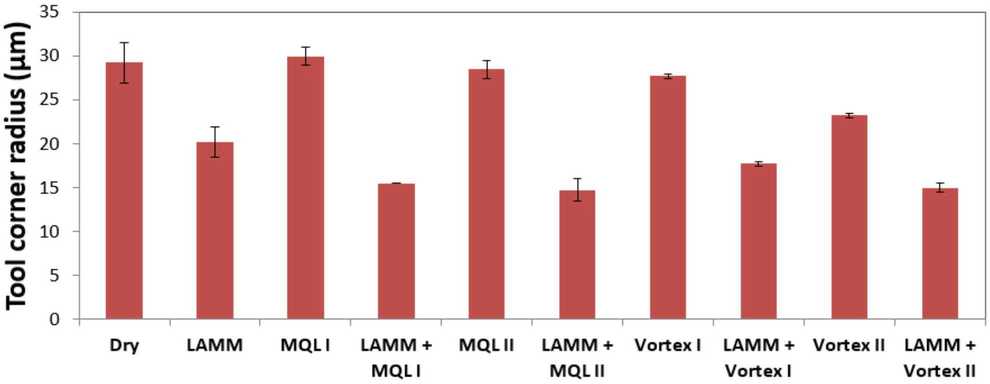

Figure 6.13: Average tool corner radius (error bars represent range).

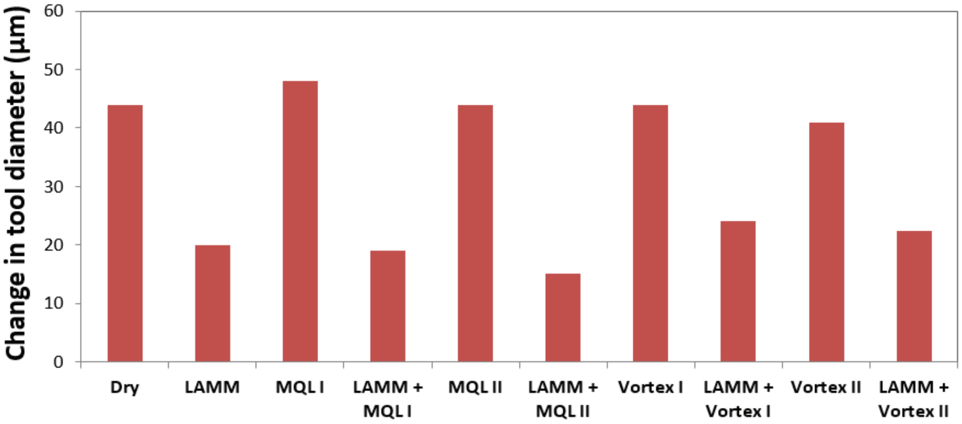

Figure 6.14: Change in tool diameter.

Confocal microscope images of the end view of the tool after each test are shown in Figure 6.15. An image of a new tool is also shown for comparison. SEM images of the peripheral edge of the tool after each test are shown in Figure 6.16.

As can be observed in Figure 6.15 and Figure 6.16, built-up edge does not form on the tool in the tests without laser assist. Visible built-up edge formation is seen in the LAMM, LAMM + Vortex I, and LAMM + Vortex II tests. Built-up edge formation is more prominent in these tests (see Figure 6.16) because the workpiece is thermally softened and is therefore more likely to adhere to the tool. Built-up edge, once formed, will eventually break off and often remove some of the coating, increase wear, or even chip the tool. Interestingly, no built-up edge was evident in the LAMM + MQL I and LAMM + MQL II tests. This is attributed to the enhanced tool surface lubrication by the MQL fluid. This is also the reason that LAMM + MQL II yielded the smallest tool corner radius and the smallest change in tool diameter, as shown earlier in Figure 6.13 and Figure 6.14.

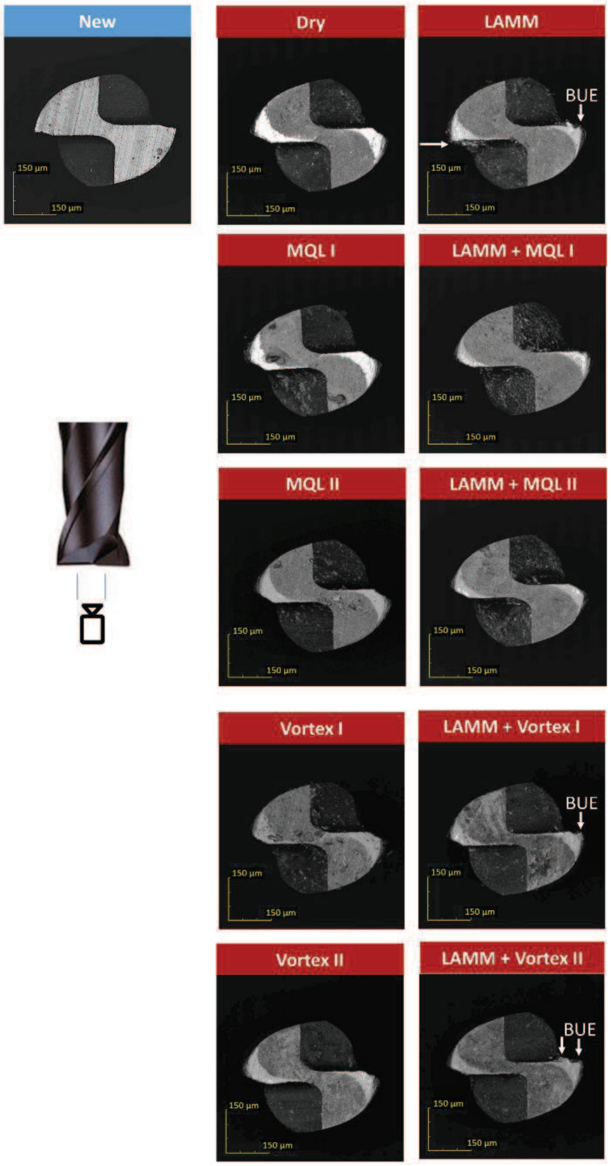

Figure 6.15: End view of tool.

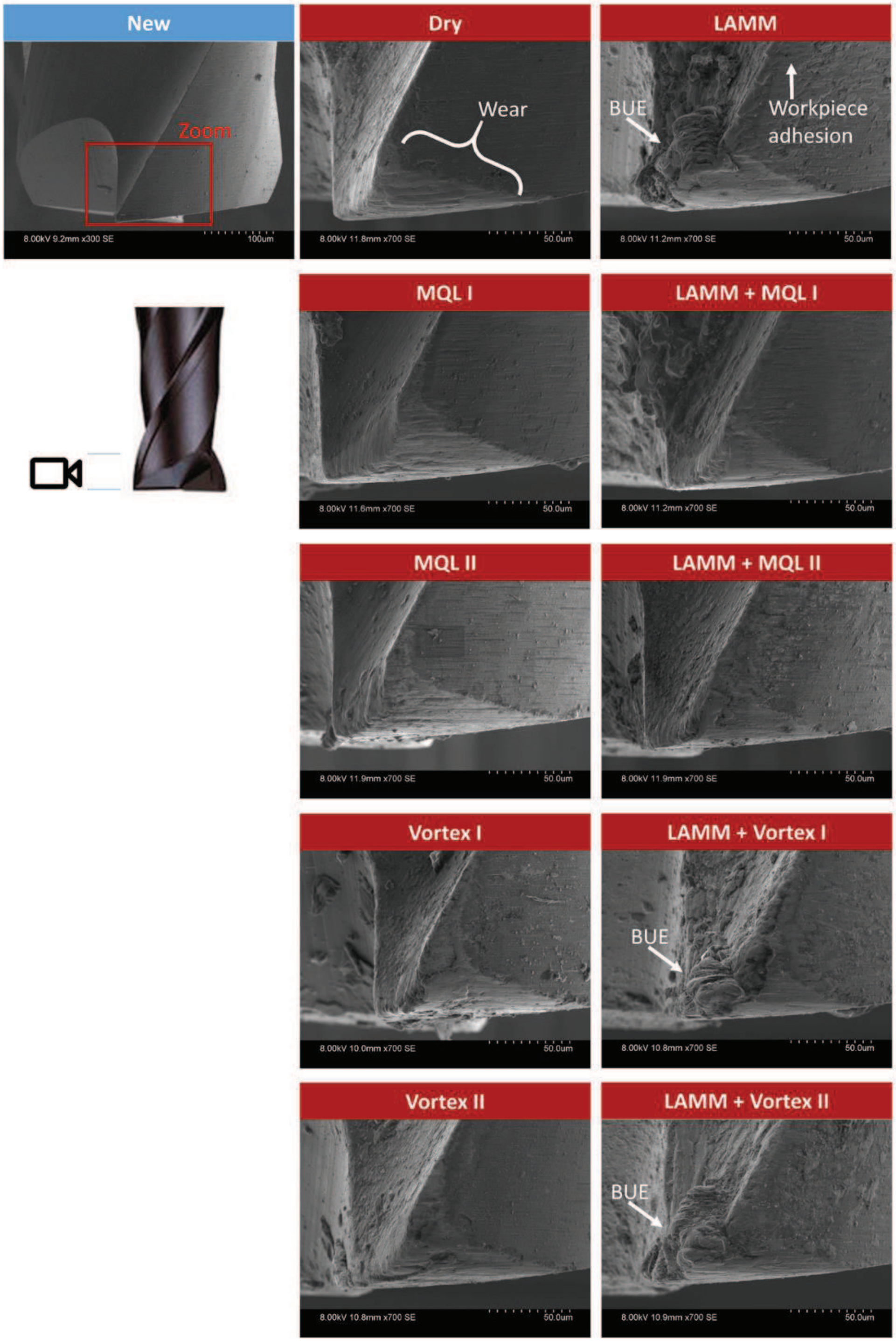

Figure 6.16: SEM images of the peripheral cutting edge of tool showing wear and built-up edge.

As seen in Figure 6.16, a flank wear scar can be observed along the peripheral edge. The maximum flank wear was measured on both cutting edges of the tool in each test according to the ISO 8688-2 standard.

In the tests without laser assist, MQL I and vortex I seemed to decrease flank wear marginally when compared to the dry test. It can be seen that LAMM significantly reduced the flank wear compared to the tests without laser assist. Of the tests with laser assist, LAMM + Vortex I did marginally better.

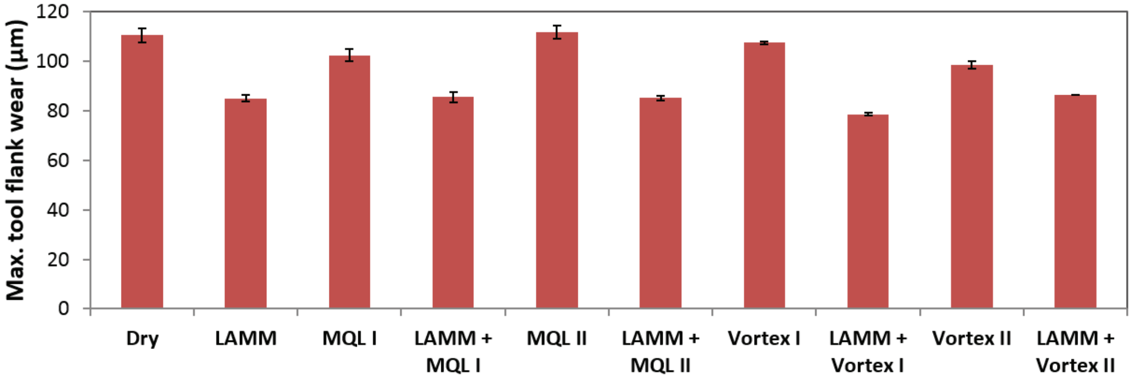

Figure 6.17: Maximum tool flank wear (error bars represent range).

Energy dispersive spectroscopy (EDS) analysis was conducted on the tool used in the LAMM and LAMM + MQL II tests to confirm that the material adhering to the tool surface was indeed built-up edge. Figure 6.18 shows the EDS maps of the tools; the corresponding legend for the observed elements is given in Table 6.3. Red dots on the maps represent iron (Fe) which is prevalent in A-286. Blue dots represent tungsten (W) which is the tool substrate material. Green dots represent titanium (Ti), which is prevalent in the tool coating. Dots are threshold based and show up only for a 1,000 count or stronger signal for the corresponding element. Note that, since the mapping is threshold based, it only shows the locations of built-up edge formation but not how much build-up occurs. As seen in the figure, LAMM is characterized by a large clump of A-286 welded at the tip of the tool along with workpiece adhesion to the right of the cutting edge as well. In contrast, LAMM + MQL II exhibits no A-286 build-up. Yet, in both cases, some of the tool coating is worn exposing the base tungsten.

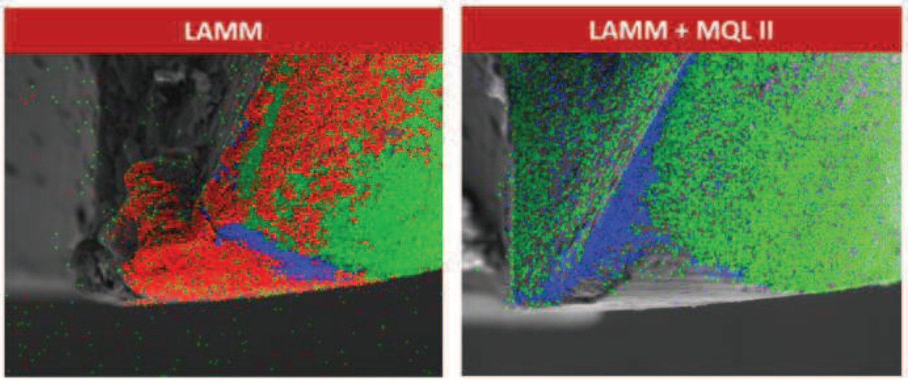

Figure 6.18: EDS maps for LAMM (left) and LAMM + MQL II (right).

Table 6.3: EDS map legend.

| Color | Element | Represents |
|---|---|---|
| Red | Iron | A-286 |
| Blue | Tungsten | Tool base substrate |
| Green | Titanium | Tool coating |

To determine the amount of built-up edge, EDS was performed on a 100μm X 60μm area along the peripheral edge of only the five laser assisted tests. The weight percentages (wt. %) of the main elements of the tool and workpiece materials are shown in Figure 6.19. Minor elements (O, N, and C) were not included because of their prevalent nature in the atmosphere while Cu and Ca were neglected due to their very small weight percentages. In LAMM, almost 45 wt. % of the mapped area of the tool surface was made of chemical elements from the workpiece material (A-286), indicating that there was significant workpiece adhesion. In comparison, the LAMM + MQL II test only had 23 wt. % of A-286 elements, implying considerably less workpiece material adhesion (built-up edge) on the tool surface. The LAMM + MQL II test also preserved more of the tool coating than any other test, as indicated by the presence of Al and Ti in the EDS spectrum. Compared to LAMM, the LAMM + Vortex I and the LAMM + Vortex II tests did marginally better in minimizing workpiece adhesion.

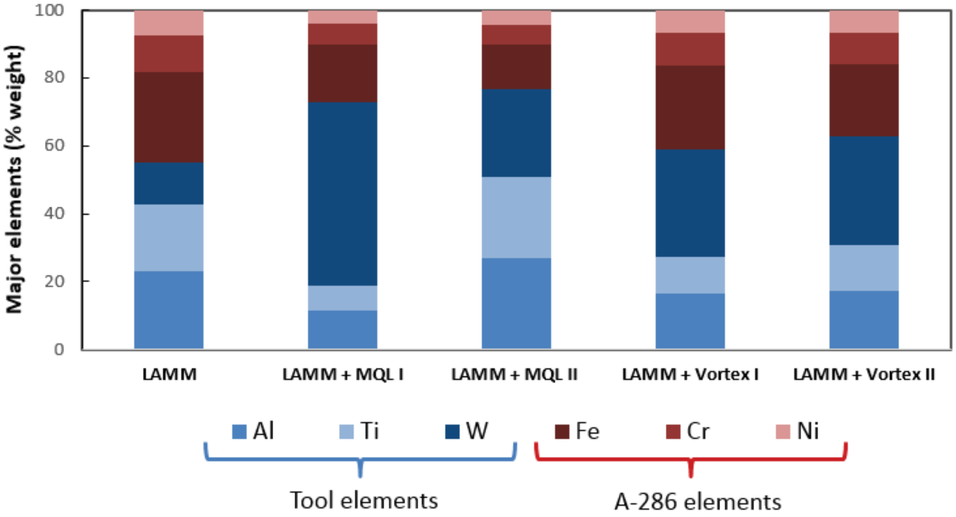

Figure 6.19: Elemental composition of the mapped area of tool surface in the LAMM tests.

### 6.3.3 Cutting forces

The average resultant cutting forces were computed from the measured X, Y, Z forces.The average resultant force results for the ten test conditions are shown in Figure 6.20. In all tests, the force was always lower for groove 1 than for groove 4, which is due to tool wear. Comparing the results for groove 1, as expected, the dry test yielded the highest average resultant force while the LAMM + Vortex I test gave the lowest average resultant force. Groove 4 was a better indicator because it showed how each assist method affects the cutting forces after a prolonged period of cutting. Of the tests without laser assist, Vortex I was an anomaly with the lowest resultant force. Vortex I also has the lowest groove depth results as shown earlier in Figure 6.6, which explains the anomaly. As expected, the tests with laser assist yielded lower forces than their non-laser assisted counterparts. Compared to the dry test, the average resultant force in the LAMM test decreased by 39%. In comparison to LAMM, the LAMM + MQL II test reduced forces an additional 10%. This is likely due to reduced friction and built-up edge due to lubrication. Compared to LAMM, LAMM + Vortex I and LAMM + Vortex II showed ~15% reductions in the average resultant force.

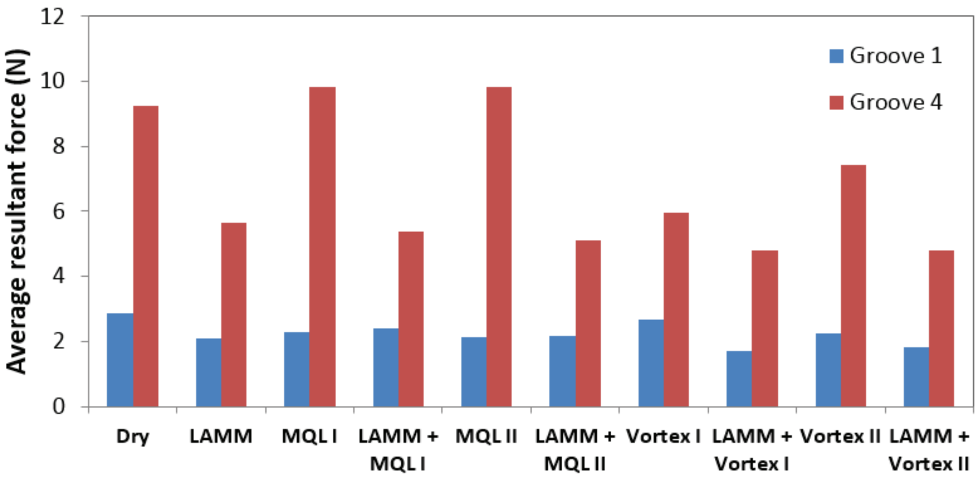

Figure 6.20: Average resultant force.

Because the depth of cut was seen to vary in some of the experiments, the average resultant force was normalized by the measured depth of cut and is shown in Figure 6.21. In this case, it was seen that LAMM + MQL I yielded the lowest forces per unit depth, while LAMM + MQL II was a close second. As a consequence of the shallow measured depth of cut, Vortex I yielded an unusually high average resultant force per unit depth. Otherwise, the overall trends are similar to those seen in Figure 6.20.

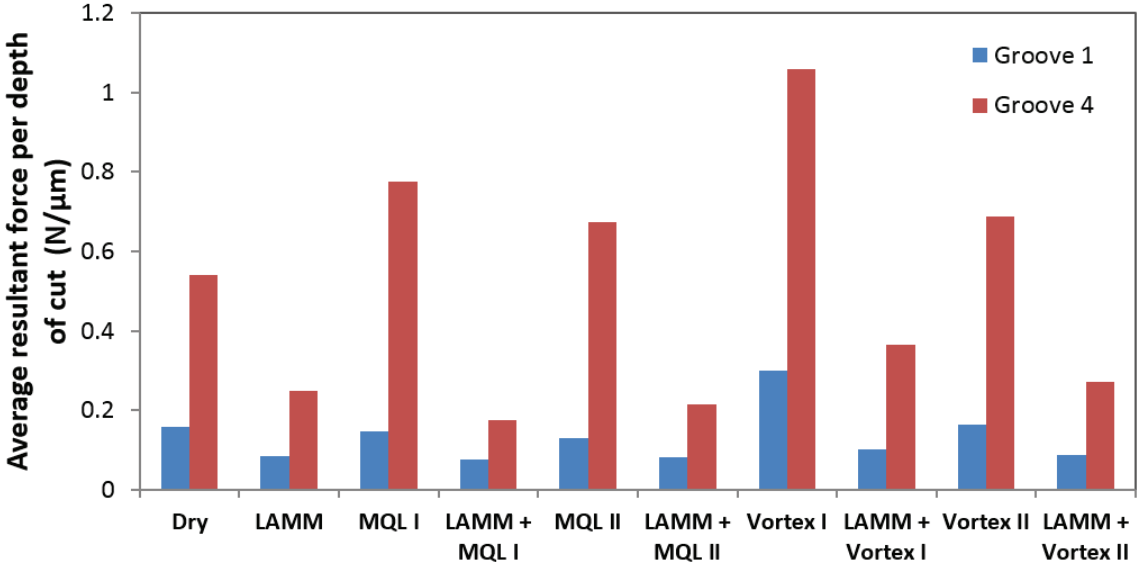

Figure 6.21: Average resultant force per unit depth of cut.

## 6.4 Summary

This chapter investigates the use of MQL and vortex cooling in the LAMM process to further enhance micromachinability of a high nickel content metal (A-286). The main conclusions of the study are:

- Vortex cooling typically produces shallower and narrower grooves, which is attributed to thermal contraction of the workpiece.
- Compared to dry cutting, LAMM yielded more accurate groove dimensions. It reduced the change groove width by 64%. The addition of MQL further enhanced the groove accuracy. In particular, compared to LAMM, LAMM + MQL II further lowered the change in groove width by 41%.
- Compared to dry cutting, LAMM increased burr size. In addition to LAMM, vortex cooling typically decreased burr size, and MQL increased burr size.
- Compared to tests without laser assist, the use of LAMM generally yielded higher surface roughness due to increased ductility of the work material and reduced burnishing effect because of the sharper tool cutting edges. LAMM + Vortex II resulted in the highest surface roughness.
- When using MQL, higher air flows (as in MQL II) allowed for better lubrication of the tool surfaces and less adhesion of work material to the tool.
- When using vortex cooling, higher air flows (as in Vortex II) allowed for better chip removal and cooling of the tool.
- Laser assist was the dominant method to reduce tool wear. Compared to dry, LAMM reduced the change in tool corner radius by 31%. MQL further aided laser

assist. Compared to LAMM, LAMM + MQL II decreased the tool corner radius by an additional 27%.

- Addition of MQL to LAMM prevents built-up edge formation.
- Laser assist greatly reduced the resultant force. Compared to dry, LAMM reduced the average resultant force by 39%. Compared to LAMM, LAMM + MQL II and LAMM + Vortex II reduced the average resultant force by an additional 10% and 15%, respectively.
- Overall, LAMM + MQL II was found to be the best test condition with the least tool wear, least built-up edge, and the least change in groove width.

# CHAPTER 7: CONCLUSIONS AND RECOMMENDATIONS

This chapter summarizes the main conclusions of this thesis and suggests related areas for further investigation. The main conclusions of this thesis are as follows.

## 7.1 Comparison of dry cutting, wet assist, and LAMM

In Chapter 4, micro milling experiments were run with dry, wet, and laser assist methods under a wide range of cutting conditions. Compared to the dry cutting and wet assist methods, LAMM was found to yield the best results overall. The following specific conclusions related to LAMM can be drawn from the results presented in this chapter:

- LAMM improved the groove condition and maintained a more precise depth of cut.
- LAMM reduced tool diameter wear by 29% and 22% compared to dry cutting and use of wet assist, respectively. Overall, LAMM preserved the tool condition better than the wet assist case.
- LAMM decreased the mean resultant force on average by 10% when compared to the dry case.
- The 18 W LAMM process combined with machining condition 3 (cutting speed of 19 m/min, feed of 0.03 mm/tooth, axial depth of cut of 0.02 mm) was found to be the best combination of assist mechanism and machining conditions to micro mill A-286.

## 7.2 Tool life in LAMM

Chapter 5 presented the results of an extended duration (25 minutes) LAMM tool life test carried out using the previously identified cutting conditions for micromachining of hardened A-286 (41.8 $HR_c$). The groove condition, tool wear, and cutting forces were monitored during the test. The main conclusions of Chapter 5 are:

- When the tool was new and sharp, the initial shallow groove had a square cross-section and its bottom surface showed distinct cutter marks. As the tool wore, the shallow grooves developed a tapered and rounded cross section, and a burnishing effect could be seen on the bottom surface of the groove. Non-uniform burrs on the groove edges became more prevalent over the test duration.
- Throughout the test, the shallow groove depth was quite consistent and overshot the programmed or target depth by an average of 6.3 μm. This is attributed to the thermal expansion of the workpiece due to laser heating.
- As more material was removed, the tool wore, and the shallow groove width decreased rapidly in the first 50 mm3, but reached a steady state thereafter.
- Similar to the shallow grooves, the initial deep groove had distinct cutter marks, but as time progressed, burnishing of the groove surface became more prevalent, and burrs were observed along the edges of the groove. As the tool wore, the deep grooves exhibited mild tapering and rounding of the cross-sectional profile, which was not as significant as seen in the shallow grooves. This was due to the groove being cut by multiple passes.
- Built-up edge formation was prevalent and tended to increase over the test duration.

- The tool corner radius and tool diameter exhibited rapid changes in the first 20 mm3 of material removal, after which they changed gradually.
- The average and peak resultant forces increased linearly due to tool wear over the test duration.

## 7.3 Effect of MQL and vortex cooling on micromachinability in LAMM

Chapter 6 investigated the use of MQL and vortex cooling in the LAMM process to further enhance micromachinability. The main conclusions of this work are:

- Vortex cooling typically produces shallower and narrower grooves, which is attributed to thermal contraction of the workpiece.
- Compared to dry cutting, LAMM yielded more accurate groove dimensions. It reduced the change in groove width by 64%. The addition of MQL further enhanced the groove accuracy. In particular, compared to LAMM, LAMM + MQL II further lowered the change in groove width by 41%.
- Compared to dry cutting, LAMM increased burr size. In addition to LAMM, vortex cooling typically decreased burr size, and MQL increased burr size.
- Compared to tests without laser assist, the use of LAMM generally yielded higher surface roughness due to increased ductility of the work material and reduced burnishing effect because of the sharper tool cutting edges. LAMM + Vortex II resulted in the highest surface roughness.
- When using MQL, higher air flows (as in MQL II) allowed for better lubrication of the tool surfaces and less adhesion of work material to the tool.

- When using vortex cooling, higher air flows (as in Vortex II) allowed for better chip removal and cooling of the tool.
- Laser assist was the dominant method to reduce tool wear. Compared to dry, LAMM reduced the change in tool corner radius by 31%. MQL further aided laser assist. Compared to LAMM, LAMM + MQL II decreased the tool corner radius by an additional 27%.
- The addition of MQL to LAMM prevents built-up edge formation.
- Laser assist greatly reduced the resultant force. Compared to dry, LAMM reduced the average resultant force by 39%. Compared to LAMM, LAMM + MQL II and LAMM + Vortex II reduced the average resultant force by an additional 10% and 15%, respectively.
- Overall, LAMM + MQL II was found to be the best test condition with the least tool wear, least built-up edge, and the least change in groove width.

## 7.4 Overall remarks and recommendations for future work

The results presented in Chapters 4-6 show that hybrid processes, like LAMM, have the potential to significantly enhance micromachinability of difficult-to-cut metals compared to dry cutting, cutting using wet assist, MQL, and vortex cooling alone. With the addition of MQL, the micromachinability of LAMM improved and built-up edge formation was greatly reduced. Future work should further investigate the effects of MQL. A heat affected zone was observed in the LAMM + MQL cases, but not when using LAMM alone. A better understanding of how the oil in MQL alters the absorption of laser irradiation is needed to optimize the laser parameters to prevent the formation of a heat affected zone in the workpiece.

Studies have been done in macroscale turning using a hybrid process consisting of LAM combined with cryogenic cooling [54]. Cryogenic cooling of the tool could be implemented in LAMM. Cryogenic cooling would have to be properly focused on the tool to prevent excessive thermal contraction of the workpiece as was shown in Chapter 6 when using vortex cooling. Further investigations are needed to understand the benefits and limitations of cryogenic cooling in LAMM.

AlCrN coated tools have recently proven to be highly effective for nickel based alloys [28] [29]. Although LAMM studies have used various tool coatings [63], work to examine the viability of AlCrN coated tools in LAMM is lacking.

# APPENDIX

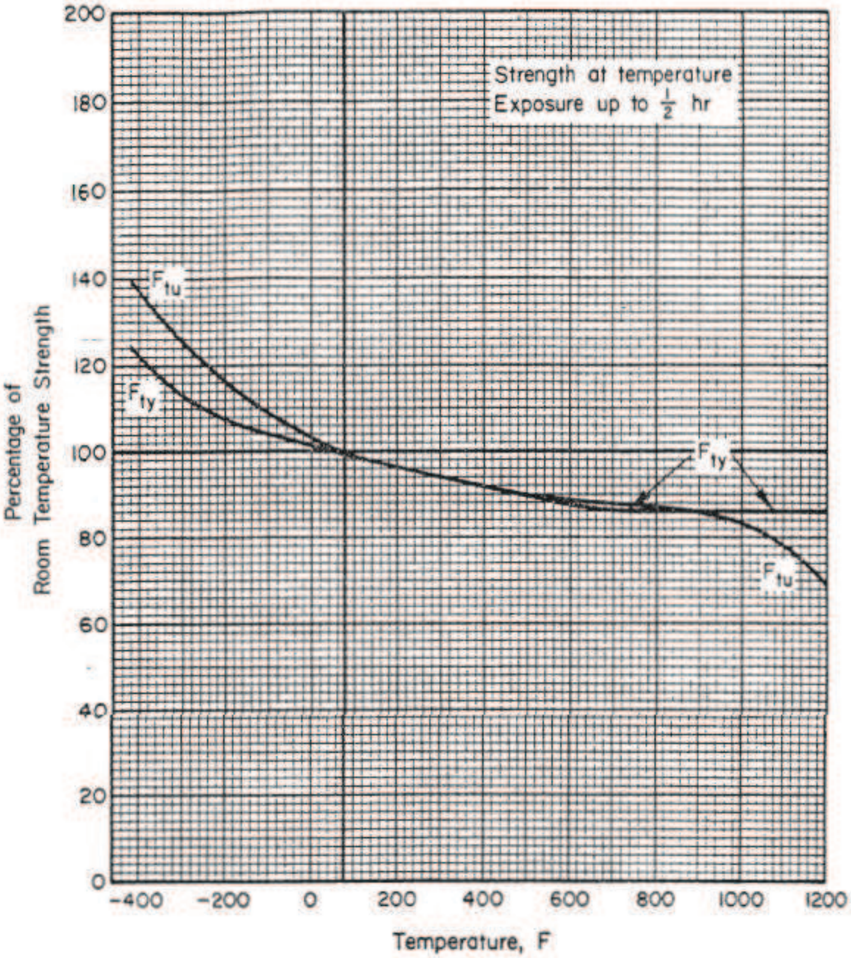

Figure A.1: A-286 tensile yield, $F_{ty}$, and ultimate tensile strength, $F_{tu}$, as a function of temperature. At room temperature $F_{ty} = 85$ ksi and $F_{tu} = 130$ ksi [67].

Table A.1: Tool wear measurement frequency.

| Groove | Type of groove | Machining time (mins) | Tool diameter | Tool corner radius | Tool bottom edge | Flank wear |
|---|---|---|---|---|---|---|
| 1 | Shallow | 0.05 | Yes | Yes | Yes | Yes |
| 2 | Medium | 0.28 | | | | |
| 3 | Shallow | 0.33 | Yes | Yes | Yes | Yes |
| 4 | Deep | 1.17 | | | | |
| 5 | Deep | 2.02 | | | | |
| 6 | Deep | 2.86 | | | | |
| 7 | Shallow | 2.91 | Yes | Yes | Yes | Yes |
| 8 | Deep | 3.76 | | | | |
| 9 | Deep | 4.60 | | | | |
| 10 | Deep | 5.45 | | | | |
| 11 | Shallow | 5.49 | Yes | Yes | Yes | |
| 12 | Deep | 6.34 | | | | |
| 13 | Deep | 7.18 | | | | |
| 14 | Deep | 8.03 | | | | |
| New | Workpiece | | | | | |
| 15 | Shallow | 8.07 | Yes | Yes | Yes | Yes |
| 16 | Deep | 8.92 | | | | |
| 17 | Deep | 9.76 | | | | |
| 18 | Shallow | 9.81 | Yes | Yes | Yes | |
| 19 | Deep | 10.66 | | | | |
| 20 | Deep | 11.50 | | | | |
| 21 | Deep | 12.35 | | | | |
| 22 | Shallow | 12.39 | Yes | Yes | Yes | Yes |
| 23 | Deep | 13.24 | | | | |
| 24 | Deep | 14.08 | | | | |
| 25 | Deep | 14.93 | | | | |
| 26 | Shallow | 14.97 | Yes | Yes | Yes | |
| 27 | Deep | 15.82 | | | | |
| 28 | Deep | 16.66 | | | | |
| New | Workpiece | | | | | |
| 29 | Shallow | 16.71 | Yes | Yes | Yes | Yes |
| 30 | Deep | 17.56 | | | | |
| 31 | Deep | 18.40 | | | | |
| 32 | Shallow | 18.45 | Yes | Yes | Yes | |
| 33 | Deep | 19.29 | | | | |
| 34 | Deep | 20.14 | | | | |
| 35 | Deep | 20.98 | | | | |
| 36 | Shallow | 21.03 | Yes | Yes | Yes | Yes |
| 37 | Deep | 21.88 | | | | |
| 38 | Deep | 22.72 | | | | |
| 39 | Deep | 23.56 | | | | |

|  |  |  |  |  |  |  |
|---|---|---|---|---|---|---|
| 40 | Shallow | 23.61 | Yes | Yes | Yes |  |
| 41 | Deep | 24.46 |  |  |  |  |
| 42 | Deep | 25.30 |  |  |  |  |
| Post | Analysis |  | Yes | Yes | Yes | Yes |

# REFERENCES

[1] Câmara, M. A., Rubio, J. C. C., Abrão, A. M., Davim, J. P. State of the art on micromilling of materials, a review. Journal of Materials Science & Technology 2012; 28:673-685.

[2] Lee, K., Dornfeld, D. A. Micro-burr formation and minimization through process control. Precision Engineering 2005; 29:246-252.

[3] Debnath, S., Reddy, M. M., Qua Sok, Y. Environmental friendly cutting fluids and cooling techniques in machining: A review. Journal of Cleaner Production 2014; 83:33-47.

[4] Nevala, S. E., Wifvat, V. T., Johnson, S. A., Wentz, J. E. Relative effects of cooling and lubrication in micro-milling of aluminum and the design of atomization cooling and lubrication systems. ASME 2012 International Mechanical Engineering Congress and Exposition, IMECE 2012, November 9, 2012 - November 15, 2012, 2012, Houston, TX, United states; pp. 1979-1986.

[5] Cong, W., Pei, Z. J. Dry machining using vortex-tube generated cold air as coolant: A literature review. ASME International Manufacturing Science and Engineering Conference, MSEC2008, October 7, 2008 - October 10, 2008, 2009, Evanston, IL, United states; pp. 447-455.

[6] Rubio, E. M., Agustina, B., Marín, M., Bericua, A. Cooling systems based on cold compressed air: A review of the applications in machining processes. Procedia Engineering 2015; 132:413-418.

[7] Kumar, M., Laser assisted micro milling of hard materials, PhD Thesis, 2011, School of Mechanical Engineering, Georgia Institute of Technology.

[8] Mian, A. J., Driver, N., Mativenga, P. T. Identification of factors that dominate size effect in micro-machining. International Journal of Machine Tools and Manufacture 2011; 51:383-394.

[9] Vollertsen, F., Biermann, D., Hansen, H. N., Jawahir, I. S., Kuzman, K. Size effects in manufacturing of metallic components. CIRP Annals - Manufacturing Technology 2009; 58:566-587.

[10] Simoneau, A., Ng, E., Elbestawi, M. A. Grain size and orientation effects when microcutting aisi 1045 steel. CIRP Annals - Manufacturing Technology 2007; 56:57-60.

[11] Filiz, S., Conley, C. M., Wasserman, M. B., Ozdoganlar, O. B. An experimental investigation of micro-machinability of copper 101 using tungsten carbide micro-endmills. International Journal of Machine Tools and Manufacture 2007; 47:1088-1100.

[12] Lucca, D. A., Rhorer, R. L., Komanduri, R. Energy dissipation in the ultraprecision machining of copper. 41st General Assembly of CIRP, Aug 18 - 24 1991, 1991, Palo Alto, CA, United states; pp. 69-72.

[13] Piljek, P., Keran, Z., Math, M. Micromachining -review of literature from 1980 to 2010. Interdisciplinary Description of Complex Systems 2014; 12:1-27.

[14] Leo Kumar, S. P., Jerald, J., Kumanan, S., Prabakaran, R. A review on current research aspects in tool-based micromachining processes. Materials and Manufacturing Processes 2014; 29:1291-1337.

[15] Cardoso, P., Davim, J. P. Micro milling of metallic materials: A brief overview. Transactions of Famena 2012; 36:79-85.

[16] Cardoso, P., Davim, J. P. A brief review on micromachining of materials. Reviews on Advanced Materials Science 2012; 30:98-102.

[17] Bissacco, G., Hansen, H. N., Slunsky, J. Modelling the cutting edge radius size effect for force prediction in micro milling. CIRP Annals - Manufacturing Technology 2008; 57:113-116.

[18] Ku, M. S., Kang, I. S., Kim, J. S. An investigation of machining characteristics in micro-scale milling process. AIP Conference Proceedings 2011; 1315:1627-1632.

[19] Jin, X., Altintas, Y. Slip-line field model of micro-cutting process with round tool edge effect. Journal of Materials Processing Technology 2011; 211:339-355.

[20] Lai, X., Li, H., Li, C., Lin, Z., Ni, J. Modelling and analysis of micro scale milling considering size effect, micro cutter edge radius and minimum chip thickness. International Journal of Machine Tools and Manufacture 2008; 48:1-14.

[21] Huo, D., Cheng, K., Wardle, F. Design of a five-axis ultra-precision micro-milling machine—ultramill. Part 1: Holistic design approach, design considerations and specifications. The International Journal of Advanced Manufacturing Technology 2010; 47:867-877.

[22] Dornfeld, D., Min, S., Takeuchi, Y. Recent advances in mechanical micromachining. CIRP Annals - Manufacturing Technology 2006; 55:745-768.

[23] Chae, J., Park, S. S., Freiheit, T. Investigation of micro-cutting operations. International Journal of Machine Tools and Manufacture 2006; 46:313-332.

[24] Yao, S. H. Evaluation of tin/aln nano-multilayer coatings on drills used for micro-drilling. Surface and Coatings Technology 2005; 197:351-357.

[25] Yao, S. H., Kao, W. H., Su, Y. L., Liu, T. H. On the tribology and micro-drilling performance of tin/aln nanolayer coatings. Materials Science and Engineering: A 2004; 386:149-155.

[26] Kao, W. H. High-speed drilling performance of coated micro-drills with zr–c:H:Nx% coatings. Wear 2009; 267:1068-1074.

[27] Aramcharoen, A., Mativenga, P. T., Yang, S., Cooke, K. E., Teer, D. G. Evaluation and selection of hard coatings for micro milling of hardened tool steel. International Journal of Machine Tools and Manufacture 2008; 48:1578-1584.

[28] Biermann, D., Steiner, M., Krebs, E. Investigation of different hard coatings for micromilling of austenitic stainless steel. Procedia CIRP 2013; 7:246-251.

[29] Ucun, İ., Aslantas, K., Bedir, F. An experimental investigation of the effect of coating material on tool wear in micro milling of inconel 718 super alloy. Wear 2013; 300:8-19.

[30] Thepsonthi, T., Özel, T. Multi-objective process optimization for micro-end milling of ti-6al-4v titanium alloy. The International Journal of Advanced Manufacturing Technology 2012; 63:903-914.

[31] Arif, M., Rahman, M., San, W. Y. Ultraprecision ductile mode machining of glass by micromilling process. Journal of Manufacturing Processes 2011; 13:50-59.

[32] Arif, M., Rahman, M., San, W. Y. An experimental investigation into micro ball end-milling of silicon. Journal of Manufacturing Processes 2012; 14:52-61.

[33] Attanasio, A., Gelfi, M., Pola, A., Ceretti, E., Giardini, C. Influence of material microstructures in micromilling of ti6al4v alloy. Materials 2013; 6:4268-4283.

[34] Wu, J. Experimental evaluation of surface roughness in orthogonal micro-milling processes. 2nd International Conference on Advanced Design and Manufacturing Engineering, ADME 2012, August 16, 2012 - August 18, 2012, 2012, Taiyuan, China; pp. 1912-1916.

[35] Pei, Y., Yiming, R., Gang, W. The effect of cutting fluids applied in metal cutting process. Proceedings of the Institution of Mechanical Engineers, Part B (Journal of Engineering Manufacture) 2016; 230:19-37.

[36] Perçin, M., Aslantas, K., Ucun, İ., Kaynak, Y., Çicek, A. Micro-drilling of ti–6al–4v alloy: The effects of cooling/lubricating. Precision Engineering 2016; 45:450-462.

[37] Monroy-Vazquez, K. P., Attanasio, A., Ceretti, E., Siller, H. R., Hendrichs-Troeglen, N. J., Giardini, C. Evaluation of superficial and dimensional quality features in metallic micro-channels manufactured by micro-end-milling. Materials 2013; 6:1434-1451.

[38] Wada, T., Morigo, Y., Tanaka, H. Tool wear of sintered cubic boron nitride compact in cutting high-nickel alloy with high-pressure coolant supplied. Funtai Oyobi Fummatsu Yakin/Journal of the Japan Society of Powder and Powder Metallurgy 2016; 63:157-165.

[39] Al-Falahi, M., Baharudin, B. T., Hong, T. S., Matori, K. A. Surface defects in groove milling of hastelloy-c276 under fluid coolant. 2015; 1-9.

[40] Pei, Y., Xiang, S., Gang, W., Yiming, R. Preliminary experimental study on effect of cutting fluid on milled surface quality of iron-base superalloy. Advanced Materials Research 2015; 1077:61-65.

[41] Kajaria, S., Chittipolu, S., Adera, S., Hung, W. N. Micromilling in minimum quantity lubrication. Machining Science and Technology 2012; 16:524-546.

[42] Vazquez, E., Gomar, J., Ciurana, J., Rodríguez, C. A. Analyzing effects of cooling and lubrication conditions in micromilling of ti6al4v. Journal of Cleaner Production 2015; 87:906-913.

[43] Vazquez, E., Kemmoku, D. T., Noritomi, P. Y., Da Silva, J. V. L., Ciurana, J. Computer fluid dynamics analysis for efficient cooling and lubrication conditions in micromilling of ti6al4v alloy. Materials and Manufacturing Processes 2014; 29:1494-1501.

[44] Ming, C., Li, J., Bowen, S., Zhigiang, L., Qinglong, A. Cfd analysis on the flow field of minimum quantity lubrication during external thread turning. Materials Science Forum 2012; 723:113-118.

[45] Li, K.-M., Chou, S.-Y. Experimental evaluation of minimum quantity lubrication in near micro-milling. Journal of Materials Processing Technology 2010; 210:2163-2170.

[46] Yalcin, B., Ozgur, A. E., Koru, M. The effects of various cooling strategies on surface roughness and tool wear during soft materials milling. Materials &amp; Design 2009; 30:896-899.

[47] Liu, J., Kevin Chou, Y. On temperatures and tool wear in machining hypereutectic al–si alloys with vortex-tube cooling. International Journal of Machine Tools and Manufacture 2007; 47:635-645.

[48] Liu, J., Kevin Chou, Y. Vortex-tube cooling for tool wear reduction in a390 dry machining. 2005 World Tribology Congress III, September 12, 2005 - September 16, 2005, 2005, Washington, D.C., United states; pp. 837-838.

[49] Su, Y., He, N., Li, L., Iqbal, A., Xiao, M. H., Xu, S. , et al. Refrigerated cooling air cutting of difficult-to-cut materials. International Journal of Machine Tools &amp; Manufacture 2007; 47:927-933.

[50] Venkatesan, K., Ramanujam, R., Kuppan, P. Laser assisted machining of difficult to cut materials: Research opportunities and future directions - a comprehensive review. Procedia Engineering 2014; 97:1626-1636.

[51] Rajagopal, S., Plankenhorn, D. J., Hill, V. L. Machining aerospace alloys with the aid of a 15 kw laser. Journal of Applied Metalworking 1982; 2:170-184.

[52] Anderson, M., Patwa, R., Shin, Y. C. Laser-assisted machining of inconel 718 with an economic analysis. International Journal of Machine Tools and Manufacture 2006; 46:1879-1891.

[53] Bermingham, M. J., Sim, W. M., Kent, D., Gardiner, S., Dargusch, M. S. Tool life and wear mechanisms in laser assisted milling ti–6al–4v. Wear 2015; 322–323:151-163.

[54] Dandekar, C. R., Shin, Y. C., Barnes, J. Machinability improvement of titanium alloy (ti–6al–4v) via lam and hybrid machining. International Journal of Machine Tools and Manufacture 2010; 50:174-182.

[55] Mohid, Z., Warap, N. M., Ibrahim, R., Rhim, E. A. Laser assisted micro-groove ball milling of ti6al4v. 5th International Conference on Mechanical and Manufacturing Engineering, Oct 29-30, 2014, Bandung, Indonesia; pp. 55-59.

[56] Rahim, E. A., Warap, N. M., Mohid, Z., Ibrahim, R. Investigation on laser assisted micro ball milling of inconel 718. 5th International Conference on Mechanical and Manufacturing Engineering, October 29- 30, 2014, Bandung, Indonesia; pp. 79-83.

[57] Hongtao, D., Ninggang, S., Shin, Y. C. Thermal and mechanical modeling analysis of laser-assisted micro-milling of difficult-to-machine alloys. Journal of Materials Processing Technology 2012; 212:601-613.

[58] Shelton, J. A., Shin, Y. C. An experimental evaluation of laser-assisted micromilling of two difficult to machine alloys. ASME International Manufacturing Science and Engineering Conference, Oct 7-10, 2008, Evanston, IL; pp. 311-320.

[59] Shelton, J. A., Shin, Y. C. Experimental evaluation of laser-assisted micromilling in a slotting configuration. Journal of Manufacturing Science and Engineering 2010; 132:021008-021008.

[60] Jeon, Y., Pfefferkorn, F. Effect of laser preheating the workpiece on micro end milling of metals. Journal of Manufacturing Science and Engineering 2008; 130:011004-011004.

[61] Pfefferkorn, F., Lei, S. A metric for defining the energy efficiency of thermally-assisted machining. International Conference on Manufacturing Science and Engineering, Oct 8-11, 2006, Ypsilanti, MI; pp. 59-66.

[62] Ozel, T., Pfefferkorn, F. Pulsed laser assisted micromilling for die/mold manufacturing. ASME International Manufacturing Science and Engineering Conference, Jan 15 - Oct 18, 2007, Atlanta, GA; pp. 337-342.

[63] Kumar, M., Melkote, S. N., M'Saoubi, R. Wear behavior of coated tools in laser assisted micro-milling of hardened steel. Wear 2012; 296:510-518.

[64] Kumar, M., Melkote, S. N. Process capability study of laser assisted micro milling of a hard-to-machine material. Journal of Manufacturing Processes 2012; 14:41-51.

[65] Kumar, M., Chang, C.-J., Melkote, S. N., Roshan Joseph, V. Modeling and analysis of forces in laser assisted micro milling. Journal of Manufacturing Science and Engineering 2013; 135:041018-041018.

[66] Wang, Z. Y., Rajurkar, K. P., Fan, J., Lei, S., Shin, Y. C., Petrescu, G. Hybrid machining of inconel 718. International Journal of Machine Tools and Manufacture 2003; 43:1391-1396.

[67] Military handbook - mil-hdbk-5h: Metallic materials and elements for aerospace vehicle structures U.S Department of Defense, 2008.

[68] Carslaw, H. S., Jaeger, J. C., Conduction of heat in solids: Clarendon Press, 1986.

[69] Cverna, F. Thermal properties of metals. ASM International, Materials Park, OH 2002;

[70] Loewen, E., Shaw, M. On the analysis of cutting tool temperatures. Trans. ASME 1954; 76:217-225.

[71] Wright, P. K. Predicting the shear plane angle in machining from workmaterial strain-hardening characteristics. Journal of Engineering for Industry 1982; 104:285-292.

[72] Kumar, M., Dotson, K., Melkote, S. N. An experimental technique to detect tool-workpiece contact in micromilling. Journal of Manufacturing Processes 2010; 12:99-105.

[73] Kasim, M. S., Che Haron, C. H., Ghani, J. A., Gusri, A. I., Yazid, M. Z. A., Sulaiman, M. A. Tool life of tiain pvd coated carbide tool in high-speed end milling of untreated inconel 718 under minimum quantity lubrication condition. Sains Malaysiana 2013; 42:1721-1726.

[74] Karandikar, J. M., Schmitz, T. L., Abbas, A. E. Spindle speed selection for tool life testing using bayesian inference. Journal of Manufacturing Systems 2012; 31:403-411.

[75] Lihui Wang, R. X. G., Condition monitoring and control for intelligent manufacturing: Springer Science & Business Media, 2006.

[76] Bergström, D., Powell, J., Kaplan, A. F. H. The absorptance of steels to nd:Ylf and nd:Yag laser light at room temperature. Applied Surface Science 2007; 253:5017-5028.

[77] Anna Grazia Mignani, L. C., Andrea Azelio Mencaglia, and Antonio Cimato, Olive oil - constituents, quality, health properties and bioconversions. Rijeka, Croatia: InTech, 2012.

[78] Bucciarelli, A., Kuila, P. D., Melkote, S. N., Fortunato, A. Micro-machinability of a-286 steel with and without laser assist. 7th HPC 2016 CIRP Conference on High Performance Cutting, 2016, Chemnitz, Germany.

[79] Schäfer, F., Breuninger, F., Sauer, H., Schuh, B., Seyderhelm, W., Winter, H.-J. , et al., Entgraten: Theorie, verfahren, anlagen: Krausskopf, 1975.